Title
The Role of Zebrafish Adhesion GPCR Eltd1 in Left-Right Asymmetry and Cardiovascular Development

Author
Saleem, Arif Hussain

Publication Date
2013

Peer reviewed|Thesis/dissertation

The Role of Zebrafish Adhesion GPCR Eltd1 in Left-Right Asymmetry and Cardiovascular Development

by

Arif Saleem

DISSERTATION

Submitted in partial satisfaction of the requirements for the degree of

DOCTOR OF PHILOSOPHY

in

Biomedical Sciences

[redacted]

This dissertation is dedicated to my parents, who selflessly have given me the opportunity to obtain a world-class education, and to my wife Victoria, who has been my most loving and dedicated supporter from the very beginning of this long journey.

Acknowledgements

My graduate school tenure lasted longer than I expected. Though at times this was a source of incredible frustration, it also provided ample opportunity to work with extraordinary individuals both inside and outside our laboratory and gain valuable skills for lifelong learning.

I must first thank my graduate advisor, Shaun Coughlin, for his willingness to host me in his laboratory for my graduate training. He gave me tremendous intellectual freedom for a graduate student and was willing to explore areas and projects I found interesting, even if they weren't in his lab's "strike zone." Over the course of the last seven years, Shaun has been a source of brilliant ideas, thought-provoking scientific discussion, unwavering support, and incredible patience. I am deeply indebted to him for all that I have learned during my stay in his laboratory, not only about experimental design, but also about the academic career path and the twists and turns along the way. I have met few individuals with his combination of brilliance and humility – it is what drew me to him as a mentor in the first place and what I will remember most.

I must also thank all of the Coughlin Lab members, past and present, who have taught me so much over the years. In particular, I appreciate the work that Hiroshi Kataoka and Justin Hamilton performed in beginning the project that first kindled my interest in joining the lab. Jean Regard was one of the best scientific teachers I've had the pleasure of learning from. Stephen Wilson was of tremendous help in all things cell culture. In the past year, Yamini Bynagari has been a vibrant and enthusiastic collaborator within our lab and I excitedly anticipate her carrying our work forward.

Yao-Wu Zheng, Yoga Srinivasan, and Daniel Duong provided tremendous technical expertise and wisdom.

I must in particular acknowledge Hilary Clay's contribution to my education. In joining our lab, Hilary brought with her the expertise we needed to establish our own zebrafish facility and research program. Without her, my project would not have been possible and I would not have gained experience with, and more importantly, an appreciation of, this important model organism. Mai Baalbaki was instrumental in helping our facility run smoothly, devoting countless hours to keeping the fish happy.

I would also like to thank Oliver Stone from Didier Stainier's laboratory. He handled an awkward situation with class and shared beautiful *in situ* data with us.

I am thankful to my committee members Kevin Shannon, Brian Black, and Jeremy Reiter for their advice and support, and to faculty members Pao-Tien Chuang, Orion Weiner, and Ben Braun for their help, particularly in the early years of my training.

Most of all I am grateful for countless family and friends that have supported me during the ups and downs of this [still young] career path. They have picked me up when I have fallen, stayed with me when I've pushed away, and forgiven my many weaknesses.

Abstract

The Role of Zebrafish *Adhesion* GPCR Eltd1 in Left-Right Asymmetry and Cardiovascular Development

Arif Saleem

The *Adhesion* family of G protein-coupled receptors (AdGCPRs) is a unique set of cell-surface receptors with relatively unknown signaling capabilities and physiological functions. Previous work has revealed physiological roles for some AdGPCRs, ranging from orchestrating planar cell polarity in *Drosophila* epithelium to mediating cell-extracellular matrix interactions in the developing central nervous system. Mutations in some AdGPCRs have been linked to human disease. However, most AdGPCRs remain orphans, with unidentified binding partners, unclear physiological roles, and unknown downstream signaling.

Eltd1 (also referred to as ETL) is a member of the AdGPCR subfamily known to be expressed in cardiovascular tissues including heart and blood vessels. I performed morpholino-mediated knockdown of *eltd1* in zebrafish to elucidate its physiological function and attempt to gain insight into binding partners and putative signaling pathways. I found that knockdown of *eltd1* in zebrafish produced a defect in the establishment of left-right (LR) asymmetry as well as the processes of convergence and extension. Using targeted morpholino injections and fluorescent timelapse microscopy, I was able to show that loss of *eltd1* disrupts nodal flow in Kuppfer's vesicle, the organ responsible for establishing LR asymmetry in zebrafish. Interestingly, the early

developmental phenotypes associated with *eltd1* knockdown are similar to those often observed in morphants and mutants of various planar cell polarity (PCP) genes.

Eltd1 morphants also displayed defects in cardiovascular development, consistent with expression data from mouse and rat that localize *eltd1* transcripts most strongly to heart and blood vessels. I sought to characterize this phenotype and implement cell-culture assays to visualize Eltd1 in primary and cultured cells. Finally, I developed a strategy to isolate N-terminal binding partners of Eltd1. This work provides a foundation for further investigation of candidate Eltd1 binding partners and putative downstream signaling pathways.

Table of Contents

List of Tables

Chapter 1

List of Figures

Chapter 1

Chapter 2

Chapter 3

Chapter 1

Introduction

Introduction to GPCRs

The G-protein-coupled receptor (GPCR) superfamily of cell-surface receptors comprises a diverse group of proteins that are grouped together based on the presence of seven membrane-spanning domains. GPCRs bind a variety of ligands, including small organic compounds, eicosanoids, peptides, and proteins, and translate that binding into an intracellular signal, the majority via physical interaction with G-proteins. They have also proven to be reliable drug targets, and it has been estimated that more than half of modern drugs target GPCRs (Flower, 1999). A comprehensive search of the human genome revealed 342 non-odorant GPCRs and 460 odorant GPCRs, for a total of over 800, or 2% of human genes (Fredriksson *et al*., 2003). Although the name suggests otherwise, not all proteins grouped into the GPCR superfamily are proven to bind G-proteins.

During the years following the discovery of the primary structure of the first GPCR, rhodopsin, various classification schemes were employed to categorize seven-transmembrane (7TM)-spanning proteins. Division of these receptors into subgroups, or clans, was first attempted in 1993 by Attwood and Findlay on the basis of hydrophobic sequence fingerprints. One year later, the A-F classification system was published by Kolakowski, and included vertebrate and invertebrate receptors that had been proven to bind to G-proteins. The A-F classification placed seven transmembrane (7TM)-spanning proteins for which there was no proven G-protein binding into the O (Other) family (Kolakowski, 1994). This system is used by the International Union of Pharmacology, Committee on Receptor Nomenclature and Classification (NC-IUPHAR), with the

exception that the frizzled receptors are placed in a separate family instead of the O family.

In 2003, Fredriksson and colleagues published a phylogenetic classification of human GPCRs consisting of five families, termed *Glutamate*, *Rhodopsin*, *Adhesion*, *Frizzled/Taste2*, and *Secretin* and referred to by the acronym GRAFS. This classification for the first time placed *Adhesion* GPCRs (AdGPCRs) into their own family, distinct from *Frizzled* receptors (Fredriksson *et al*., 2003). Table 1 describes the properties of the GPCR families.

Property	Rhodopsin	Secretin	Adhesion	Glutamate	Frizzled	Taste2
Number of full-length receptor proteins	672 (388 ORs)	15	33	22	11	25
Number of identified major drug targets	>39	4	0	3	0	0
Number of orphans	63 (not including ORs)	0	30 *	7	0	21
Type of ligand	Peptides, proteins (including enzymes), small organic compounds, lipid-like substances, nucleotides	Peptides, proteins	Proteins, glycosaminoglycan	Amino acids, cations, small organic compounds, carbohydrates	Proteins	Small organic compounds
Extended N termini	No	No	Yes	Yes	Yes	Yes
Conserved functional domains in the N termini	No	No	Yes	Yes	Yes	Yes
Type of functional domains in the N termini (not including transmembrane)	Proteolytic sites, LRR, LDLa	HBD	GPS, TSP1, HBD, PTX, EGF, OLF, GBL, CA, LamG, EGF-Lam, LRR, Ig, SEA, Calx-beta, EAR, CUB, C-type lectin	VFTM, SUSHI	Wnt binding domain	–
Proteolytic processing of the N termini in family members	Yes	No	Yes	No	No	No
Conserved cysteine residues in EL1 and EL2	Yes	Yes	Yes	Yes	Yes	No
Suitable as drug targets?	Yes	Yes	Yes	Yes	Yes	No

Table 1. Properties of GPCR families. Adapted from Lagerström *et al*., *Nat Rev Drug Disc* (2008). *As of 2008, three AdGPCRs were considered to be de-orphanized: GPR56 (transglutaminase-2, Xu *et al*., 2006), EMR2 (chondroitin sulphate, Stacey *et al*., 2003), and CD97 (decay-accelerating factor/CD55, Hamann *et al*., 1996; chondroitin sulphate, Stacey *et al*., 2003; integrin $\alpha_5\beta_1$, Wang *et al*., 2005). Recent work has led to the de-orphanization of LEC2 (teneurin-2, Silva *et al*., 2011) and the addition of a

physiological ligand for GPR56 (collagen III, Luo *et al*., 2011). Thus, there are 29 orphans in the *Adhesion* family at present time.

Classical GPCR Signaling

Although this work focuses on *Adhesion* GPCRs, which can be considered "non-classical" from a GPCR signaling perspective, it is worthwhile to first briefly review "classical" GPCR signaling.

The binding of an endogenous ligand to a GPCR facilitates the interaction of the intracellular portions of the receptor with a heterotrimeric G-protein. This occurs via a conformational shift of the transmembrane helices of the GPCR. The interaction in turn produces a conformational shift within the G-protein, leading to its activation (Gether, 2000).

Heterotrimeric G-proteins consist of α-, ß-, and γ-subunits that form a complex. The α-subunit binds and hydrolyzes GTP, and undergoes an activation-inactivation cycle. Coupling of the GDP-bound trimeric G-protein to an activated GPCR promotes exchange of GDP for GTP and dissociation of the α-subunit from the complex. The resulting GTP-bound α-subunit and ßγ dimer then go on to modulate a variety of effectors, such as enzymes or ion channels. Signaling is terminated when the α-subunit hydrolyzes the bound GTP, a process that is intrinsic to the α-subunit and subject to regulation by modifying proteins. The GDP-bound α-subunit then reassociates with a ßγ complex to reform the heterotrimeric protein and enter a new cycle if activated receptors are present.

The α-subunit largely defines the properties of a heterotrimeric G-protein. There are four families of α-subunits: $G\alpha_s$, $G\alpha_i/G\alpha_o$, $G\alpha_q/G\alpha_{11}$, and $G\alpha_{12}/G\alpha_{13}$. Each family consists of various members that often show very specific expression patterns. The ßγ complex is composed from one of five ß-subunits and one of twelve γ-subunits. Bγ complexes do not differ significantly in their ability to modulate effector functions (Clapham & Neer, 1997). Most GPCRs are able to couple to more than one subtype of G-protein, and thus the cellular and biological response is determined by the pattern of G-proteins, and therefore different signaling cascades, activated by a given receptor (Wettschureck & Offermanns, 2005).

Adhesion GPCR family characteristics and classification

The *Adhesion* family of GPCRs, the second-largest GPCR family in humans, consists of 33 full-length receptor proteins that share two important properties: (1) The presence of long N-termini and (2) a conserved domain known as GPS (GPCR proteolytic site). The family is also sometimes referred to as LNB-7TM, whereby LN stands for long N-termini and B for the sequence similarity between the transmembrane regions of *Adhesion* GPCRs and *Secretin* family receptors (class B).

Members of the *Adhesion* family are divided into eight subgroups I-VIII based on phylogenetic analyses of the transmembrane regions. The composition of functional domains in the N-termini also seems to support this phylogenetic classification, as receptors with most closely-related transmembrane regions also have similar N-terminal extracellular domains. Group I includes the lectomedin receptors (LECs 1-3) and Eltd1.

Group II, the EGF-like module containing receptors (EMRs), includes EMR1-4 and CD97. Group III consists of three receptors, GPR123-125. GPR123 is the only AdGPCR that lacks a GPS domain. CELSR1, -2, and -3 (mammalian homologs of *Drosophila* flamingo) constitute Group IV. The remainder of AdGPCR groups is summarized in Figure 1. As noted in Table 2, the vast majority of AdGPCRs are orphans. As of this writing, non-homotypic extracellular binding partners have been identified for only four out of thirty-three AdGPCRs, and thus the *Adhesion* family has the largest proportion of receptors awaiting de-orphanization.

Receptor	Ligand(s)	Expression / relevant tissues	Selected references
LEC1	None, same as LEC2?	CNS, lung, liver, heart	Matsushita *et al*., 1999
LEC2	Lasso/teneurin-2	CNS	Matsushita *et al*., 1999 Silva *et al*., 2011
LEC3	None, same as LEC2?	CNS	Matsushita *et al*., 1999
ELTD1	None	Heart, smooth muscle, microvascular endothelium	Nechiporuk *et al*., 2001 Wallgard *et al*., 2008
EMR1	None	Leukocytes	Hamann *et al*., 2007
EMR2	Chondroitin sulphate	Leukocytes	Stacey *et al*., 2003
EMR3	None, ligand on surface of macrophages and neutrophils	Leukocytes	Stacey *et al*., 2001
EMR4	None, ligand on A20 B-lymphoma cells	Leukocytes	Stacey *et al*., 2002
CD97	Decay-accelerating factor/CD55, chondroitin sulfate, integrin $a_5\beta_1$	Leukocytes, smooth muscle, GI tract	Hamann *et al*., 1996 Stacey *et al*., 2003 Becker *et al*., 2010
GPR123	None	CNS	Lagerstrom *et al*., 2007
GPR124	None, integrin binding possible	CNS endothelium	Kuhnert *et al*., 2010 Vallon *et al*., 2012
GPR125	None	Spermatogonia, choroid plexus	Seandel *et al*., 2008 Pickering *et al*., 2008
CELSR1	Homotypic interactions likely	CNS, eye, kidney, lung, spleen, testis	Shima *et al*., 2004 Beall *et al*., 2005
CELSR2	Homotypic interactions likely	CNS, eye, heart, kidney, lung, spleen, testis	Shima *et al*., 2004 Beall *et al*., 2005 Tissir *et al*., 2010
CELSR3	Homotypic interactions likely	CNS, eye, testis	Beall *et al*., 2005 Zhou *et al*., 2008 Tissir *et al*., 2010
GPR133	None	CNS	Vanti *et al*., 2003
GPR144	None	Unknown	
GPR110	None	Kidney	Prömel *et al*., 2012
GPR111	None	Skin	Prömel *et al*., 2012
GPR113	None	Taste receptor cells	LopezJimenez *et al*., 2005
GPR115	None	Skin	Prömel *et al*., 2012
GPR116	None	Lung, heart, kidney	Abe *et al*., 1999 Prömel *et al*., 2012
BAI1	None	CNS, bone marrow	Park *et al*., 2007
BAI2	None	CNS, heart, skeletal muscle	Shiratsuchi *et al*., 1997
BAI3	None	CNS, heart	Shiratsuchi *et al*., 1997
GPR56	Transglutaminase-2, collagen III	CNS	Xu *et al*., 2006 Luo *et al*., 2011
GPR97	None	Leukocytes	Peng *et al*., 2011

GPR112	None	Mucosal layer of GI tract	Ito *et al*., 2009
GPR114	None	Leukocytes	Peng *et al*., 2011
GPR126	None	PNS, endothelium, placenta	Moriguchi *et al*., 2004 Stehlik *et al*., 2004 Monk *et al*., 2011
GPR128	None	Unknown	
HE6	None	Male reproductive tract	Kirchhoff *et al*., 2006
VLGR1	None	Inner ear, retina	Reiners *et al*., 2005 McGee *et al*., 2006

Table 2. Summary of *Adhesion* GPCR ligands and expression. De-orphanized receptors are highlighted in blue. Selected/seminal references are given for each receptor where applicable.

AdGPCR-like sequences are found in animals as primitive as *Nematostella* and *Dictyostelium* (Nordstrom *et al*., 2009). Interestingly, neither genome contains *Secretin* family GPCRs, leading to the belief that AdGPCRs comprise a more ancient family of receptors. Iterative phylogenetic analysis has suggested that the *Secretin* GPCRs arose from Group V AdGPCRs (Schioth *et al*., 2011). Almost the entire *Adhesion* family is thought to share a common ancestry, having arisen from gene duplication events. During vertebrate evolution, two rounds of large-scale gene duplications are believed to have resulted in up to four copies of each gene in mammals. This is known as the "2R hypothesis" or "one-to-four" model (Lundin *et al*., 1993; Holland *et al*., 1994). Indeed, most of the genes for AdGPCRs are found on the human paralogon 1/5p-q21/6p21-p25/9/15q11-q26/19p (Fredriksson *et al*., 2003).

AdGPCR genes are extremely large, spanning up to over 7,000 nucleotides and multiple introns (up to 100), which can also be alternatively spliced (Bjarnadottir *et al*., 2007). This, in addition to unique protein features discussed below, has contributed an additional degree of difficulty to their study.

The long N-termini of AdGPCRs, which range from approximately 200 to 2,600 amino acid residues in length, are notable for containing a variety of functional domains including EGF-like domains, thrombospondin repeats, leucine-rich repeats, lectin-like

domains, and cadherins. In other proteins, many of these domains are involved in protein-protein interactions and cell adhesion; hence the '*Adhesion* GPCR' nomenclature has been proposed to reflect potential roles in both cellular adhesion and signal transduction. Given their size, likely accessibility at the cell surface, and numerous binding domains, the lengthy N-termini are also intriguing targets for drug development.

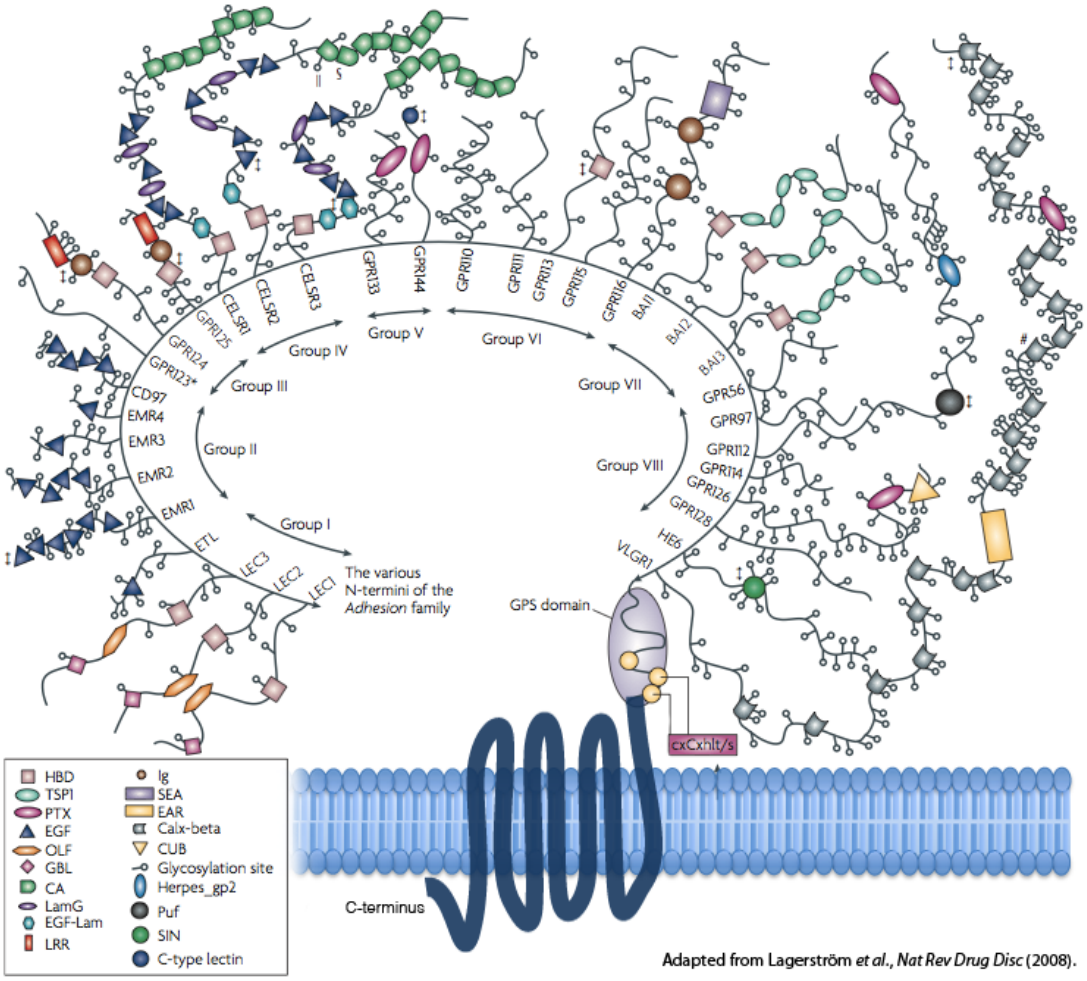

Figure 1. The 33 human Adhesion GPCRs. Each receptor contains seven TM domains (bottom center) attached to a long N-terminal extracellular domain with various binding motifs. Between the TM region and the extracellular domain is the GPS, a proteolytic site that yields two protein subunits for each receptor after cleavage. HBD, hormone-binding domain; TSP1, thrombospondin1 domain; PTX, pentraxin domain; EGF, epidermal growth factor domain; OLF, olfactomedin domain; GBL, galactose-binding lectin domain; CA, cadherin domain; LamG, laminin G domain; EGF-Lam, Laminin EGF-like domain; LRR, leucine-rich repeat; Ig, immunoglobulin domain; SEA, domain found in sea urchin sperm protein; EAR, epilepsy-associated repeat; Calx-beta, domain found in Na-Ca exchangers; CUB, an immunoglublin-like domain; Herpes_gp2, resembles equine herpes virus glycoprotein 2 structure; Puf, structural similarity to RNA-

binding protein from the Puf family; SIN, resembles primary structure of SIN component of histone deacetylase complex; C-type lectin, carbohydrate recognition domain.

The functional domains are located N-terminal to a region of these receptors that is rich in glycosylation sites and proline residues. It is thought that this forms a rigid, "mucin-like" stalk structure that protrudes from the cell surface. The functional significance of this rigidity is currently unknown – it may provide mechanical integrity essential for some function of the receptor or it may allow presentation of the functional/binding domains of the receptor at a greater distance from the cell surface.

The transmembrane regions of AdGPCRs are generally thought not to be involved in ligand-binding as they are for many "classical" GPCRs. In support of this, the TM regions for many AdGPCR mouse/human orthologs share less than 70% sequence identity. The low degree of evolutionary constraint on the TM regions of some AdGPCRs has also led to speculation that AdGPCRs may not couple to second messenger systems in specific or important fashion, with the 7TM acting merely as a membrane anchor (Bjarnadottir *et al*., 2007). However, it should be noted that several pairs of AdGPCR mouse/human orthologs, such as BAI3, share over 90% amino acid identity in the TM regions, arguing for a more specific and conserved role for the 7TM (Schioth *et al*., 2011). Thus, on the basis of sequence conservation through vertebrate evolution, it can be concluded that the purpose of the 7TM may be highly variable amongst AdGPCR family members.

AdGPCRs do not share many features with other families of GPCRs; however, they do contain a conserved Cys between TMI and TMII and a second conserved Cys between TMIII and TMIV as with all other families of GPCRs (Fredriksson *et al*., 2003).

These Cys residues are believed to form disulfide linkages between intracellular loops and contribute to the overall structural integrity of the protein. Similar to *Rhodopsin* family GPCRs, which contain a conserved DRY motif in the ascending portion of TMIII, human and mouse AdGPCRs have three conserved residues in the ascending portion of TMIII, including hydrophilic His and Trp residues (Bjarnadottir *et al*., 2004). The DRY motif of TMIII is essential for keeping several *Rhodopsin* GPCRs in an inactive conformation (Chung *et al*., 2002). If AdGPCRs share a similar topology to bovine rhodopsin (Palczewski *et al*., 2000), rotation of TMIII may allow for signal transduction into the cell, as has been hypothesized for all *Rhodopsin* GPCRs. TMIV of AdGPCRs contains a Trp residue that is found in the consensus sequences for *Rhodopsin*, *Secretin*, and *Frizzled* family receptors (Fredriksson *et al*., 2003). This conserved Trp is followed by a PAL/V motif that is found in *Secretin* and *Frizzled* families.

Arguably the most compelling feature of AdGPCRs is the presence of the GPS motif, a conserved arrangement of four Cys residues N-terminal to the first TM domain. Contained within this region is a cleavage site that undergoes autoproteolysis in the endoplasmic reticulum or early compartment of the Golgi apparatus. This biosynthetic event yields two non-covalently attached subunits, and the crystal structure of this interaction has been recently elucidated for two particular AdGPCRs and is discussed below.

GPS Proteolytic Cleavage of Adhesion GPCRs

One of the most striking and unique structural features of AdGPCRs is the presence of the GPS motif, which results in the biosynthetic separation of the receptor into an extracellular α-subunit and a 7TM ß-subunit. The region was first studied in the AdGPCR latrophilin. Krasnoperov and colleagues noted that mutations introduced into this motif prevented cleavage of the protein (1999). No protease was identified, and based on the presence of a cis-proteolytic signature, it was hypothesized that the cleavage is autocatalytic (Lin *et al*., 2004). Hydrolysis of the peptide bond at the cleavage site is thought to be mediated by a N > O or N > S acyl shift enabled by nucelophilic attack on critical residues around the cleavage site (Figure 2). This is the same autoproteolytic mechanism that Ntn hydrolases and hedgehog proteins employ (Brannigan *et al*., 1995; Perler *et al*., 1997).

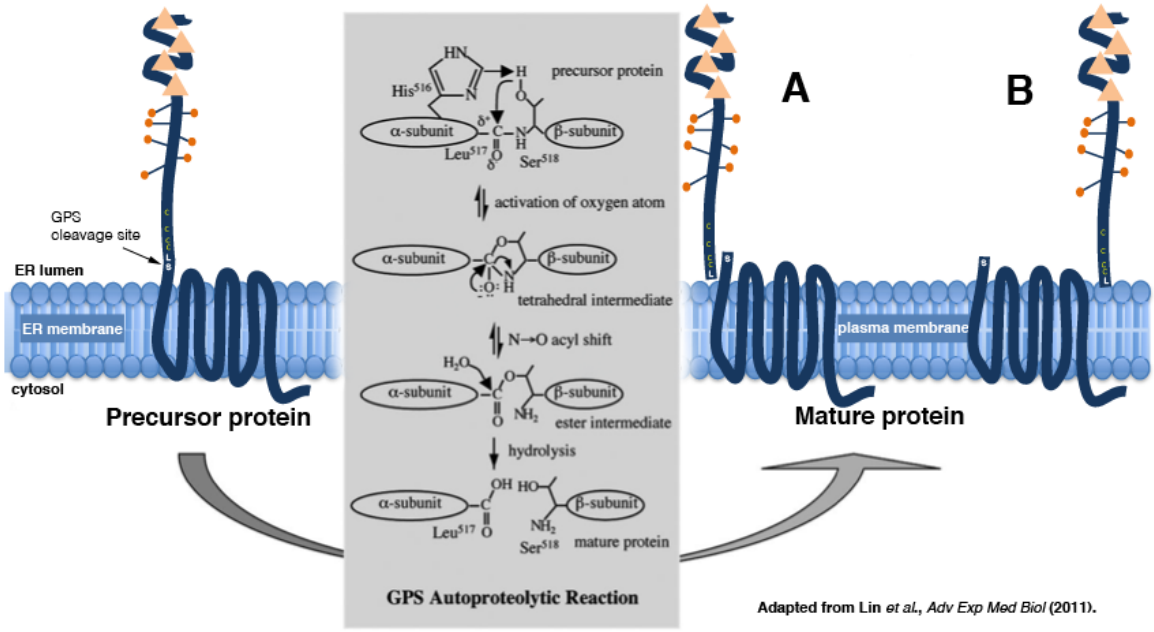

Figure 2. Proposed mechanism of *Adhesion* GPCR autoproteolysis of the GPS. The reaction takes place in the ER lumen with EMR2 as an example. Only the cleavage tripeptide is depicted in the shaded box. The reaction begins with a nucleophilic attack and electron transfer (arrow) from P_2 (His516), resulting in a tetrahedral intermediate. An N>O acyl shift in the P_1' residue (Ser518) cleaves the C-N bond. Finally, water hydrolyzes the ester bond resulting in an extracellular α-subunit and 7TM ß-subunit that may remain associated (A) at the plasma membrane or may separate (B).

Until recently, it was believed that the stalk region preceding the GPS motif was unstructured and largely non-functional. This notion was refuted in a study that solved the crystal structures for LEC2 and BAI3, two distantly related AdGPCRs. The authors found that the ~40 residue GPS motif itself does not form a single folded domain, but rather is an integral part of a much larger ~320 residue domain that they termed the GPCR-Autoproteolysis Inducing (GAIN) domain (Arac *et al*., 2012).

Several studies have suggested that GPS proteolysis is essential for receptor trafficking, and until recently this was a prevailing notion in the field. The discovery of the GAIN domain suggests that observations of impaired receptor trafficking in many earlier studies were likely due to disrupted folding of the larger GAIN domain. Cleavage site mutants have now been described for several AdGPCRs which inhibit cleavage at the GPS but still allow the receptor to traffic to the plasma membrane (Arac *et al*., 2012; Prömel *et al*., 2012). Thus, it is evident that GPS cleavage likely has a role in AdGPCR function that is distinct from trafficking.

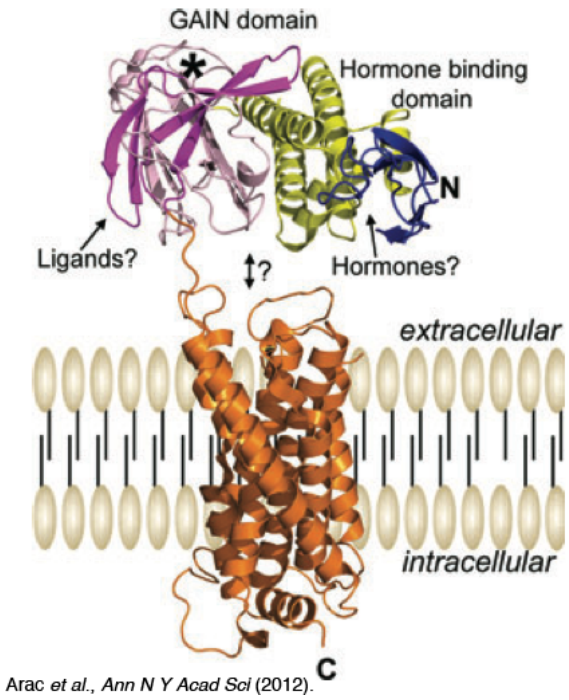

Figure 3. Crystal structure of the GAIN domain. The A and B subdomains of the GAIN domain are colored yellow and light pink, respectively. The GPS domain is colored magenta. The HormR domain, which is found in 12 AdGPCRs, is colored blue. The transmembrane helices are colored orange. The GPS cleavage site is identified by the asterisk.

Given that the GAIN domain remains attached to the membrane-embedded portion of the receptor after GPS cleavage, it is possible that the domain regulates receptor signaling via the transmembrane helices. Results from deletion experiments undertaken by Paavola and colleagues suggest that the GAIN domain of one AdGPCR, GPR56, may have inhibitory effects on receptor signaling. Truncation of the large N-terminus of GPR56 resulted in constitutive activation of receptor signaling as measured by a Rho activation assay. In addition, enhanced binding of ß-arrestins to, and extensive ubiquitination of, the truncated protein were observed (Paavola *et al*., 2011). These results argue for a model in which the GAIN domain may serve as an "off switch" for signal transduction that can be removed transiently or permanently via several potential

mechanisms, including ligand binding to the functional domains of the N-terminus, mechanical forces acting on the N-terminus, or proteolytic cleavage (Figure 4).

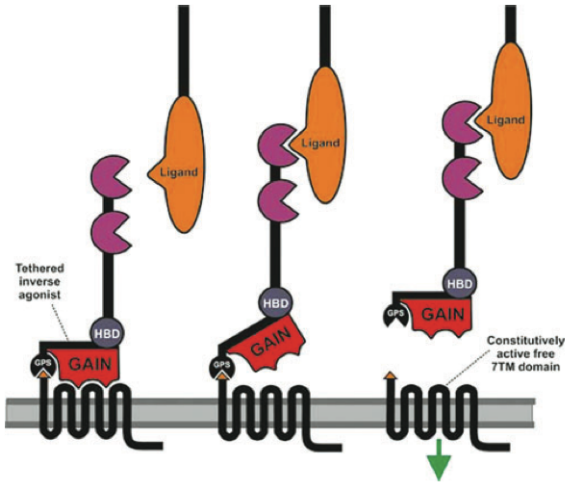

Figure 4. A general model for Adhesion GPCR signaling. It is proposed that the extracellular domain acts as a tethered inverse agonist which silences the constitutive activity of the 7TM via the GAIN domain. When a ligand binds the extracellular domain, the GAIN domain is removed from the 7TM, either partly or completely if GPS autoproteolytic cleavage has occurred. The 7TM is now free to signal with its high constitutive activity.

A line of investigation that may illuminate the functional role of the GPS motif and GAIN domain in AdGPCRs comes from work on polycystin-1, one of only five human non-AdGPCRs to contain the GAIN domain. Polycystin-1 (PC1) is an 11-transmembrane protein approximately 4,300 amino acid residues in length, with a ~2,500 aa extracellular domain containing leucine-rich repeats, a C-type lectin, 16 Ig-like repeats, and four type III fibronectin-related domains (Hughes *et al*., 1995). Mutations in the gene encoding PC1, *Pkd1*, are responsible for 85% of autosomal dominant polycystic kidney disease (ADPKD) (Tsiokas *et al*., 2007), a relatively frequent genetic disorder characterized by progressive cyst formation and enlargement typically leading to end stage renal disease. PC1 forms heterodimers with polycystin-2 (PC2) that localize to the primary cilium in a variety of cell types including renal epithelial cells (Nauli *et al*.,

2003). Based on evidence from several studies, it is thought that the complex acts as a mechanosensitive ion channel, allowing Ca^{2+} entry in response to mechanical stimuli such as fluid shear stress (Nauli *et al*., 2003; Nauli & Zhou, 2004; Rohatgi *et al*., 2008; Xia *et al*., 2010). The long N-terminus of PC1, strikingly reminiscent of AdGPCRs with its numerous functional domains preceding a GAIN domain, is thought to mediate this mechanosensory function (Qian *et al*., 2005).

Certain disease-associated point mutations in polycystin-1 inhibit GPS cleavage but allow for normal cell surface expression (Qian *et al*., 2002). However, these mutant proteins showed impaired tubulogenic functions in an *in vitro* tubulogenesis model compared to wild-type polycystin-1. This study also noted that disruption of the so-called REJ domain of PC1 (mostly analogous to the GAIN domain of AdGPCRs identified ten years later by Arac and colleagues) inhibited cleavage at the GPS, supporting the model that sequences outside of the GPS are required for cleavage. *In vivo* validation of the functional role of PC1 GPS cleavage was provided by mutant knock-in mice in which the wild-type *Pkd1* gene was replaced by an allele expressing uncleavable polycystin-1. These mice displayed different phenotypes than *Pkd1*-null animals (Yu *et al*., 2007). From these experiments it was concluded that uncleaved full-length and GPS-cleaved PC1 possess distinct functions. Taken together, these data strongly argue that GPS cleavage has a functional role in PC1 biology and provide hints that GPS cleavage of AdGPCRs may be similarly important.

Functional cross-interaction is an intriguing model for how GPS cleavage may direct and enable the functional capabilities of AdGPCRs. It was previously believed that the α- and ß-subunits remain tightly but non-covalently bound to one another during

trafficking and remain so at the plasma membrane. This was largely due to the observation in multiple AdGPCRs that α-subunits can readily be pulled down by antibodies specific to ß-subunits (Gray *et al*., 1996; Krasnoperov *et al*., 1997; Abe *et al*., 2002). Further, soluble chimeric proteins containing the α-subunit fused to a protein tag such as the immunoglobulin Fc region were found to be cleaved normally and the entire protein could be affinity-purified by Protein A column chromatography (Chang *et al*., 2003; Lin *et al*., 2004).

Some studies have challenged this model, however. In one report, isotope-labeled α-latrotoxin, a non-physiologic ligand of latrophilin, was observed to bind the surface of cells transfected with a soluble latrophilin molecule. This suggests that cleaved N-terminal latrophilin can somehow attach to the plasma membrane by itself. Moreover, confocal immunofluorescence imaging revealed incomplete co-localization of the two latrophilin subunits, which exhibited different lateral diffusion rates. The binding of α -latrotoxin was also shown to induce reassociation of the α -subunit with the 7TM ß-subunit, and the authors concluded that the extracellular α -subunit of latrophilin was a separate molecular entity able to anchor itself to the plasma membrane (Volynski *et al*., 2004). A follow-up article from the same laboratory demonstrated that it is possible to detect the cross-interaction, by immunoprecipitation, of independent α- and ß-subunits derived from different AdGPCRs transfected into cultured cells. The authors also demonstrated cross-precipitation of GPR56 ß-subunit by the α-subunit of latrophilin from solubilized rat brain (Silva *et al*., 2009). This ability of AdGPCRs, enabled by GPS cleavage, creates the potential for combinatorial diversity in AdGPCR signal transduction.

Adhesion GPCR Signal Transduction: G-proteins or not?

Downstream signaling through AdGPCRs has been historically difficult to identify because most AdGPCRs are orphan receptors, have poorly-characterized ligand interactions, or have only non-physiological, non-specific ligands available for signaling studies. Even in the case of AdGPCRs that are well-studied and for which putative ligands have been identified, convincing evidence for G-protein coupling exists in a few cases. We examine some of those instances here.

G-protein-dependent signaling of GPR56

Point mutations in human GPR56, an AdGPCR with no identifiable functional domains in its N-terminus, cause a disease of cerebral cortical development known as bilateral frontoparietal polymicrogyria (BFPP) (Piao *et al*., 2004). In one study aiming to de-orphanize this receptor, the authors demonstrated a physical interaction between GPR56 and tissue transglutaminase (TG2), an enzyme found in the extracellular matrix (Xu *et al*., 2006). The strategy involved using the N-terminus of GPR56 fused to human IgG Fc fragment as a probe on frozen tissue sections and as bait to pull the ligand out of mouse lung extracts, followed by mass spectrometric analysis. However, agonism by TG2 was not shown, nor has it been demonstrated in other studies as of this writing. Another study utilizing a luciferase-based reporter system identified ligand-independent signaling via $G\alpha_{12/13}$ in HEK293T cells overexpressing GPR56, and used an agonistic anti-GPR56 antibody to show GPR56-dependent Rho activation. Importantly, ERK,

JNK, or p38 activation were not detected, nor was a calcium response, arguing against coupling to $G\alpha_{i/o}$ or $G\alpha_{q/11}$ (Iguchi *et al*., 2008). More recently, collagen III has been identified as a second, and perhaps more physiologically relevant, ligand for GPR56. *Col3a1* null mice were shown to exhibit cortical malformations similar to *GPR56* null mice, and recombinant collagen III-stimulated activation of RhoA was blunted by dominant-negative $G\alpha_{13}$ in NIH3T3 cells (Luo *et al*., 2011). Taken together, these data strongly argue for collagen III and GPR56 as a physiological ligand-receptor pair that signals through $G\alpha_{12/13}$. Further studies from the same group demonstrated that four BFPP-causing human point mutations in *GPR56* abolish collagen III binding (Luo *et al*., 2012). The example of GPR56 underscores the importance of animal knockout studies, in addition to biochemistry, for the establishment of AdGPCR-ligand pairs and identification of their immediate downstream signaling partners. A direct physical interaction between GPR56 and $G\alpha_{12/13}$ has yet to be demonstrated.

Lack of G-protein-dependent signaling of CD97

CD97 was the first AdGPCR for which a putative ligand was identified and is of particular interest here because it possesses only EGF-domains in its N-terminus, much like the AdGPCR we have been studying, Eltd1. Hamann *et al*. identified a monoclonal antibody that blocked binding of erythrocytes and lymphocytes to CD97-expressing COS cells (1996). This antibody was shown to be directed to a portion of decay-accelerating factor (DAF, CD55), a GPI-linked cell-surface protein found on most leukocytes. Erythrocytes lacking CD55, obtained from patients with the CD55- phenotype, failed to adhere to CD97-expressing COS cells. Intriguingly, splice variants of CD97 vary in

CD55 binding affinity (Hamann *et al*., 1998). The CD97-CD55 complex has been shown to regulate the complement system (Abbott *et al*., 2007). Despite well-characterized binding site and affinity studies, functional data regarding relevant cell types, and the existence of a blocking antibody, a downstream signal, G-protein or otherwise, remains elusive for CD97 and its ligand CD55. The difficulty in establishing G-protein coupling for a relatively well-defined receptor-ligand pair suggests that G-protein-independent signal transduction may be relevant for some or all AdGPCRs. The observation that AdGPCRs BAI1, GPR124, and GPR125 have a xTxV motif, which interacts with PDZ, in the C-terminus of their 7TM region (Shiratsuchi *et al*., 1998; Yamamoto *et al*., 2004) while other AdGPCRs such as GPR56 and latrophilin do not, supports this hypothesis.

G-protein-dependent signaling of latrophilin

A third example of AdGPCR receptor signaling is that of latrophilin (LEC), arguably the most biochemically characterized AdGPCR. Latrophilin was originally isolated as the target molecule of α-latrotoxin (LTX), a component of black widow spider venom. LTX induces calcium signaling and neurotransmitter release in neurons and also forms cation-permeable pores in the plasma membrane. Although it is not the endogenous ligand for latrophilin, LTX has been a useful tool to study its signal transduction. LTX action can be blocked by U73122 (a phospholipase C inhibitor), thapsigargin (a drug that depletes intracellular Ca^{2+} stores), and 2-aminoethoxydiphenyl borate (an inhibitor of inositol(1,4,5)-triphosphate-induced Ca^{2+} release), suggesting that G-protein signaling may regulate LTX action. Several studies have contributed to the model that latrophilin induces $G\alpha_q$ or Gßγ-mediated PLCß activation, leading to Ca^{2+}

mobilization (Davletov *et al*., 1998; Ashton *et al*., 2001; Capogna *et al*., 2003). Additionally, latrophilin has been co-purified with $G\alpha_o$ (Lelianova *et al*., 1997) when expressed in COS cells and with $G\alpha_q$ (Rahman *et al*., 1999) from rat brain extracts.

A putative ligand for latrophilin was isolated from rat brain extracts by utilizing the extracellular domain as bait (Silva *et al*., 2011). A splice variant of teneurin-2, the 275 kDa protein was termed Lasso. Both proteins are enriched at synapses of cultured hippocampal neurons, with LPH-1 adopting a presynaptic localization and Lasso postsynaptic. A C-terminal fragment was also shown to induce Ca^{2+} signals in hippocampal neurons and neuroblastoma cells expressing LPH-1. However, despite the availability of pharmacological agents used previously to establish G-protein-dependent signaling from LPH-1, the G-protein dependence of Lasso-induced Ca^{2+} signaling was not tested.

G-protein-independent signaling of Flamingo/CELSR

A final example of AdGPCR signaling is that of *Drosophila* flamingo and the orthologous CELSR1, CELSR2, and CELSR3 in humans and mice. These are some of the largest AdGPCRs with N-termini that extend over 2,000 amino acids. The functional domains present in flamingo include nine cadherin repeats, three cysteine-rich domains (EGF), and two laminin A globular domains (Usui *et al*., 1999). In contrast to GPR56 and latrophilin, no G-protein signaling has yet been described for flamingo or its mammalian orthologs. However, flamingo has been studied extensively and is considered to be a central player in planar cell polarity (PCP), or non-canonical Wnt, signaling. While canonical Wnt signaling involves the binding of wnt ligands to *Frizzled*

family receptors and signal transduction via activation of disheveled to inhibit the degradation of ß-catenin, non-canonical Wnt signaling diverges at disheveled to multiple downstream pathways including JNK, Ca^{2+}, and small GTPases rho/rac/cdc42, and does not involve ß-catenin. These pathways are also downstream targets of G-proteins and other signaling pathways; thus a specific biochemical assay for non-canonical Wnt activation remains an unrealized tool as of this writing.

Unlike G-protein signaling, which can be assayed biochemically in relatively simple cell culture experiments, non-canonical Wnt signaling must be studied in a context that offers coordinated interactions and physiological polarization of groups of cells – planar cell polarity - typically, this is during epithelial development in a model organism such as *Drosophila* or *Danio*. In *Drosophila*, one traditional phenotypic readout for PCP signaling has been the planar polarization of wing epithelium, and at the subcellular level, the asymmetric distribution of "core" PCP molecules disheveled (Dsh), van gogh (Vang), frizzled (Fz), prickle (Pk), diego (Dgo), and flamingo (Fmi) in wing epithelial cells. Flamingo exhibits homophilic interaction *in trans* (Usui *et al*., 1999), and this interaction is thought to establish molecular asymmetry across polarized epithelial cells that directs the other core PCP proteins to the proximal or distal edge of each wing epithelial cell in a Fz activity-dependent manner (Gray *et al.*, 2011).

Loss of any one of the core PCP genes in *Drosophila* wing epithelium leads to loss of the polarized localization of all the other components, suggesting that complex positive and negative interactions regulate this process. Observed physical interactions between core PCP molecules support this idea. Specifically, murine CELSR1 was shown to co-immunoprecipitate with vangl2 when both were expressed as tagged proteins in

primary keratinocyte cultures (Devenport & Fuchs, 2008), and *Drosophila* frizzled can be co-immunoprecipitated with flamingo when expressed in S2 cells and natively from 24h after puparium formation (APF) pupae. Further, the data suggested flamingo interacts with frizzled via its transmembrane domains (Chen *et al*., 2008). The role of flamingo and its mammalian orthologs in the establishment of planar cell polarity and its physical interactions with core PCP molecules raise the question of whether these functions and interactions may extend to other AdGPCR family members.

In Vivo Roles for AdGPCRs – Lessons from Animal Models

Genetic analysis of AdGPCRs is made challenging by the complexity of the gene family, including the presense of up to 3-5 paralogs for some receptor subfamilies, possibly indicating functional overlap and/or compensation between paralogs. Although the majority of *Adhesion* GPCRs remain orphans and relatively little has been established regarding their signaling, mouse knockouts and other transgenic model organisms have contributed significantly to our understanding of the potential function of these receptors *in vivo*. We attempt to summarize these efforts here with the goal of extracting general principles related to AdGPCR function and signaling that may direct future studies, particularly on those *Adhesion* family members for which less is currently known, including Eltd1.

CELSR

Flamingo has been well-studied in *Drosophila* in the context of planar cell polarization of wing epithelial cells, where it is thought to direct the asymmetric localization of core PCP molecules which in turn establish the proximal-distal polarization of each wing epithelial cell and therefore, the coordinated distal placement of each cell's single cuticular hair. The current understanding is that this occurs via homotypic flamingo interactions across neighboring cells, which in turn recruit core PCP proteins frizzled, disheveled, and diego to the distal side of each cell and van gogh and prickle to the proximal side (McNeill, 2010).

Wing epithelium is composed of a relatively uniform array of hexagonal-shaped cells on a structure that is amenable to visualization without laborious tissue processing, making the demonstration of asymmetric protein distribution somewhat less difficult than in other tissues and organisms. However, other studies have established a similar role for flamingo/CELSR in less uniform murine epithelial tissues, including inner ear sensory epithelium, epidermis, and brain ventricular ependyma.

The *crash* (*Crsh*) and *spin cycle* (*Scy*) mouse mutant alleles were mapped to *celsr1* in 2003 (Curtin, *et al*.). The *Crsh* allele contains a point mutation resulting in an aspartate to glycine transition (D1040G) in the eighth cadherin repeat of the extracellular domain while *Scy* harbors a point mutation converting asparagine to lysine (N1110K) within a linker region between cadherin repeats that is likely to coordinate Ca^{2+} binding based on sequence similarity to E-cadherin. In addition to neural tube defects, these mice exhibit vestibular dysfunction in the form of head-spinning behavior, belly curling, and spinning during tail suspension. The vestibular phenotypes are caused by a defective

planar polarization of sensory hair cells in the organ of Corti, as noted by the disorganization of the stereocilia found on these cells.

Devenport and Fuchs reported the anterior-posterior polarization of hair follicles in mouse epidermis (2008), which is responsible for the alignment of hairs that give the fur its uniform appearance. Similar to flamingo distribution within *Drosophila* wing epithelial cells, CELSR1 and Vangl2 were found enriched on the anterior-posterior axis of interfollicular epithelial cells. *Crsh/Crsh* mutant mice exhibited disorganized and mis-angled hair follicles by E18.5, and the mutant allele eliminated the asymmetric distribution of CELSR1 without altering its overall expression or transport to the plasma membrane. Vangl2 asymmetry within epidermal cells was lost in *Crsh*/*Crsh* mutants, showing the same dependence on CELSR1 that van gogh/strabismus has on flamingo in *Drosophila* wing epithelium. Intriguingly, the Vangl2 point mutant allele *looptail* (*Lp*) causes CELSR1 to adopt a uniform distribution at the plasma membrane of basal layer epidermal cells instead of an asymmetric A-P pattern, supporting the idea that flamingo/CELSR1 and van gogh/Vangl2 are interdependent for their polarized distribution.

Mouse knockouts for CELSR1, CELSR2, and CELSR3 have been generated. Tissir *et al*. found that CELSR2$^{-/-}$ mice developed hydrocephalus as a result of perturbed planar organization of the coordinated motile cilia that direct fluid flow in the brain ventricles. These cilia are found on the apical surface of the ependymal cells that line the brain ventricles. The defect was even more pronounced in CELSR2/3 double mutant animals, leading to a fatal hydrocephalus. Similar to Devenport and Fuchs' report of CELSR1 in mouse epidermis (2008), CELSR2 mutant ependymal cells did not express

Fzd3 and Vangl2 in the wild-type polygonal pattern. Importantly, this defect was found not to be secondary to defective junctional organization, as the ZO-1 immunostaining pattern was preserved in mutant animals.

Additional phenotypes in vertebrates that are associated with mutant or knocked out CELSR, as well as other PCP molecules, include impaired convergent extension during gastrulation, neural tube closure, and eyelid closure (Curtin *et al*., 2003; Formstone & Mason, 2005). In these processes, planar cell polarity proteins including CELSR govern the coordinated movements of groups of cells that allow for tissue narrowing and lengthening during morphogenesis. The mechanism is hypothesized to be a more dynamic version of the events observed in more "static" epithelium, in which transient polarization and interactions between PCP proteins dictate appropriate cell intercalation.

From multiple cell and tissue types in multiple model organisms, the role of CELSR in the planar polarization of epithelial tissues is abundantly clear. Recent studies in other cell types have provided information on the *in vivo* roles of flamingo/CELSR in tissues that are not planar polarized, or those in which observing a phenomenon akin to planar cell polarity may be difficult due to the three-dimensional structure of the tissue.

Zhou *et al*. conditionally-deleted *celsr3* in mouse brain to study its role in the central nervous system, where all three *celsr* genes are abundantly expressed. Animals in which both *celsr3* alleles were deleted in the telencephalon (using *Foxg1-Cre*) lacked the anterior commissure (AC), a major axonal tract connecting the two cerebral hemispheres across the midline. This was also observed when *celsr3* was deleted from the neocortex using *Emx1-Cre*, but *celsr3* mRNA was still observed in so-called guidepost cells along

the AC, suggesting that CELSR3 activity is required cell-autonomously in the neurons that originate the AC. With respect to the internal capsule (IC), an axonal tract that runs between the cerebral cortex and medullary pyramids, CELSR3 was found to be required in both neurons and guidepost cells, consistent with the idea that it participates in homophilic interactions (Zhou *et al*., 2008).

Matsubara *et al*. studied the role of flamingo during sensory neuron development in *Drosophila*. The hypomorphic mutant allele fmi^{E86}, which expresses a flamingo protein that does not display normal polarization in wing epithelium, causes loss of the repulsion between dendritic branches that results in appropriate arborization of the dendritic "tree." Importantly, other members of the PCP pathway, such as van gogh, frizzled, and prickle, were also shown to participate in dendritic self-avoidance and genetically interact with flamingo with respect to this phenotype (Matsubara *et al*., 2011). These results are interesting because they suggest that signaling partners for flamingo are conserved beyond the single physiological context of epithelial planar cell polarity.

LATROPHILIN / LEC

The lectin-like latrophilins were originally described as cellular receptors for the main neurotoxin found in Black Widow spider (*Latrodectus mactans*), alpha-latrotoxin (α-LTX) (Krasnoperov *et al*., 1997). Studies have implicated them as modulators of neurotransmitter release, and they are thought to be components of the fusion machinery that regulates the discharge of biogenic amine vesicles (Südof, 2001; Capogna *et al*., 2003). Additionally, G-protein-dependent signaling has been demonstrated for latrophilin (see the section *G-protein-dependent signaling of latrophilin*, above).

Perhaps most relevant to our own studies on Eltd1 is recent work that describes *in vivo* studies detailing the contribution of latrophilin to embryonic development. Much like flamingo, latrophilin exhibits highly conserved domain architecture across invertebrate and vertebrate species (Nordström *et al*., 2009), possibly representing core functions of AdGPCRs that are highly conserved in the evolution of bilateral animals.

Langenhan et al. utilized the nematode *C. elegans* as a model system to study the role of latrophilin (*lat-1*) during early development. *C. elegans* exhibits an essentially invariant embryonic cell lineage resulting from a series of asymmetric cell divisions and intercellular induction events. The small number of cells and their precisely reproduced locations and interactions are regulated and coordinated tightly. This is well-established from the study of *C. elegans* mutants in various signaling pathways and experimental ablation of blastomeres using laser microbeam dissection (Sulston *et al*., 1983; Schnabel, 1997). The Wnt/ß-catenin pathway has been shown to be important for cell fate decisions during these early divisions while a noncanonical Wnt/Frizzled pathway is required for the orientation of mitotic spindles (Walston & Hardin, 2006; Mizumoto & Sawa, 2007).

The offspring of mutant *lat-1(ok1465)* homozygotes show severe defects in early embryonic development. Examination of early cell divisions revealed a specific and novel defect in the division plane of 8-cell *lat-1(ok1465)* embryos. ABal, the most anterior blastomere, exhibited a division plane perpendicular to the A-P axis in *lat-1* mutants, in contrast to wild-type embryos in which the division plane of ABal is along the A-P axis. The altered division plane of ABal changed the positions and neighboring cell contacts of its daughter cells ABala and ABalp. This observation suggested that A-P

tissue polarity is affected by *lat-1* mutation (Langenhan *et al*., 2009). A posterior signaling center is thought to arise from the descendants of the P1 blastomere, producing a Wnt-dependent relay signal to orient the cleavage planes of the embryo relative to the A-P axis (Bischoff & Schnabel, 2006). It is possible that latrophilin is a component of the propagation machinery that translates either a Wnt-dependent, or –independent, signal into ABal spindle orientation in the developing *C. elegans* embryo.

The lectin-like RBL domain, a defining feature of the latrophilins, was required for all functions of *lat-1* in *C. elegans* (Langenhan *et al*., 2009). This was in contrast to results reported for flamingo in which deletion of most of the extracellular domain resulted in a protein with some activity during sensory axon advance (Steinel & Whitington, 2009), supporting a model in which an extracellular interaction results in an "outside-in" signal for latrophilin during *C. elegans* early morphogenesis.

Prömel *et al*. followed up the previous study by Langenhan *et al*. with a detailed structure-function analysis of LAT-1 in the context of the embryonic lethality (tissue polarity) and fertility phenotypes previously described for *lat-1(ok1465)* mutants. Intriguingly, the 7TM and extracellular domains were found to have different activities; mutants lacking the 7TM rescued the fertility defect but not the tissue polarity defect of *lat-1(ok1465)* mutants. This *in vivo* 7TM-independent function of LAT-1 supports several models that attempt to describe AdGPCR function, including the "split personality" model which suggests that GPS cleavage may allow ectodomains to interact with 7TMs of other AdGPCRs. However, Prömel *et al*. found that GPS proteolytic cleavage was dispensable for LAT-1 function, as cleavage-site mutant alleles abolishing

the autocatalytic cleavage but not surface expression of LAT-1 (H528A and T530A) were able to rescue defects in *lat-1* mutants.

A proposed ligand of latrophilin-1, Lasso/teneurin-2, was isolated from rat brain (Silva *et al*., 2011). A mutant null allele of the nematode homolog, *ten-1(ok461)*, was also studied by Prömel *et al*. Interestingly, they found that while *ten-1(ok461)* homozygotes phenocopied the *lat-1(ok1465)* mutants, double mutants exhibited a more severe phenotype. The two mutant alleles also displayed nonallelic non-complementation, indicating the two genes are acting at least partly in parallel. This led the authors to speculate that LAT-1 and TEN-1 may be functioning as co-receptors for an as-of-yet unidentified ligand as opposed to a receptor-ligand pair.

In sum, the studies on nematode latrophilin reveal a vital role for this receptor in the establishment of early anterior-posterior tissue polarity in *C. elegans*, reminiscent of the functions established for flamingo/CELSR in planar cell polarity. Both flamingo and latrophilin also exhibit roles in both early tissue polarity and in regulating various aspects of CNS development and function. In part, the ability of LAT-1 to adopt distinct 7TM-dependent and –independent functions explains how these seemingly unrelated activities may arise for both receptors. However, unlike flamingo, interactions with the Wnt/Frizzled signaling pathway have not been described for latrophilin.

GPR126

Monk and colleagues utilized a genetic screen in zebrafish to search for genes involved in the regulation of myelination in the developing peripheral nervous system. Two mutants, *st49* and *st63*, were found to lack myelin basic protein (Mbp) in peripheral

nerves. The mutations mapped to *GPR126*, one truncating the protein before the GPS and the other changing a highly conserved cysteine residue to a tyrosine in the 7TM. A splice-blocking morpholino phenocopied the mutants. Promyelinating Schwann cells in *GPR126* mutants seemed to adhere normally to peripheral nerve axons but produced a much smaller number of myelin wraps around the axons compared to wild-type embryos or mutant embryos with transplanted wild-type Schwann cells. The mutant Schwann cells arrested at the promyelination stage as determined by the lack of expression of transcriptional markers *krox20* and *oct6*, but could be differentiated by the elevation of cAMP levels via forskolin treatment (Monk *et al*., 2009). These results suggest that GPR126 on Schwann cells initiates myelination by elevating cAMP levels in response to some unknown cue. Additionally, the role of GPR126 in peripheral nerve myelination is conserved in mice, as *GPR126*$^{-/-}$ embryos, which die during mid-gestation due to cardiovascular failure (Waller-Evans *et al*., 2010), exhibit very similar Schwann cell defects to the zebrafish mutants (Monk *et al*., 2011). It is tempting to speculate that GPR126 binds an as-of-yet unidentified axonal or extracellular matrix ligand that directs the promyelinating Schwann cell to fully differentiate.

CD97

CD97 is capable of binding two distinct ligands depending on the splice variance. Splice variants with EGF domain 4 bind chondroitin sulfate (Stacey *et al*., 2003), while the presence of EGF domains 1, 2, and 5 confers binding specificity to CD55, as described above.

The observation that CD97 overexpression in HT1080 fibrosarcoma cells stimulates single cell motility and promotes invasive growth in a tumor model led to the development of a CD97-overexpressing transgenic mouse to test the hypothesis that CD97 may affect colorectal carcinogenesis (Becker *et al*., 2010). CD97 was constitutively overexpressed in intestinal epithelial cells (Tg(villin-CD97)). Unexpectedly, the authors found that CD97-overexpressing animals were less susceptible to dextran sodium sulfate (DSS)-induced injury and tumorigenesis in a transgene copy number-dependent manner. Ultrastructural examination revealed that adherens junctions between intestinal epithelial cells were strengthened in Tg(villin-CD97) mice and weakened in $CD97^{-/-}$ mice as compared to wild-type. Further, the amount of membrane-associated ß-catenin was increased in CD97-overexpressing mice, as were phospho-GSK-3ß and phospho-Akt, indicating inhibition of the ß-catenin degradation complex occurred as a result of CD97 overexpression. A potential ligand for CD97 in this context was not identified, nor was an immediate downstream signaling transducer that leads to ß-catenin protection. Further studies on the role of CD97 during early intestinal epithelial development, when contacts between epithelial cells are initially made, may help to clarify the mechanism by which this AdGPCR regulates adherens junction formation.

VLGR1

VLGR1 is the largest member of the Adhesion GPCR family, spanning approximately 6,300 amino acids in length in mouse and human. The largest splice variant, VLGR1b, contains an ectodomain notable for the presence of thirty-five Calx-ß repeats, a calcium-binding domain found in Na^{+}/Ca^{2+} exchangers. The protein also

contains a single pentraxin domain and an epilepsy-associated repeat (EAR), which is found on another family of secreted proteins often mutated in one particular form of human epilepsy (McMillan & White, 2011). The highest expression levels of *VLGR1* in mouse are observed in the developing central nervous system (CNS) during embryogenesis (McMillan *et al*., 2002; Yagi *et al*., 2005).

Four *VLGR1* mutant mouse lines have been studied – two early truncation mutants, a knock-out, and a knock-in expressing a tagged, 7TM-less version of the receptor. While no defects in brain development have been detected in any of the lines, all four develop susceptibility to audiogenic seizures and an early onset, progressive hearing impairment (Skradski *et al*., 1998; Zheng *et al*., 1996; Klein *et al*., 2005; Mcgee *et al*., 2006). VLGR1 protein has been localized to the base of cochlear hair cells by immunofluorescence microscopy until 10 days of age in perinatal mice, the approximate time period during which inner ear development proceeds. Stereociliary ankle links, transient thin filaments forming a mesh-like structure connecting the bases of adjacent stereocilia, are absent in mice with *VLGR1* mutations. Additionally, hair cell bundles in *VLGR1* mutant mice become progressively disorganized (McGee *et al*., 2006; Yagi *et al*., 2007; Michalski *et al*., 2007). The mechanism by which VLGR1 contributes to stereociliary ankle link formation and hair cell bundle organization is not well-understood, but homotypic interactions are one possibility given the predicted distance the extracellular domain of VLGR1 would be able to span (180 nm) and the 150 nm gap between adjacent stereocilia (McMillan *et al*., 2002; McGee *et al*., 2006). Alternatively, VLGR1 may participate in heterophilic interactions with other proteins believed to be components of the ankle link complex, such as usherin (Adato *et al*., 2005).

An important observation that stems from the body of work on *VLGR1* mouse mutants is that different spice variants of *VLGR1* appear to have distinct roles *in vivo*. VLGR1a has a significantly shorter extracellular N-terminus than VLGR1b and the pentraxin domain and twenty-six Calx-ß repeats are missing. These domains seem to be important for normal auditory development as VLGR1b is the only splice variant that is affected in all four *VLGR1* mouse mutants. It can be inferred from this that it is the isoform with the most vital role in the development and maintenance of normal hearing (McMillan & White, 2011).

Like GPR56, VLGR1 represents another AdGPCR in which mutations are a known cause of human disease. VLGR1 mutations result in Usher Syndrome type 2C, a commonly diagnosed cause of human deaf-blindness with symptoms including moderate to severe hearing loss, normal vestibular function, and late onset retinitis pigmentosa (RP). The clinical symptoms are phenocopied quite well by the mouse mutants, with the exception of RP; despite VLGR1 expression in the mouse retina, the mutants have no gross retinal defects (McGee *et al*., 2006; Maerker *et al*., 2008). As with the mouse, an analysis of the 14 known human mutations in *VLGR1* suggests that the full-length isoform, VLGR1b, is the variant required for normal auditory function. Additionally, two mutations found in the 100 amino acid C-terminus highlight the importance of this region of VLGR1. Indeed, several studies have demonstrated a direct physical interaction between the C-terminus of VLGR1, which contains a PDZ domain, and cytoplasmic PDZ-containing scaffolding proteins *in vitro* (Reiners *et al*., 2005; Adato *et al*., 2005; van Wijk *et al*., 2006). However, no direct associations with the eight other Usher Syndrome proteins cloned so far have been observed for VLGR1.

HE6

Human epididymis-specific protein 6 (HE6/GPR64) is an AdGPCR with high expression in the proximal epididymis and efferent ductules. To study the possible role of HE6 in male fertility, one group generated a transgenic mouse in which the 7TM region of HE6 was deleted (Davies *et al*., 2004). The hemizygous mutant male mice exhibit an age-dependent infertility that was nearly complete by the age of 15 weeks, and showed reduced spermatozoa counts. Histological examination revealed dilated efferent ductules with lumens frequently blocked by large accumulations of spermatozoa. A buildup of fluid was also observed in the testes of mutant mice, with reduced spermatogenesis in many of the seminiferous tubules. The authors found that these defects preceded the production of spermatozoa, as 2 week-old mutant mice already exhibited an enlarged rete testis, which led them to hypothesize that HE6 controls fluid reabsorption in the male reproductive tract. HE6 regulation of fluid reabsorption likely involves interactions with the actin cytoskeleton. It was found to co-localize to F-actin-containing microvilli and subapical actin cytoskeleton. Additionally, Yeast-2-Hybrid screening led to the cloning and characterization of a profilin-like protein that can bind the C-terminus of HE6 (Kirchhoff *et al*., 2006). These findings begin to offer glimpses of a mechanism by which HE6 may contribute to male reproductive tract function. Taking cues from other AdGPCRs, it is possible that defects in the oriented cell division of efferent duct epithelium (i.e., planar cell polarity, as for CELSR) or integrity of cell-cell contacts (as for CD97 in intestinal homeostasis) are at the root of the dilation phenotype observed in HE6 mutant mice.

GPR124

GPR124 was first identified as a cell-surface protein upregulated in tumor endothelium (St. Croix *et al*., 2000; Carson-Walter *et al*., 2001). Kuhnert and colleagues found that in mouse embryos, GPR124 was expressed in endothelial cells and pericytes, mostly strongly in the brain and neural tube, and in certain non-vascular tissues such as lung and esophageal epithelium. In adult mice, expression was exclusively vascular. In order to study the role of GPR124 in angiogenesis, a global *gpr124* knockout mouse was generated. *Gpr124*$^{-/-}$ embryos exhibited a completely penetrant, progressive cerebral hemorrhage and embryonic lethality from E15.5 onward. Angiogenic sprouting into the forebrain was reduced as part of an overall CNS vascular patterning defect, with *Gpr124*$^{-/-}$ endothelial cells showing markedly reduced or absent filopodia. Interestingly, the angiogenic defect was confined to the forebrain and neural tube, as the diencephalon, midbrain, and hindbrain, as well as non-neural tissues, were vascularized normally. This phenotype was reproduced in endothelial-specific knockouts using a floxed *gpr124* allele and both *Tie2-Cre* and *PDGFß-Cre* mouse lines, establishing the endothelial cell-autonomy of the angiogenic defect. A gain-of-function transgenic mouse overexpressing GPR124 in endothelial cells was also generated and displayed a brain-specific vascular phenotype characterized by focal areas of hypervascularity.

Finally, the authors utilized bEND3 cells, a brain endothelial cell line which expresses GPR124, to test cell migration in response to chemoattractive gradients. GPR124-overexpressing bEND3 cells migrated towards a gradient of conditioned medium from E12.5 forebrain cortical cells, and this migration was abrogated by short

hairpin RNA (shRNA) against GPR124 (Kuhnert *et al*., 2010). In sum, these results suggest GPR124 regulates CNS endothelial cell migration in response to a soluble ligand produced by forebrain cortical cells, but do not rule out membrane-bound or extracellular matrix ligand involvement in GPR124 function *in vivo*. The role of GPR124 in CNS angiogenesis reported by Kuhnert and colleagues was corroborated by two additional independent groups (Anderson *et al*., 2011; Cullen *et al*., 2011).

Introduction to Eltd1

Eltd1 is a member of Group I of the AdGPCRs, phylogenetically classified with the latrophilins on the basis of transmembrane domain homology. However, its extracellular domain much more closely resembles the Group II Adhesion GPCRs, which include the leukocyte receptors EMR1-4 and CD97. The ~475 amino acid extracellular domain of Eltd1 is notable for two calcium-binding EGF domains and one EGF-like domain, followed by the "stalk" region and GPS motif. As reported for latrophilin and BAI3, it is likely that the stalk and GPS motif together are part of the larger GAIN domain.

When we began our line of experimentation on Eltd1 in 2009, very little was published on this receptor. Only Nechiporuk *et al*. had reported studies on Eltd1 (2001), naming the protein ETL (for EGF-TM7-latrophilin-related protein). They identified Eltd1 in a screen for mRNAs that were differentially expressed during postnatal heart development in rat cardiomyocytes. Eltd1 was upregulated 4.9-fold by postnatal day 12 as compared to embryonic day 16. A similar finding was made in human hearts.

In COS-7 cells, myc-tagged rEltd1 was found to possibly dimerize, showing 85 kDa and 175 kDa bands on Western blot analysis. Additionally, the protein was detected both in 85-kDa and 35-kDa forms when sample and gel buffers contained 8M urea, likely the result of GPS proteolytic cleavage. Using a Fc-tagged extracellular domain of Eltd1, the authors also showed that dimerization of the receptor required the transmembrane region. Finally, expression of rEltd1 was demonstrated by *in situ* hybridization in cardiomyocytes, vascular smooth muscle in coronary and lung blood vessels, and bronchiolar smooth muscle (Nechiporuk *et al*., 2001). These results formed the initial characterization of Eltd1.

In a study aiming to identify the core transcriptome of endothelial cells, Eltd1 was found to be one of 58 genes with broad and specific expression in microvascular endothelium (Wallgard *et al*., 2008). Coupled with data from Nechiporuk *et al*., it is clear that Eltd1 is widely expressed throughout the cardiovascular system, making it a worthy candidate for our laboratory to investigate.

We set out to determine the physiological roles of Eltd1 in the cardiovascular system using morpholino-mediated gene knockdown in zebrafish. In Chapter 2, we discuss somewhat unexpected early developmental phenotypes in *eltd1* morphants. We show that *eltd1* morphants exhibit left-right asymmetry defects that localize to Kupffer's vesicle, establishing the requirement for Eltd1 in the formation of this organ. Further, we demonstrate perturbed nodal flow as the cause of this defect, suggesting a role for Eltd1 in the development or organization of motile cilia within Kupffer's vesicle.

In Chapter 3, we describe cardiovascular phenotypes in *eltd1* morphants. Consistent with reported expression patterns, we found *eltd1* morphants to exhibit signs

of cardiovascular failure by 48 hours post-fertilization (hpf). *Eltd1* morphants display defective angiogenesis of several vessels as early as 24 hpf, possibly one contributing factor to their cardiovascular collapse.

References

1. Abbott, R. J. M. *et al.* Structural and functional characterization of a novel T cell receptor co-regulatory protein complex, CD97-CD55. *J Biol Chem* **282,** 22023–22032 (2007).

2. Abe, J., Suzuki, H., Notoya, M., Yamamoto, T. & Hirose, S. Ig-hepta, a novel member of the G protein-coupled hepta-helical receptor (GPCR) family that has immunoglobulin-like repeats in a long N-terminal extracellular domain and defines a new subfamily of GPCRs. *J Biol Chem* **274,** 19957–19964 (1999).

3. Abe, J., Fukuzawa, T. & Hirose, S. Cleavage of Ig-Hepta at a 'SEA' module and at a conserved G protein-coupled receptor proteolytic site. *J Biol Chem* **277,** 23391–23398 (2002).

4. Adato, A. *et al.* Interactions in the network of Usher syndrome type 1 proteins. *Hum Mol Genet* **14,** 347–356 (2005).

5. Anderson, K. D. *et al.* Angiogenic sprouting into neural tissue requires Gpr124, an orphan G protein-coupled receptor. *Proceedings of the National Academy of Sciences* **108,** 2807–2812 (2011).

6. Araç, D. *et al.* A novel evolutionarily conserved domain of cell-adhesion GPCRs mediates autoproteolysis. *EMBO J* **31,** 1364–1378 (2012).

7. Ashton, A. C. *et al.* alpha-Latrotoxin, acting via two Ca2+-dependent pathways, triggers exocytosis of two pools of synaptic vesicles. *J Biol Chem* **276,** 44695–44703 (2001).

8. Attwood, T. K. & Findlay, J. B. Design of a discriminating fingerprint for G-protein-coupled receptors. *Protein Eng.* **6,** 167–176 (1993).

9. Beall, S. A., Boekelheide, K. & Johnson, K. J. Hybrid GPCR/cadherin (Celsr) proteins in rat testis are expressed with cell type specificity and exhibit differential Sertoli cell-germ cell adhesion activity. *J. Androl.* **26,** 529–538 (2005).

10. Becker, S. *et al.* Overexpression of CD97 in intestinal epithelial cells of transgenic mice attenuates colitis by strengthening adherens junctions. *PLoS ONE* **5,** e8507 (2010).

11. Bischoff, M. & Schnabel, R. A posterior centre establishes and maintains polarity of the Caenorhabditis elegans embryo by a Wnt-dependent relay mechanism. *PLoS Biol.* **4,** e396 (2006).

12. Bjarnadóttir, T. K., Fredriksson, R. & Schiöth, H. B. The adhesion GPCRs: a unique family of G protein-coupled receptors with important roles in both central and peripheral tissues. *Cell Mol Life Sci* **64,** 2104–2119 (2007).

13. Bjarnadóttir, T. K. *et al.* Identification of novel splice variants of Adhesion G protein-coupled receptors. *Gene* **387,** 38–48 (2007).

14. Bjarnadóttir, T. K. *et al.* The human and mouse repertoire of the adhesion family of G-protein-coupled receptors. *Genomics* **84,** 23–33 (2004).

15. Brannigan, J. A. *et al.* A protein catalytic framework with an N-terminal nucleophile is capable of self-activation. *Nature* **378,** 416–419 (1995).

16. Capogna, M., Volynski, K. E., Emptage, N. J. & Ushkaryov, Y. A. The alpha-latrotoxin mutant LTXN4C enhances spontaneous and evoked transmitter release in CA3 pyramidal neurons. *J Neurosci* **23,** 4044–4053 (2003).

17. Carson-Walter, E. B. *et al.* Cell surface tumor endothelial markers are conserved in mice and humans. *Cancer Res.* **61,** 6649–6655 (2001).

18. Chang, G.-W. *et al.* Proteolytic cleavage of the EMR2 receptor requires both the extracellular stalk and the GPS motif. *FEBS Lett* **547,** 145–150 (2003).

19. Chen, W.-S. *et al.* Asymmetric homotypic interactions of the atypical cadherin flamingo mediate intercellular polarity signaling. *Cell* **133,** 1093–1105 (2008).

20. Chung, D. A. *et al.* Mutagenesis and peptide analysis of the DRY motif in the alpha2A adrenergic receptor: evidence for alternate mechanisms in G protein-coupled receptors. *Biochem Biophys Res Commun* **293,** 1233–1241 (2002).

21. Clapham, D. E. & Neer, E. J. G protein beta gamma subunits. *Annu. Rev. Pharmacol. Toxicol.* **37,** 167–203 (1997).

22. Cullen, M. *et al.* GPR124, an orphan G protein-coupled receptor, is required for CNS-specific vascularization and establishment of the blood-brain barrier. *Proceedings of the National Academy of Sciences* **108,** 5759–5764 (2011).

23. Curtin, J. A. *et al.* Mutation of Celsr1 disrupts planar polarity of inner ear hair cells and causes severe neural tube defects in the mouse. *Curr Biol* **13,** 1129–1133 (2003).

24. Davies, B. *et al.* Targeted deletion of the epididymal receptor HE6 results in fluid dysregulation and male infertility. *Mol Cell Biol* **24,** 8642–8648 (2004).

25. Davletov, B. A. *et al.* Vesicle exocytosis stimulated by alpha-latrotoxin is mediated by latrophilin and requires both external and stored Ca2+. *EMBO J* **17,** 3909–3920 (1998).

26. Devenport, D. & Fuchs, E. Planar polarization in embryonic epidermis orchestrates global asymmetric morphogenesis of hair follicles. *Nat Cell Biol* **10,** 1257–1268 (2008).

27. Flower, D. R. Modelling G-protein-coupled receptors for drug design. *Biochim Biophys Acta* **1422,** 207–234 (1999).

28. Formstone, C. J. & Mason, I. Combinatorial activity of Flamingo proteins directs convergence and extension within the early zebrafish embryo via the planar cell polarity pathway. *Dev Biol* **282,** 320–335 (2005).

29. Fredriksson, R., Lagerström, M. C., Lundin, L.-G. & Schiöth, H. B. The G-

protein-coupled receptors in the human genome form five main families. Phylogenetic analysis, paralogon groups, and fingerprints. *Mol. Pharmacol.* **63,** 1256–1272 (2003).

30. Gether, U. Uncovering molecular mechanisms involved in activation of G protein-coupled receptors. *Endocr Rev* **21,** 90–113 (2000).

31. Gray, J. X. *et al.* CD97 is a processed, seven-transmembrane, heterodimeric receptor associated with inflammation. *J Immunol* **157,** 5438–5447 (1996).

32. Gray, R. S., Roszko, I. & Solnica-Krezel, L. Planar cell polarity: coordinating morphogenetic cell behaviors with embryonic polarity. *Dev Cell* **21,** 120–133 (2011).

33. Hamann, J. *et al.* Characterization of the CD55 (DAF)-binding site on the seven-span transmembrane receptor CD97. *Eur. J. Immunol.* **28,** 1701–1707 (1998).

34. Hamann, J., Vogel, B., van Schijndel, G. M. & van Lier, R. A. The seven-span transmembrane receptor CD97 has a cellular ligand (CD55, DAF). *J Exp Med* **184,** 1185–1189 (1996).

35. Hamann, J. *et al.* EMR1, the human homolog of F4/80, is an eosinophil-specific receptor. *Eur. J. Immunol.* **37,** 2797–2802 (2007).

36. Holland, P. W., Garcia-Fernàndez, J., Williams, N. A. & Sidow, A. Gene duplications and the origins of vertebrate development. *Dev. Suppl.* 125–133 (1994).

37. Hughes, J. *et al.* The polycystic kidney disease 1 (PKD1) gene encodes a novel protein with multiple cell recognition domains. *Nat Genet* **10,** 151–160 (1995).

38. Iguchi, T. *et al.* Orphan G protein-coupled receptor GPR56 regulates neural progenitor cell migration via a G alpha 12/13 and Rho pathway. *J Biol Chem* **283,** 14469–14478 (2008).

39. Ito, J. *et al.* Anatomical and histological profiling of orphan G-protein-coupled receptor expression in gastrointestinal tract of C57BL/6J mice. *Cell Tissue Res.* **338,** 257–269 (2009).

40. Kirchhoff, C., Obermann, H., Behnen, M. & Davies, B. Role of epididymal receptor HE6 in the regulation of sperm microenvironment. *Mol. Cell. Endocrinol.* **250,** 43–48 (2006).

41. Klein, B. D., Fu, Y.-H., Ptacek, L. J. & White, H. S. Auditory deficits associated with the frings mgr1 (mass1) mutation in mice. *Dev. Neurosci.* **27,** 321–332 (2005).

42. Kolakowski, L. F. GCRDb: a G-protein-coupled receptor database. *Recept. Channels* **2,** 1–7 (1994).

43. Krasnoperov, V., Bittner, M. A., Holz, R. W., Chepurny, O. & Petrenko, A. G. Structural requirements for alpha-latrotoxin binding and alpha-latrotoxin-stimulated secretion. A study with calcium-independent receptor of alpha-latrotoxin (CIRL) deletion mutants. *J Biol Chem* **274,** 3590–3596 (1999).

44. Krasnoperov, V. G. *et al.* alpha-Latrotoxin stimulates exocytosis by the interaction with a neuronal G-protein-coupled receptor. *Neuron* **18,** 925–937 (1997).

45. Kuhnert, F. *et al.* Essential regulation of CNS angiogenesis by the orphan G protein-coupled receptor GPR124. *Science* **330,** 985–989 (2010).

46. Lagerström, M. C. & Schiöth, H. B. Structural diversity of G protein-coupled receptors and significance for drug discovery. *Nature reviews Drug discovery* **7,** 339–357 (2008).

47. Lagerström, M. C. *et al.* The evolutionary history and tissue mapping of GPR123: specific CNS expression pattern predominantly in thalamic nuclei and regions containing large pyramidal cells. *J. Neurochem.* **100,** 1129–1142 (2007).

48. Langenhan, T. *et al.* Latrophilin signaling links anterior-posterior tissue polarity and oriented cell divisions in the C. elegans embryo. *Dev Cell* **17,** 494–504 (2009).

49. Lelianova, V. G. *et al.* Alpha-latrotoxin receptor, latrophilin, is a novel member of the secretin family of G protein-coupled receptors. *J Biol Chem* **272,** 21504–21508 (1997).

50. Lin, H.-H. *et al.* Autocatalytic cleavage of the EMR2 receptor occurs at a conserved G protein-coupled receptor proteolytic site motif. *J Biol Chem* **279,** 31823–31832 (2004).

51. LopezJimenez, N. D. *et al.* Two novel genes, Gpr113, which encodes a family 2 G-protein-coupled receptor, and Trcg1, are selectively expressed in taste receptor cells. *Genomics* **85,** 472–482 (2005).

52. Lundin, L. G. Evolution of the vertebrate genome as reflected in paralogous chromosomal regions in man and the house mouse. *Genomics* **16,** 1–19 (1993).

53. Luo, R., Jin, Z., Deng, Y., Strokes, N. & Piao, X. Disease-associated mutations prevent GPR56-collagen III interaction. *PLoS ONE* **7,** e29818 (2012).

54. Luo, R. *et al.* G protein-coupled receptor 56 and collagen III, a receptor-ligand pair, regulates cortical development and lamination. *Proceedings of the National Academy of Sciences* **108,** 12925–12930 (2011).

55. Maerker, T. *et al.* A novel Usher protein network at the periciliary reloading point between molecular transport machineries in vertebrate photoreceptor cells. *Hum Mol Genet* **17,** 71–86 (2008).

56. Matsubara, D., Horiuchi, S.-Y., Shimono, K., Usui, T. & Uemura, T. The seven-pass transmembrane cadherin Flamingo controls dendritic self-avoidance via its binding to a LIM domain protein, Espinas, in Drosophila sensory neurons. *Genes Dev* **25,** 1982–1996 (2011).

57. Matsushita, H., Lelianova, V. G. & Ushkaryov, Y. A. The latrophilin family: multiply spliced G protein-coupled receptors with differential tissue distribution. *FEBS Lett* **443,** 348–352 (1999).

58. McGee, J. *et al.* The very large G-protein-coupled receptor VLGR1: a component of the ankle link complex required for the normal development of auditory hair bundles. *J Neurosci* **26,** 6543–6553 (2006).

59. McMillan, D. R. & White, P. C. Studies on the very large g protein-coupled receptor: from initial discovery to determining its role in sensorineural deafness in higher animals. *Adv. Exp. Med. Biol.* **706,** 76–86 (2011).

60. McMillan, D. R., Kayes-Wandover, K. M., Richardson, J. A. & White, P. C. Very large G protein-coupled receptor-1, the largest known cell surface protein, is highly expressed in the developing central nervous system. *J Biol Chem* **277,** 785–792 (2002).

61. McNeill, H. Planar cell polarity: keeping hairs straight is not so simple. *Cold Spring Harb Perspect Biol* **2,** a003376 (2010).

62. Michalski, N. *et al.* Molecular characterization of the ankle-link complex in cochlear hair cells and its role in the hair bundle functioning. *J Neurosci* **27,** 6478–6488 (2007).

63. Mizumoto, K. & Sawa, H. Two betas or not two betas: regulation of asymmetric division by beta-catenin. *Trends Cell Biol* **17,** 465–473 (2007).

64. Monk, K. R., Oshima, K., Jörs, S., Heller, S. & Talbot, W. S. Gpr126 is essential for peripheral nerve development and myelination in mammals. *Development* **138,** 2673–2680 (2011).

65. Monk, K. R. *et al.* A G protein-coupled receptor is essential for Schwann cells to initiate myelination. *Science* **325,** 1402–1405 (2009).

66. Moriguchi, T. *et al.* DREG, a developmentally regulated G protein-coupled receptor containing two conserved proteolytic cleavage sites. *Genes Cells* **9,** 549–560 (2004).

67. Nauli, S. M. & Zhou, J. Polycystins and mechanosensation in renal and nodal cilia. *Bioessays* **26,** 844–856 (2004).

68. Nauli, S. M. *et al.* Polycystins 1 and 2 mediate mechanosensation in the primary cilium of kidney cells. *Nat Genet* **33,** 129–137 (2003).

69. Nechiporuk, T., Urness, L. D. & Keating, M. T. ETL, a novel seven-transmembrane receptor that is developmentally regulated in the heart. ETL is a member of the secretin family and belongs to the epidermal growth factor-seven-transmembrane subfamily. *J Biol Chem* **276,** 4150–4157 (2001).

70. Nordström, K. J. V., Lagerström, M. C., Wallér, L. M. J., Fredriksson, R. & Schiöth, H. B. The Secretin GPCRs descended from the family of Adhesion GPCRs. *Mol. Biol. Evol.* **26,** 71–84 (2009).

71. Paavola, K. J., Stephenson, J. R., Ritter, S. L., Alter, S. P. & Hall, R. A. The N terminus of the adhesion G protein-coupled receptor GPR56 controls receptor signaling activity. *Journal of Biological Chemistry* **286,** 28914–28921 (2011).

72. Palczewski, K. *et al.* Crystal structure of rhodopsin: A G protein-coupled

receptor. *Science* **289,** 739–745 (2000).

73. Park, D. *et al.* BAI1 is an engulfment receptor for apoptotic cells upstream of the ELMO/Dock180/Rac module. *Nature* **450,** 430–434 (2007).

74. Peng, Y.-M. *et al.* Specific expression of GPR56 by human cytotoxic lymphocytes. *J Leukoc Biol* **90,** 735–740 (2011).

75. Perler, F. B., Xu, M. Q. & Paulus, H. Protein splicing and autoproteolysis mechanisms. *Curr Opin Chem Biol* **1,** 292–299 (1997).

76. Piao, X. *et al.* G protein-coupled receptor-dependent development of human frontal cortex. *Science* **303,** 2033–2036 (2004).

77. Pickering, C. *et al.* The Adhesion GPCR GPR125 is specifically expressed in the choroid plexus and is upregulated following brain injury. *BMC Neurosci* **9,** 97 (2008).

78. Prömel, S. *et al.* Characterization and functional study of a cluster of four highly conserved orphan adhesion-GPCR in mouse. *Dev Dyn* **241,** 1591–1602 (2012).

79. Qian, F., Wei, W., Germino, G. & Oberhauser, A. The nanomechanics of polycystin-1 extracellular region. *J Biol Chem* **280,** 40723–40730 (2005).

80. Qian, F. *et al.* Cleavage of polycystin-1 requires the receptor for egg jelly domain and is disrupted by human autosomal-dominant polycystic kidney disease 1-associated mutations. *Proc Natl Acad Sci USA* **99,** 16981–16986 (2002).

81. Rahman, M. A. *et al.* Norepinephrine exocytosis stimulated by alpha-latrotoxin

requires both external and stored Ca2+ and is mediated by latrophilin, G proteins and phospholipase C. *Philos Trans R Soc Lond, B, Biol Sci* **354,** 379–386 (1999).

82. Reiners, J. *et al.* Scaffold protein harmonin (USH1C) provides molecular links between Usher syndrome type 1 and type 2. *Hum Mol Genet* **14,** 3933–3943 (2005).

83. Rohatgi, R. *et al.* Mechanoregulation of intracellular Ca2+ in human autosomal recessive polycystic kidney disease cyst-lining renal epithelial cells. *Am J Physiol Renal Physiol* **294,** F890–9 (2008).

84. Schiöth, H. B., Nordström, K. J. V. & Fredriksson, R. The Adhesion GPCRs; Gene Repertoire, Phylogeny and Evolution. *Adv. Exp. Med. Biol.* **706,** 1–13 (2011).

85. Schnabel, R. Why does a nematode have an invariant cell lineage? *Semin Cell Dev Biol* **8,** 341–349 (1997).

86. Seandel, M. *et al.* Niche players: spermatogonial progenitors marked by GPR125. *Cell Cycle* **7,** 135–140 (2008).

87. Shima, Y., Kengaku, M., Hirano, T., Takeichi, M. & Uemura, T. Regulation of dendritic maintenance and growth by a mammalian 7-pass transmembrane cadherin. *Dev Cell* **7,** 205–216 (2004).

88. Shiratsuchi, T. *et al.* Cloning and characterization of BAI-associated protein 1: a PDZ domain-containing protein that interacts with BAI1. *Biochem Biophys Res*

Commun **247,** 597–604 (1998).

89. Shiratsuchi, T., Nishimori, H., Ichise, H., Nakamura, Y. & Tokino, T. Cloning and characterization of BAI2 and BAI3, novel genes homologous to brain-specific angiogenesis inhibitor 1 (BAI1). *Cytogenet. Cell Genet.* **79,** 103–108 (1997).

90. Silva, J.-P. *et al.* Latrophilin 1 and its endogenous ligand Lasso/teneurin-2 form a high-affinity transsynaptic receptor pair with signaling capabilities. *Proceedings of the National Academy of Sciences* **108,** 12113–12118 (2011).

91. Silva, J.-P., Lelianova, V., Hopkins, C., Volynski, K. E. & Ushkaryov, Y. Functional cross-interaction of the fragments produced by the cleavage of distinct adhesion G-protein-coupled receptors. *J Biol Chem* **284,** 6495–6506 (2009).

92. Skradski, S. L., White, H. S. & Ptácek, L. J. Genetic mapping of a locus (mass1) causing audiogenic seizures in mice. *Genomics* **49,** 188–192 (1998).

93. St Croix, B. *et al.* Genes expressed in human tumor endothelium. *Science* **289,** 1197–1202 (2000).

94. Stacey, M., Lin, H. H., Hilyard, K. L., Gordon, S. & McKnight, A. J. Human epidermal growth factor (EGF) module-containing mucin-like hormone receptor 3 is a new member of the EGF-TM7 family that recognizes a ligand on human macrophages and activated neutrophils. *J Biol Chem* **276,** 18863–18870 (2001).

95. Stacey, M. *et al.* The epidermal growth factor-like domains of the human EMR2 receptor mediate cell attachment through chondroitin sulfate glycosaminoglycans. *Blood* **102,** 2916–2924 (2003).

96. Stacey, M. *et al.* EMR4, a novel epidermal growth factor (EGF)-TM7 molecule up-regulated in activated mouse macrophages, binds to a putative cellular ligand on B lymphoma cell line A20. *J Biol Chem* **277,** 29283–29293 (2002).

97. Stehlik, C., Kroismayr, R., Dorfleutner, A., Binder, B. R. & Lipp, J. VIGR--a novel inducible adhesion family G-protein coupled receptor in endothelial cells. *FEBS Lett* **569,** 149–155 (2004).

98. Steinel, M. C. & Whitington, P. M. The atypical cadherin Flamingo is required for sensory axon advance beyond intermediate target cells. *Dev Biol* **327,** 447–457 (2009).

99. Südhof, T. C. alpha-Latrotoxin and its receptors: neurexins and CIRL/latrophilins. *Annu. Rev. Neurosci.* **24,** 933–962 (2001).

100. Sulston, J. E., Schierenberg, E., White, J. G. & Thomson, J. N. The embryonic cell lineage of the nematode Caenorhabditis elegans. *Dev Biol* **100,** 64–119 (1983).

101. Tissir, F. *et al.* Lack of cadherins Celsr2 and Celsr3 impairs ependymal ciliogenesis, leading to fatal hydrocephalus. *Nature Neuroscience* **13,** 700–707 (2010).

102. Tsiokas, L., Kim, S. & Ong, E.-C. Cell biology of polycystin-2. *Cell Signal* **19,** 444–453 (2007).

103. Usui, T. *et al.* Flamingo, a seven-pass transmembrane cadherin, regulates planar cell polarity under the control of Frizzled. *Cell* **98,** 585–595 (1999).

104. Vallon, M., Aubele, P., Janssen, K.-P. & Essler, M. Thrombin-induced shedding of tumour endothelial marker 5 and exposure of its RGD motif are regulated by cell-surface protein disulfide-isomerase. *Biochem. J.* **441,** 937–944 (2012).

105. Vanti, W. B. *et al.* Novel human G-protein-coupled receptors. *Biochem Biophys Res Commun* **305,** 67–71 (2003).

106. Volynski, K. E. *et al.* Latrophilin fragments behave as independent proteins that associate and signal on binding of LTX(N4C). *EMBO J* **23,** 4423–4433 (2004).

107. Waller-Evans, H. *et al.* The orphan adhesion-GPCR GPR126 is required for embryonic development in the mouse. *PLoS ONE* **5,** e14047 (2010).

108. Wallgard, E. *et al.* Identification of a core set of 58 gene transcripts with broad and specific expression in the microvasculature. *Arterioscler Thromb Vasc Biol* **28,** 1469–1476 (2008).

109. Walston, T. D. & Hardin, J. Wnt-dependent spindle polarization in the early C. elegans embryo. *Semin Cell Dev Biol* **17,** 204–213 (2006).

110. Wang, T. *et al.* CD97, an adhesion receptor on inflammatory cells, stimulates angiogenesis through binding integrin counterreceptors on endothelial cells.

Blood **105,** 2836–2844 (2005).

111. Wettschureck, N. & Offermanns, S. Mammalian G proteins and their cell type specific functions. *Physiol. Rev.* **85,** 1159–1204 (2005).

112. van Wijk, E. *et al.* The DFNB31 gene product whirlin connects to the Usher protein network in the cochlea and retina by direct association with USH2A and VLGR1. *Hum Mol Genet* **15,** 751–765 (2006).

113. Xia, S. *et al.* Polycystin-dependent fluid flow sensing targets histone deacetylase 5 to prevent the development of renal cysts. *Development* **137,** 1075–1084 (2010).

114. Xu, L., Begum, S., Hearn, J. D. & Hynes, R. O. GPR56, an atypical G protein-coupled receptor, binds tissue transglutaminase, TG2, and inhibits melanoma tumor growth and metastasis. *Proc Natl Acad Sci USA* **103,** 9023–9028 (2006).

115. Yagi, H. *et al.* Vlgr1 knockout mice show audiogenic seizure susceptibility. *J. Neurochem.* **92,** 191–202 (2005).

116. Yamamoto, Y. *et al.* Direct binding of the human homologue of the Drosophila disc large tumor suppressor gene to seven-pass transmembrane proteins, tumor endothelial marker 5 (TEM5), and a novel TEM5-like protein. *Oncogene* **23,** 3889–3897 (2004).

117. Yu, S. *et al.* Essential role of cleavage of Polycystin-1 at G protein-coupled receptor proteolytic site for kidney tubular structure. *Proceedings of the National*

Academy of Sciences **104,** 18688–18693 (2007).

118. Zheng, Q. Y., Johnson, K. R. & Erway, L. C. Assessment of hearing in 80 inbred strains of mice by ABR threshold analyses. *Hear. Res.* **130,** 94–107 (1999).

119. Zhou, L. *et al.* Early forebrain wiring: genetic dissection using conditional Celsr3 mutant mice. *Science* **320,** 946–949 (2008).

Chapter 2

Effects of *Eltd1* Knockdown on Left-Right Asymmetry and Convergence-Extension in the Developing Zebrafish Embryo

Introduction

Adhesion G-protein coupled receptors (AdGPCRs) are emerging as regulators of diverse developmental and physiological processes ranging from early tissue polarity, epithelial planar cell polarity, and adherens junction maintenance to endothelial cell migration, neuronal pathfinding, and peripheral nerve myelination (discussed in Chapter 1). AdGPCRs are particularly intriguing from a structural perspective, harboring long, stalk-like extracellular N-termini with a diverse array of functional domains, a unique autoproteolytic domain, and seven-transmembrane (7TM) units. However, the specific functions of these receptors as well as their signaling mechanisms remain unknown for the vast majority of the family. Based on the functional domains in their N-termini, AdGPCRs are presumed to participate in cell-cell and cell-matrix interactions that regulate the development of tissues and organs. As such, they are best studied *in vivo*. The zebrafish *Danio rerio* offers a number of advantages for undertaking this type of analysis (Driever *et al*., 1996; Haffter *et al*., 1996; Stainier *et al*., 1996, Peterson *et al*., 2000). The expression patterns of individual genes can be quickly determined by whole mount *in situ* hybridization, while their functions can be rapidly assessed by visual inspection of the knockdown phenotypes resulting from morpholino antisense oligonucleotide (MO) injection (Nasevicius & Ekker, 2000). Particularly relevant to the work presented herein, zebrafish are very suitable for studying both early embryonic and cardiovascular development since the embryos develop externally and do not require blood circulation for their initial development, thereby allowing even those embryos showing severe defects to be analyzed in detail.

Eltd1 (EGF, latrophilin seven transmembrane domain containing 1) is an orphan

Adhesion GPCR with strong cardiovascular expression in mouse and rat (Nechiporuk *et al*., 2001; Wallgard *et al*., 2008). In order to determine the physiological functions of Eltd1 during cardiovascular development, we undertook morpholino-mediated knockdown of Eltd1 in zebrafish. We show that Eltd1 regulates the left-right (LR) determination of the heart and other organs via its role in Kupffer's vesicle, the zebrafish organ of LR asymmetry. Additionally, we find roles for Eltd1 in the convergence-extension movements that contribute to embryo narrowing and lengthening during gastrulation. These experiments reveal an essential role for an *Adhesion* GPCR in LR patterning for the first time.

Results

Comparison of zebrafish, mouse, and human Eltd1 protein sequences

To search for the zebrafish ortholog of *eltd1*, we used the mouse *eltd1* gene to query the zebrafish genomic sequence database on Ensembl (http://www.ensembl.org) and identified *zgc:63629* (which was later renamed to *eltd1* in the subsequent Zv9 update to the zebrafish genome assembly [Howe *et al*., 2013]). We then generated a full-length zebrafish *eltd1* cDNA by reverse transcription-polymerase chain reaction (RT-PCR) of total RNA harvested from 48 hpf wild-type TL embryos. Translation of the open-reading frame predicted a 730-amino acid protein that showed 52% and 51% overall homology to the mouse and human Eltd1 proteins, respectively. Since the *Rhodopsin* family members typically bind their ligands via their seven transmembrane (7TM) domains (Schwartz *et al.*, 2006), sequence alignments of the 7TM domains are often more insightful for making cross-species comparisons (Fredriksson & Schiöth, 2005). We utilized a Kyte-Doolittle

hydrophobicity calculator to predict the 7TM regions of zebrafish, mouse, and human Eltd1 (http://www.vivo.colostate.edu/molkit/hydropathy/). The zebrafish Eltd1 protein shared 80% amino acid identity with mouse and human Eltd1 in the 7TM region (Figure 1), providing evidence of a close evolutionary relationship and suggesting transmembrane domain functions, including possible binding partners of the Eltd1 7TM module, have been conserved from fish to human.

Further analysis of the protein sequences indicated additional regions of high similarity. The intracellular IC2 loop (100% amino acid identity), extracellular EC2 loop (86% amino acid identity), intracellular IC3 loop (71% amino acid identity), and the short 23-amino acid C-terminal tail (87% amino acid identity) all exhibited a high degree of conservation, spotlighting these regions as important for conserved function of Eltd1. Additionally, the GPS motif for all three species contained the four conserved Cys residues found in other AdGPCRs. All three proteins contain a PAV motif in TMIV that is found in *Adhesion*, *Frizzled*, and *Secretin* families.

In contrast to the GPS and 7TM regions, the N-terminal regions of zEltd1, mEltd1, and hEltd1 outside of the GPS cysteine box are not well-conserved, with zEltd1 sharing just 32% overall amino acid identity with mouse and human Eltd1. This is consistent with the belief that the extracellular domains of *Adhesion* GPCRs are under relatively low evolutionary pressure. Zebrafish and mouse Eltd1 are predicted to contain three EGF-like domains in their extracellular N-termini which can be presumed to be sites of ligand interaction based on the ligand-binding of AdGPCRs CD97 and EMR2 (Stacey *et al*., 2003), two AdGPCRs with N-terminal EGF-like domains. Intriguingly, the middle EGF-like domain is absent from human Eltd1 due to a 50 amino acid deletion that shortens the

protein relative to its zebrafish and mouse orthologs. This may represent either altered Eltd1 ligand specificity during evolution or a mutation that complements evolutionary change in a conserved ligand.

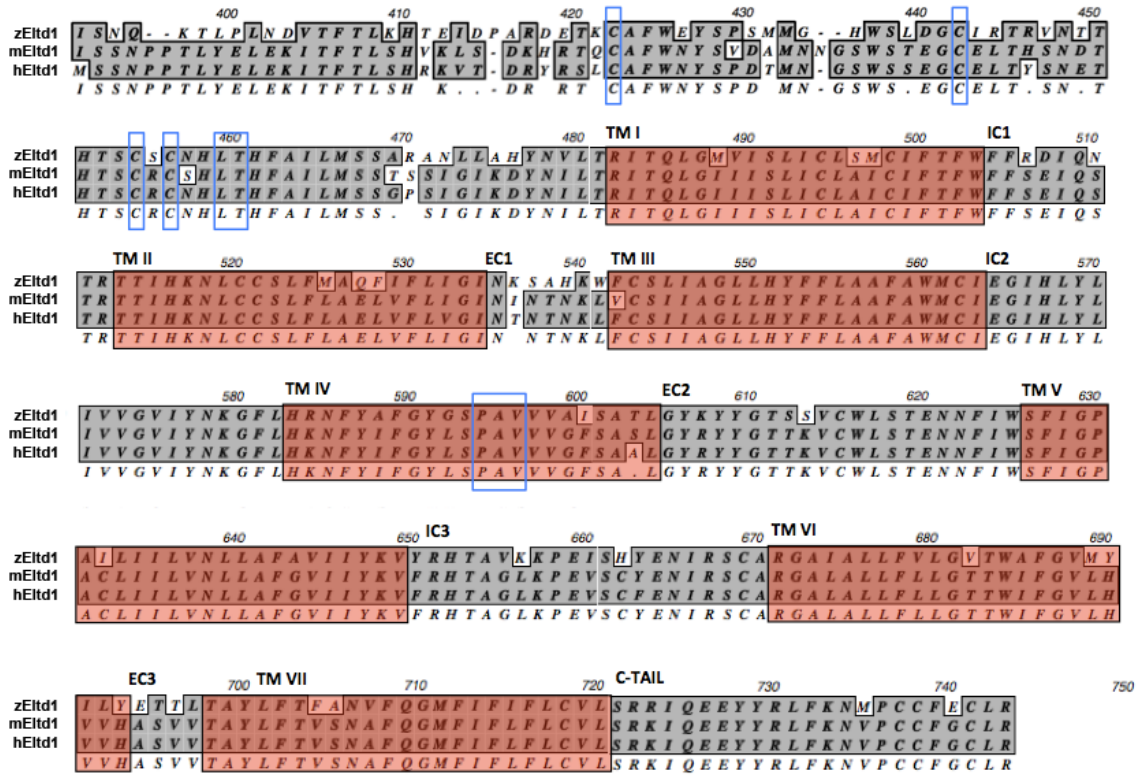

Figure 1. GPS & 7TM protein sequence alignments of zebrafish, mouse, and human Eltd1. The transmembrane (TM) helices, determined by hydrophobicity analysis, are noted with red overlays. Blue outlines highlight conserved residues of interest (PAV motif, conserved Cys residues of GPS motif, and GPS cleavage site). The overall amino acid identity for zEltd1 as compared to the mEltd1/hEltd1 consensus sequence is 80% in the displayed region from TMI to the end of the protein. The majority of the N-terminal region, which shows significantly less conservation, has been omitted.

Eltd1 is expressed during early zebrafish development

Studies in mouse and rat on Eltd1 have outlined a predominantly cardiovascular expression pattern for this receptor with cardiomyocytes, vascular smooth muscle cells, and microvascular endothelial cells as the relevant cell-types (Nechiporuk *et al*., 2001; Wallgard *et al*., 2008). Anatomical GPCR expression profiling of mouse tissues using

quantitative real-time polymerase chain reaction (qPCR) from our own laboratory showed that *eltd1* transcript is detectable in most organs, but most abundantly in lung, consistent with vascular and/or smooth muscle expression (Regard *et al*., 2008). Additionally, we observed abundant *eltd1* expression by qPCR in microvascular endothelial cells purified from neonatal and adult mouse skin. However, no previous studies had assessed *eltd1* expression in the developing embryo. In order to do so efficiently, we utilized whole mount *in situ* hybridization of zebrafish embryos at various stages of development. This showed that *eltd1* is expressed broadly throughout the embryo, visualizable as early as the 64 cell stage. Examination of 2-12 somite stage embryos indicated expression in the notochord, somites, and tailbud regions (Figure 2). Tailbud expression was particularly strong in the 2-3 somite and 10 somite stages, and persisted to the 12 somite stage. By 24 hpf, *eltd1* expression adopted a mostly vascular expression pattern. RT-PCR detected *eltd1* transcript from the 1 cell stage onward, indicating the maternal deposition of this gene (Oliver Stone, personal communication). This early and dynamic expression suggests important roles for zebrafish *eltd1* throughout embryonic development.

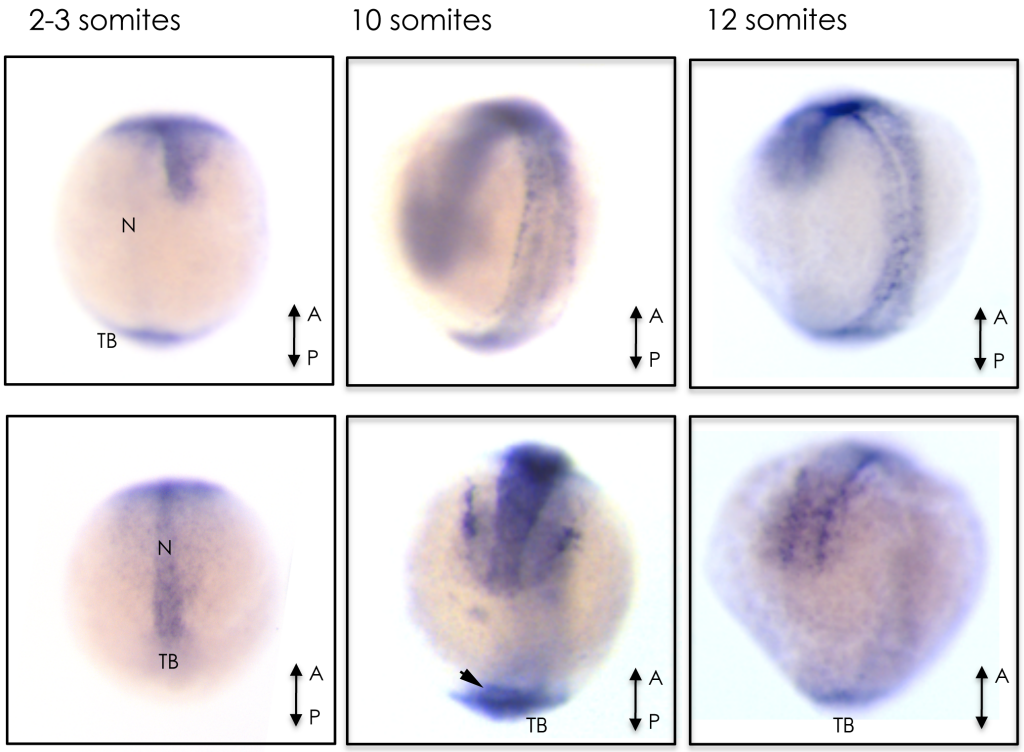

Figure 2. Expression of *eltd1* in the developing zebrafish embryo. A, anterior; P, posterior; N, notochord; TB, tailbud. The arrowhead in the bottom center panel indicates the area around Kupffer's vesicle. Contributed graciously by Oliver Stone, Stainier Laboratory.

Genetic manipulation of eltd1 disrupts embryonic development and LR asymmetry

To investigate how zebrafish *eltd1* may function in embryonic development, we used a morpholino antisense oligonucleotide (MO) approach to knock down *eltd1* in developing zebrafish embryos (Nasevicius and Ekker, 2000). To confirm the sequence specificity of any observed defects, we utilized two morpholinos, the first targeting the translation start site ($Eltd1_{ATG}MO$) and the second targeting the exon10 splice acceptor ($Eltd1_{ex10}MO$). We found the ATG-blocking morpholino to be 10-15 fold more potent than the $Eltd1_{ex10}MO$ and thus used it for most of our experiments. However, the splice-blocker was used to confirm specificity of the phenotypes observed. In this work, we use '$Eltd1_{ATG}$ morphants' and '*eltd1* morphants' interchangeably to refer to embryos injected

with Eltd1$_{ATG}$MO.

Following injection of either MO (Eltd1$_{ATG}$MO or Eltd1$_{ex10}$MO) targeting *eltd1* transcript, transgenic embryos exhibiting heart-specific, vascular-specific, or blood-specific fluorescence were collected from different stages and screened for morphological and functional defects. This analysis revealed that the majority of morphant embryos exhibited pericardial edema and other signs of cardiovascular failure as early as 30 hpf. We discuss those cardiovascular phenotypes in the next chapter.

We were surprised to note that cardiac laterality at 36 hpf was affected in *eltd1* morphants, with the heart frequently adopting right-sided or midline positions as opposed to the *situs solitus* (normal) left-sided placement (Figure 3A). Attesting to the specificity of this phenotype, the defect was observed with both morpholinos and across multiple transgenic zebrafish lines and two wild-type strains. A quantification of heart placement in embryos injected with Eltd1$_{ATG}$MO is shown in Figure 3B. 100% of embryos injected with a control morpholino targeting a mutant human ß-globin transcript exhibited *situs solitus*. In Eltd1$_{ATG}$ morphants, however, the frequency of right-sided and midline cardiac positions increased in a dose-dependent manner, attaining complete randomization (50% normal, 50% abnormal) between the 1.6 ng and 2.4 ng doses. Interestingly, the proportion of abnormal (non-left-sided heart) embryos with midline cardiac placement increased dramatically beyond the 2.4 ng dose. This has been observed for many genes that regulate cardiac laterality.

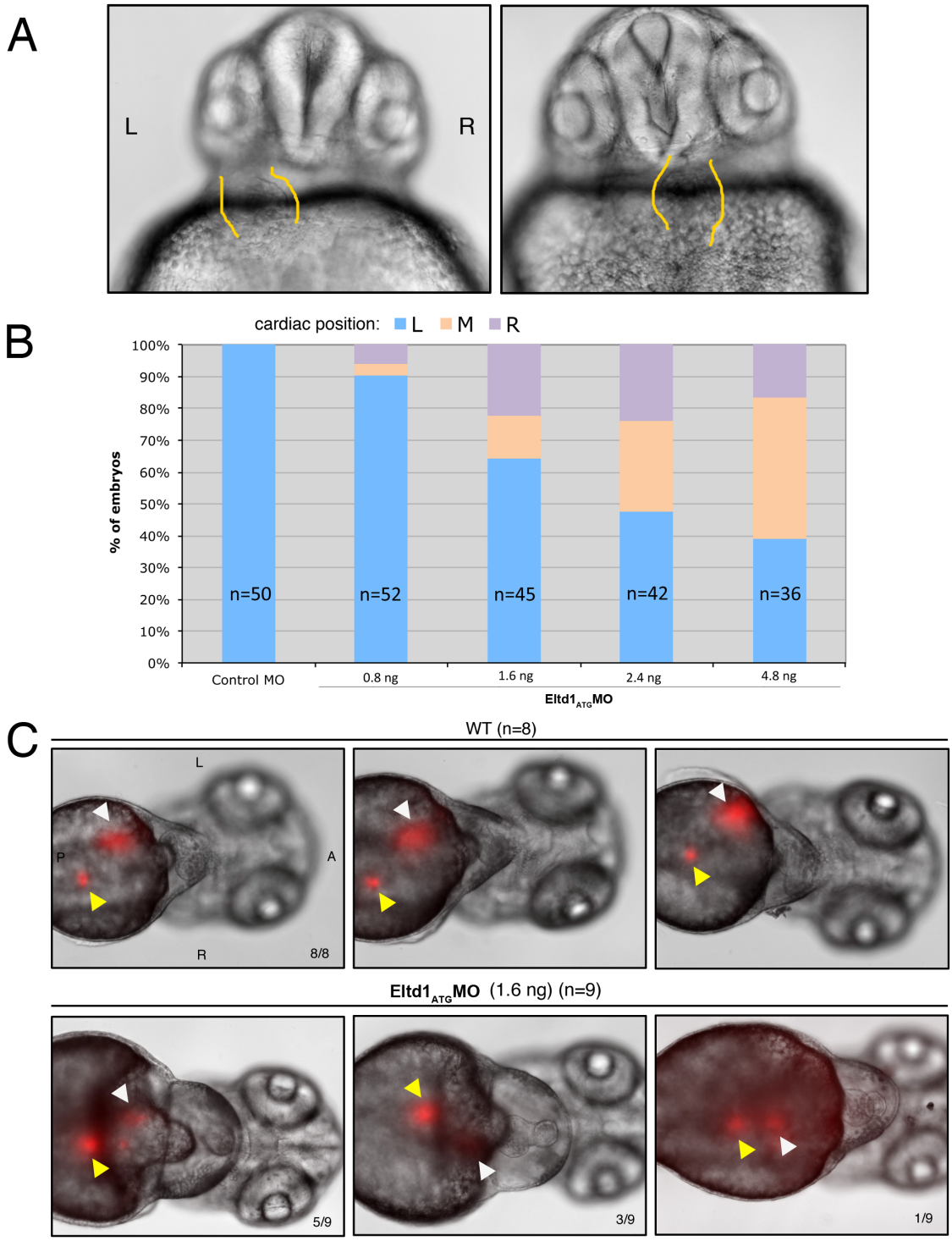

Figure 3. Defective heart and visceral organ laterality in *eltd1* morphants. (A) Representative images of *situs solitus* (left panel) and *situs inversus* (right panel) with respect to cardiac jog in 30 hpf embryos. The lateral borders of the heart are highlighted in yellow. **(B)** Quantification of cardiac laterality defect in *eltd1* morphants. L, left; R, right; M, middle define cardiac placement. **(C)** *Situs inversus* of the gut organs in *eltd1* morphants. Top row depicts three representative images of *2CLIP* transgenic embryos at 54 hpf, exhibiting *situs solitus* of the liver and pancreas. The *2CLIP* strain expresses dsRed in the developing liver (anterior, white arrowheads) and pancreas (posterior, yellow arrowheads). The dsRed signal has been overlayed on differential interference contrast (DIC) images of embryos. *Eltd1* morphants (bottom row)

exhibit *situs solitus* (5/9), *situs inversus* (3/9), and a lack of *situs* (1/9) with respect to liver and pancreas laterality.

In addition to the heart, morphological LR asymmetry of the visceral organs is also observed in zebrafish embryos (Horne- Badovinac *et al*., 2003, Field *et al*., 2003). The gut primordium begins to loop at approximately 26 hpf, with the liver bud moving to the left of midline and the pancreatic bud occupying a rightward position. To determine if L–R asymmetry of the visceral organs is also affected in *eltd1* knockdown embryos, we utilized *2CLIP* transgenic zebrafish (Farooq *et al*., 2008), which express dsRed under the control of the insulin, liver fatty-acid binding protein (lfabp), and elastase promoters. This fluorescently labels both the developing liver and pancreatic buds. Control *2CLIP* embryos exhibited stereotypical asymmetric positioning of the liver and pancreas buds in 100% (8/8) of embryos examined, with the former occupying a more anterior, left-displaced position and the latter occupying a rightward, posterior position (Figure 3C). In contrast, 44% (4/9) of *2CLIP* embryos injected with Eltd1$_{ATG}$MO exhibited *situs inversus* or heterotaxic positioning of both gut organs. Although the sample size for this experiment was small due to difficulty in breeding this transgenic line, the results suggest that Eltd1 is required for LR asymmetry of visceral organs. Taken together with the observation that loss of eltd1 affects cardiac laterality, these experiments indicate eltd1 regulate global LR axis specification, impacting the LR asymmetry of multiple developing organs.

Intriguingly, we also noted that knockdown of *eltd1* seemed to affect the size of the dsRed signal emanating from the developing gut organs (Figure 3C). Whereas the liver bud in control *2CLIP* embryos was consistently larger than the pancreatic bud, *eltd1* morphants displayed liver and pancreatic buds of similar size. This observation suggests

there may be roles for Eltd1 in the growth and development of the visceral organs in addition to LR specification. More likely, disruption of global LR specification may impact the mechanisms by which the liver and pancreas attain their normal sizes, given that many cues directing organogenesis (in addition to lateral migration of organ progenitors) are expressed asymmetrically. In support of this latter hypothesis, disruption of visceral organ laterality in *2CLIP* embryos via knockdown of another gene, *geminin*, also showed this size disparity (Huang *et al*., 2011).

Eltd1 functions in the DFC/KV cell lineage to regulate LR asymmetry

The organ of LR asymmetry in zebrafish is Kupffer's vesicle (KV), which generates the initial asymmetric signal that is translated into left-specific gene expression. We hypothesized that Eltd1 may contribute to the development or function of this organ, therefore affecting global LR asymmetry in the embryo. To test this, we utilized dorsal forerunner cell (DFC)-targeted morpholino injections (Figure 4A). DFCs comprise a group of 20-30 cells that migrate ahead of involuting dorsal blastoderm during gastrulation and subsequently organize in the tailbud to form the ciliated epithelium of KV (Cooper & D'Amico, 1996; Melby *et al*., 1996; Essner *et al*., 2002). By injecting morpholino into the yolk of embryos at a later developmental stage compared to global morpholino injections, DFCs can be exclusively targeted because the progenitor cells from which they are derived maintain cytoplasmic bridges with the yolk longer than other cells (Amack & Yost, 2004).

Embryos receiving DFC-targeted Eltd1$_{ATG}$MO exhibited disrupted cardiac laterality in a dose-dependent manner, but not display tail or vascular defects observed in

global Eltd1$_{ATG}$ morphants, indicating that the morpholino was directed exclusively to DFCs. We additionally utilized fluorescein-conjugated Eltd1$_{ATG}$MO to verify this and screen for embryos showing fluorescence in DFCs. Similar to the global morphants, 40% of injected and screened embryos at the 1.6 ng dose exhibited abnormal cardiac jog, and also as in the global morphants, the frequency of midline cardiac placement increased with increasing dose (Figure 4B). 43% (18/42) of DFC^{eltd1} embryos receiving the highest (4.8 ng) dose of morpholino exhibited significant toxicity/disruption of the yolk and were not scored. These results suggest that Eltd1 functions in DFCs or their KV descendants to contribute to LR asymmetry.

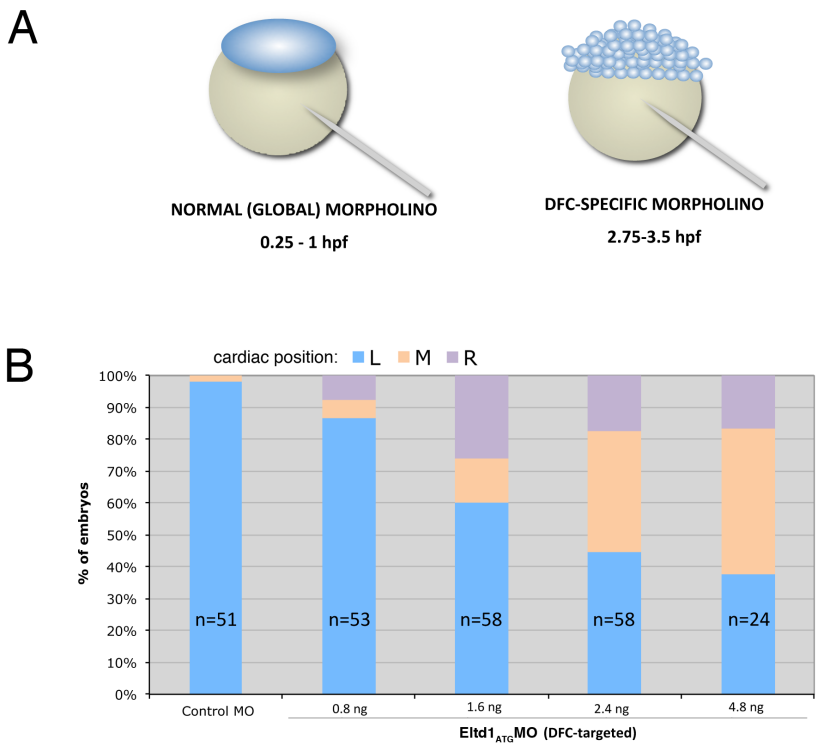

Figure 4. Defective heart laterality in DFC^{eltd1} morphants. (A) Schematic outlining the difference between global morpholino injections and DFC-targeted injections. **(B)** Quantification of cardiac laterality defect in DFC^{eltd1} morphants. L, left; R, right; M, middle define cardiac placement.

Eltd1 morphants form a grossly normal KV

One manner in which Eltd1 may regulate LR asymmetry is by contributing to the coalescing of DFCs at the tailbud and subsequent morphogenesis of the spherical KV. Consistent with such a role, *eltd1* is expressed in the posterior mesoderm surrounding the presumed location of KV (Figure 2). Using *Tg(Sox17:GFP)*^{s807} transgenic fish, which express GFP in DFCs and their descendants, we visualized DFCs and the developing KV. We found DFCs to persist, migrate, and grossly organize normally at the tailbud to form a spherical structure of GFP^{+} cells in all morphants receiving Eltd1$_{ATG}$MO, either globally or targeted to DFCs (Figure 5A). This suggests Eltd1 regulates LR asymmetry at a step following KV formation.

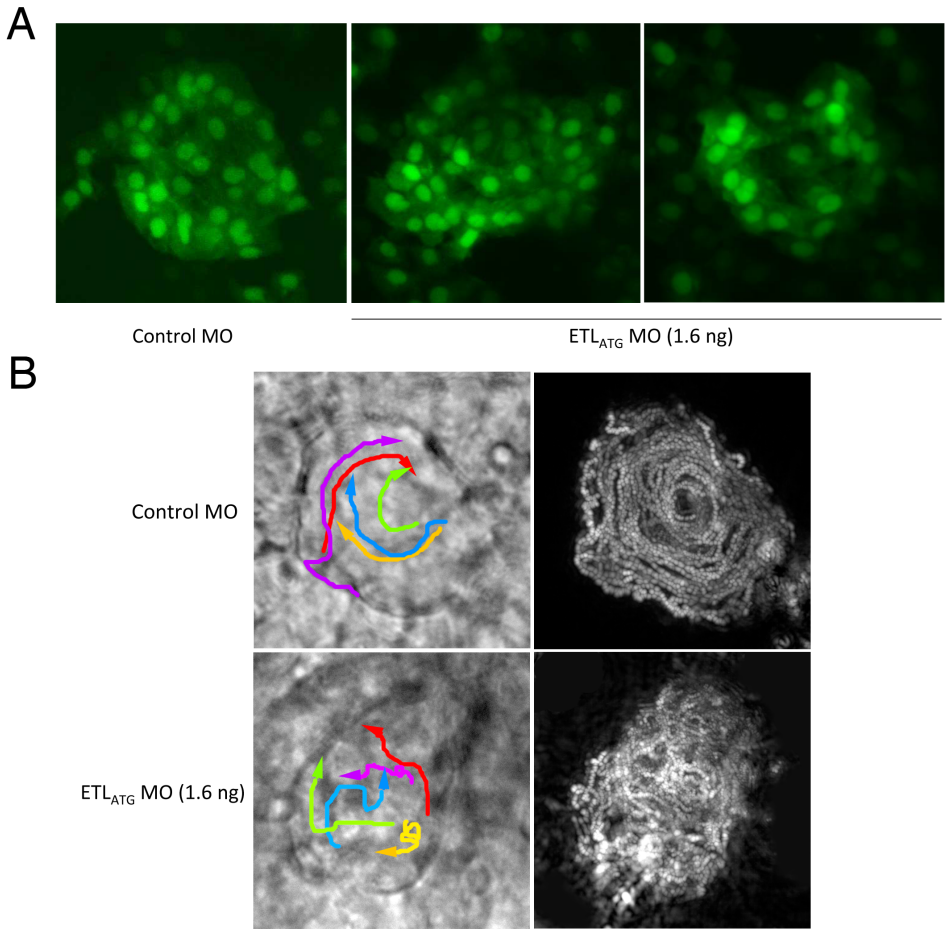

Figure 5. KV morphology and nodal flow in *eltd1* morphants. (A) Representative confocal Z-stacks of KV from control MO and Eltd1$_{ATG}$MO-injected embryos. **(B)** Tracking analysis of fluorescent beads in control and *eltd1* morphant KVs. Left panels depict the paths of five representative beads over 30 frames (□pprox.. 1.5 sec). Right panels are Z stack projections showing the paths of all beads over the entire capture from the same embryo.

Nodal flow is disrupted by eltd1 knockdown in DFC/KV

In Kupffer's vesicle, motile cilia projecting from the apical surface of KV epithelial cells are thought to generate a leftward fluid flow that stimulates sensory cilia on cells lining KV (Tabin & Vogan, 2003; Delmas, 2004; Nauli & Zhou, 2004). This process is believed to produce an asymmetric Ca^{2+} signal that leads to left-specific gene expression (McGrath *et al*., 2003, Essner *et al*., 2005, Sarmah *et al*., 2005). We examined so-called nodal flow in *eltd1* morphant KV by direct microinjection of fluorescent dye-conjugated latex beads into KV during the 6-8 somite stage, a time point when nodal flow has been established and KV is reaching its largest size. Fluorescent beads injected into control embryos were observed to move in a counter-clockwise path around the interior of KV (clockwise when viewed on an inverted microscope). Strikingly, embryos injected with Eltd1$_{ATG}$MO (global) exhibited mostly random flow with beads following arbitrary trajectories. Although movies of bead motion are more informative, bead trajectories are shown in Figure 5B.

Mutants that lack nodal flow due to absence or stasis of motile cilia exhibit slow, Brownian motion of injected beads. In contrast, we observed that injected beads in *eltd1* morphants were moving at speeds equal to or greater than in control MO-injected embryos, implying that Eltd1 is not required for ciliogenesis and ciliary motility in the KV. The further implication of these results is that Eltd1 is required for some other aspect of nodal flow generation. The appropriate positioning of motile cilia within

individual KV cells, the precise posterior tilt of these cilia, and their asymmetric anterior-posterior distribution in KV have all been shown to be required for the generation of normal nodal flow (Hirokawa *et al*., 2012). Our results seem to localize the requirement for Eltd1 in LR asymmetry to some such aspect of motile cilia within Kupffer's vesicle.

Eltd1 morphants exhibit convergence-extension defects

At higher doses of morpholino than those that produced laterality defects, *eltd1* morphants exhibited a specific convergence-extension (CE) defect that manifested with enlarged tail buds at 10 hpf, and in more severely affected embryos, significant lengthening of the body axis and yolk leading to an ovoid rather than round shape. In moderately and severely affected embryos, the tailbud was observed to extend off the yolk instead of proceeding around the yolk to the ventral side, as in control embryos. This extended tail bud went on to develop into a kinked tail by 24 hpf, and the severity of the posterior body defect correlated with the severity of embryo lengthening. We quantified the dose-dependence of this phenotype by categorizing embryos into three distinct phenotypic categories (Figure 6).

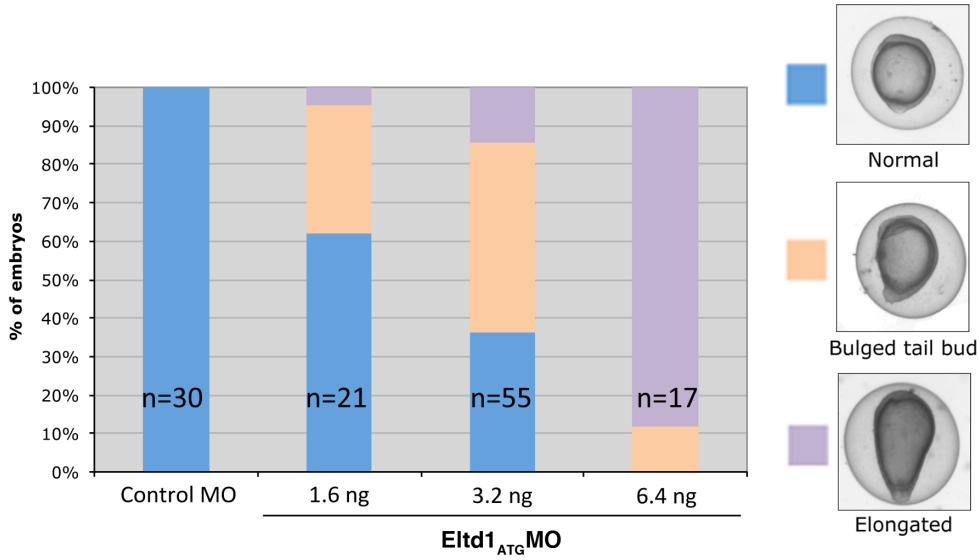

Figure 6. Convergence-extension defects in *eltd1* morphants at 10 hpf. Embryos were placed into three phenotypic categories for quantification: those that exhibited tailbuds that remained attached to the yolk (normal), those that exhibited tailbuds extending from the yolk but a mostly round yolk ball (bulged tail bud), and those that exhibited an obviously ovoid shape.

This phenotype suggests Eltd1 may regulate convergence-extension in gastrulating zebrafish embryos. In support of this, injection of *eltd1* RNA into 1-2 cell stage embryos also resulted in CE defects (Oliver Stone, personal communication). Intriguingly, with respect to the CE defect, *eltd1* morphants essentially phenocopy zebrafish mutants *swirl* (*swr*), *snailhouse* (*snh*), *piggytail* (*pgy*), and *lost-a-fin* (*laf*), all of which have been mapped to proteins involved in bone morphogenetic protein (BMP) signaling (Mullins *et al*., 1996; Lele *et al*., 2001; Mintzer *et al*., 2001).

Discussion

Although the last decade has seen much progress with respect to understanding the physiological roles of *Adhesion* GPCRs, 29 of 33 receptors in the family remain as

orphans, and most still have poorly characterized function. It is evident that these receptors participate in cell-cell or cell-extracellular matrix interactions in a variety of tissues, but these events have been difficult to study in further detail, partly because they cannot be reproduced *in vitro*. Additionally, the generation of knockout mice, a tested strategy for determining the function of thousands of genes, is a time-consuming and inefficient approach to search for phenotypes caused by loss of AdGPCRs particularly because AdGPCRs appear to contribute to more subtle organization of tissues that is difficult to decipher. We successfully utilized morpholino-mediated knockdown in zebrafish to establish a role for Eltd1 in LR asymmetry, illustrating the utility of this model organism in uncovering novel functions for AdGPCRs. Although a GPCR has previously been reported to participate in LR axis specification (Leung *et al*., 2008), our work represents the first instance of an *Adhesion* GPCR participating in LR asymmetry.

We localized the requirement for Eltd1 in LR axis specification to Kupffer's vesicle, where Eltd1 may play a role in one or more processes that regulate nodal flow. The precise spatial regulation of motile cilia in Kupffer's vesicle is considered to be vital for the generation of productive nodal flow. Recently it has been theorized that anterior-posterior (AP) axis asymmetry is translated into LR asymmetry at Kupffer's vesicle (Hashimoto & Hamada, 2010). Several aspects of ciliary function in KV appear to be regulated by the AP axis. In particular, motile cilia have been found to adopt an asymmetric AP distribution along the dorsal wall of KV, with approximately two-thirds located on the anterior side. This is thought to contribute to the higher flow velocities injected particles adopt in the anterior half of KV. The rho kinase rock2b was shown to regulate this asymmetric AP distribution of cilia as knockdown resulted in uniform ciliary

distribution, unproductive nodal flow, and laterality defects (Wang *et al*., 2011). Eltd1 may participate in this process, perhaps upstream of rock2b, warranting investigation of AP cilia distribution in *eltd1* morphant KV. Another AdGPCR, nematode latrophilin (LAT-1), has been shown to direct AP tissue polarity in the early *C. elegans* embryo (Langenhan *et al.*, 2009). It is tempting to speculate that AdGPCRs, including Eltd1, may be part of, or able to regulate, the pathways that establish AP polarity during early embryogenesis. The precise nature of these pathways is unclear, but a Wnt gradient is thought to be central to AP axis specification throughout evolution (Niehrs, 2010).

Yet another manner in which AP polarity impacts nodal flow is via the posterior tilting of nodal cilia. This tilting of the ciliary rotational axis arises from the subcellular location of the basal body, which occupies a posterior position in the majority of KV cells (Borovina *et al*., 2010) or mouse node cells (Maisonneuve *et al*., 2009; Hashimoto *et al*., 2010). Intriguingly, disheveled proteins have been found to regulate the gradual posterior shifting of nodal basal bodies in mouse and *Xenopus*, arguing for an important role for planar polarization and noncanonical Wnt signaling in this process (Park *et al*., 2008; Hashimoto *et al*., 2010). Several other studies have also implicated PCP components in basal body localization in the mouse and *Xenopus* nodes (Antic *et al*., 2010; Song *et al*., 2010). In zebrafish, the noncanonical Wnt/PCP pathway again appears to be important; mutant embryos lacking Vangl2 lose posterior tilt of primary cilia in several tissues, including KV epithelium, and display centralized localization of apically docked basal bodies (Borovina *et al*., 2010). These results suggest that planar polarization of KV cells is important for LR axis specification. Flamingo/CELSR, the AdGPCR considered to be a “core” planar cell polarity (PCP) molecule, directs planar polarization in several types

of epithelium. However, despite extensive studies on flamingo/CELSR during embryogenesis in mouse and zebrafish, no known role for flamingo orthologs has been found in the node/KV or in LR axis specification. If flamingo represents a required component of the PCP "cassette," it is possible that another AdGPCR such as Eltd1 may adopt a flamingo-like role in the planar polarization pathway in KV. Testing this hypothesis must begin with an examination of basal body subcellular localization in *eltd1* morphant KV epithelium.

We observed *eltd1* morphants to exhibit a striking convergence-extension (CE) defect, notable at higher doses of morpholino 10-12 hpf. This became increasingly relevant as we uncovered the laterality defect in *eltd1* morphants because the combination of laterality and CE defects are hallmarks of PCP pathway disruption (McNeill, 2010). While planar polarization of the node or KV is conceptually similar to *Drosophila* wing epithelium, where PCP molecules have been studied most extensively, the pathway also regulates polarized cell movements that cause tissues to narrow and lengthen, such as during cochlear extension, neural tube closure, and convergence and extension movements during gastrulation (Roszko *et al.*, 2009). Thus, the PCP pathway comprises an intriguing set of candidate genetic and molecular interactors for Eltd1 and possibly other AdGPCRs.

An alternative candidate pathway that Eltd1 may participate in, or interact with, is BMP signaling. The specific gross morphology of the CE defect in *eltd1* is strikingly reminiscent of mutants of the BMP signaling pathway (Mullins *et al.*, 1996), which exhibit CE defects as result of altered ventro-lateral cell fates that are ultimately thought to impact upon cadherin-dependent cell-cell adhesion important for proper convergence

and extension gastrulation movements (von der Hart *et al*., 2007). Additionally, the dorso-ventral (DV) axis also impacts upon KV, as cilia are distributed asymmetrically across this axis, predominantly on the dorsal side of the laterality organ (Kreiling *et al*., 2007; Okabe *et al*., 2008). We conducted initial experiments to test the hypothesis that *eltd1* knockdown perturbed BMP signaling by utilizing *Tg(Bre:GFP)* (Alexander *et al*., 2011) zebrafish to monitor BMP signaling during gastrulation, but found no overt differences between controls and morphants (data not shown). This does not exclude the possibility that Eltd1 acts downstream of BMP signaling, possibly modulating cell-cell adhesion in response to BMP-related cues.

A global *eltd1* knockout mouse has been generated by Deltagen, Inc. and deposited in the European Mouse Mutant Archive (EMMA). It was recently utilized in a study of cardiac hypertrophy in response to pressure overload (Xiao *et al*., 2012). The authors of that study report that the knockout mice they obtained were viable with no overt phenotypes. Additionally, Deltagen has reported that homozygous mutants are indistinguishable from age and gender-matched wild-type controls. This seems to indicate an absence of the early developmental phenotypes we observed in zebrafish morphants. Several possibilities may explain this. First, Eltd1 may simply not regulate LR asymmetry or convergence-extension in mice. Indeed, the organs of laterality differ slightly between species and each has its unique characteristics. For instance, the mouse node is pit-shaped while KV is spherical. Such factors may contribute to the presumed dispensability of Eltd1 in the mouse node. Redundancy may also be responsible for the presumed lack of LR defect in *eltd1* knockout mice. Several AdGPCRs from Group II exhibit N-termini composed only of EGF-like repeats, and the transmembrane domains of

the latrophilins (LECs) are closely related to those of Eltd1. Yet another possibility is that maternal deposition of Eltd1 in mouse overcomes an early developmental lack of zygotic Eltd1. Maternally-deposited protein in mouse has been reported to persist as long as embryonic day 5.5-6.5 (West *et al*., 1986), although most maternal proteins in mice do not last this long. The embryonic node in mice forms around e7.0, suggesting this is an unlikely explanation for the lack of early developmental phenotypes in *eltd1* knockout mice. Finally, these knockout mice have not been characterized extensively, and it is possible that early developmental phenotypes causing embryonic lethality and reduced litter sizes have gone unnoticed.

Our results represent the first report of an *Adhesion* GPCR participating in LR axis determination in any species. The phenotypic data strongly suggest at least two candidate pathways which should be investigated for interaction with, or regulation by, Eltd1. Additionally, they may provide one more example of an AdGPCR participating in tissue polarity, with implications for signaling pathways that may be downstream of AdGPCRs. The identification of an extracellular ligand for Eltd1 would certainly aid in interrogating the relationship between Eltd1 and candidate downstream signaling pathways.

Materials and Methods

Zebrafish strains and husbandry. Wild-type AB, wild-type TL, *Tg(cmlc2:GFP)* (Huang *et al*., 2003), *Tg(sox17:GFP)*^{s870} (Chung & Stainier, 2008), and *2CLIP* (Anderson *et al*., 2009) zebrafish (*Danio rerio*) strains were raised in the SCVRB facility at 28.5˚C. Embryos for experiments were obtained from natural matings and cultured at 28˚C – 32˚C in sterile-filtered fish water. The developmental stages of embryos were determined according to morphological criteria (Kimmel *et al*., 1995). Embryos were manually dechorionated for experiments using #5 fine forceps (Fine Science Tools, Foster City, CA).

Antisense morpholino oligos. The following morpholinos (Mos) were obtained from Gene Tools, LLC (Eugene, OR): Eltd1$_{ATG}$MO (translation-blocking morpholino targeting the start codon): 5'-AAAGCAGGAGTTTCATTGGAGAACT-3', Eltd1$_{ATG2}$MO (a second translation-blocking morpholino targeting the start codon): 5'-GGAGAACTGTGTAAAAACTCCATTT-3', Eltd1$_{ex10}$MO (splice-blocking morpholino targeting the exon 10 splice acceptor): 5'-AGCAGTAGACCAGACTTACATTAGC-3', and Gene Tools' *standard control* (targeting a human ß-globin mutant): 5'-CCTCTTACCTCAGTTACAATTTATA-3'. Morpholino oligonucleotides were solubilized in water at a concentration of 10 mM (~85 mg/ml). The resulting stock solution was diluted to working concentrations of 0.1 mM or 0.2 mM in 1x Danieau solution (58 mM NaCl, 0.7 mM KCl, 0.4 mM $MgSO_4$, 0.6 mM $Ca(NO_3)_2$, 5 mM HEPES, pH 7.6). 0.1% phenol red was added to working concentrations of MO to aid in visualization during injection. The injected volume was 0.5–8 nl, depending on the

required injected MO dose. Doses ranged from 0.8 ng to 12.8 ng. MOs were injected into the yolk of 1-2 cell stage embryos for global knockdown and into the yolk of 256-1,000 cell stage embryos for DFC-targeted knockdown. Flourescein-labeled MO of the same Eltd1$_{ATG}$MO sequence listed above was used to validate targeted delivery of MO to DFCs by visualizing shield stage embryos.

Cloning of full-length zebrafish eltd1. Total RNA was extracted from 100 pooled wild-type *Tupfel long fin* (TL) 48 hpf embryos in 1.5 ml microfuge tubes. 250 µl of Trizol reagent (Invitrogen) was added after removal of all water. Embryos were disrupted with 29g insulin syringe (BD Biosciences) followed by addition of 750 µl of Trizol reagent Samples were incubated for 5 min. at room temperature and flash frozen in liquid nitrogen or subjected to phenol-chloroform extraction. RNA cleanup was performed with the Qiagen RNEasy Mini Kit (Qiagen). cDNA was synthesized from the using the iScript cDNA Synthesis Kit (Bio-Rad). A 1:10 dilution of the resulting cDNA was used as template for PCR amplification of *eltd1* using the following primers with EcoRI and XbaI sites built-in: F z110001 5'-CTGCGAATTCAGCTCAATGAAACTCCTGCTTTTCG-3' and R z110004 5'-GCTATCTAGATCCGCGCATTGCGTTGTAGTTCACC-3'. The PCR reaction was subjected to gel electrophoresis and the ~2.2kb band was gel-purified using the QiaQuick Gel Extraction Kit (Qiagen). The purified DNA was subcloned into pCS2+ and sequenced.

Whole-mount in situ hybridization. Whole-mount in situ hybridization was performed as described (Thisse et al., 1993) using a full-length cDNA-containing plasmid.

Digoxigenin-labeled RNA probes were synthesized by *in vitro* transcription using SP6 RNA polymerase. Embryos were fixed in 4% paraformaldehyde/PBS overnight at 4˚C, manually dechorionated, and dehydrated in methanol overnight at -20˚C. After stepwise rehydration in a methanol/PBS series, embryos were digested with proteinase K (10µg/ml) for 1 min at 37˚C, then refixed in 4% paraformaldehyde/PBS for 20 min. Following 5 washes of 5 min. in PBT (0.1% Tween20/PBS), embryos were prehybridized in 200 µl of hydridization mix (50% formamide, 5x SSC, 0.1% Tween-20, pH 6.0, 50 µg/ml tRNA, 50 µg/ml heparin) for 2-6 hrs at 65˚C. The hybridization mix was removed and replaced with fresh containing 200-500ng of antisense RNA probe, and incubated overnight at 65-70˚C. The following day, embryos were washed in the series: 100% hybridization mix without tRNA or heparin (HM), 1 min. at 70˚C; 66% HM/33% 2x SSC, 15 min. at 65˚C; 33% HM/66% 2x SSC, 15 min. at 65˚C; 2x SSC, 15 min. at 65˚C; two washes of 30 min. each in 0.2x SSC at 65˚C; 66% 0.2x SSC/33% PBT, 10 min. at RT; 33% 0.2x SSC/66% PBT, 10 min. at RT; PBT, 10 min. at RT. Embryos were then blocked in Roche Blocking Buffer in PBT for 3 hours at RT. Anti-DIG antibody was diluted in 1x blocking buffer/PBT and embryos were incubated overnight with agitation at 4˚C, followed by 6 washes of 10 min. each the next day.

Whole-mount immunohistochemistry of Kupffer's vesicle. Embryos were fixed in 4% paraformaldehyde (Sigma) overnight at 4˚C, then rinsed 3-5 times in PBST (0.1% Triton X-100 in 0.1M PBS, pH 7.3). For staining of Kupffer's vesicle, the tailbud region of 2-10 somite stage embryos was dissected out using No.5 Dumont forceps and a tungsten needle (Fine Science Tools, Foster City, CA) after fixation and rinsing. Samples were then treated in pre-chilled acetone for 7 min. at -20˚C, followed by 3 x 5 min. washes in

PBST. Blocking was performed in 10% fetal bovine serum (Hyclone), 2% bovine serum albumin (BSA), and 1% DMSO in PBST at room temperature for 1 hr, followed by 3 x 5 min. washes in PBST. Incubation with primary antibodies was carried out at 4˚C overnight in blocking solution. Primary antibodies and dilutions used were mouse monoclonal anti-acetylated tubulin (Sigma), 1:400, polyclonal rabbit anti-Eltd1 (Sigma), 1:200, goat polyclonal anti-Vangl2 N-13 (Santa Cruz Biotechnology, Dallas, TX), 1:200. Samples were rinsed 3-5 x 20 min. in PBST, followed by incubation with secondary antibodies in blocking solution at 4˚C overnight. Secondary antibodies and dilutions used were goat anti-mouse Alexa594, 1:500, goat-anti-mouse Alexa488, 1:500, goat anti-rabbit Alexa594, 1:500, and donkey anti-goat Alexa488, 1:500 (Invitrogen). After rinsing 5 x 20 min. in PBST, samples were mounted in Vectashield mounting medium with or without DAPI (Vector Laboratories, Burlingame, CA) on glass microscope slides. KV samples were mounted ventral side up.

Microscopy. Live embryos were manually dechorionated, anesthetized with 0.1% w/v tricaine (Sigma), and mounted in 50 µl drops of 1.2% low-melt agarose (Sigma) on 22mm square glass coverslips or in glass-bottomed 35mm petri dishes (Mattek, Ashland, MA). Embryos were visualized on a Nikon Eclipse TE300 inverted microscope using both DIC or epifluorescence. Images and video were captured with a Coolsnap ES2 CCD camera (Photometrics, Tuscon, AZ). Confocal imaging was carried out on a Bio-Rad MRC 1024ES confocal system attached to a Nikon TE300 microscope. Images were captured using Lasersharp2000 v5.2 (Bio-Rad, Hercules, CA) and further processed using ImageJ v1.44 (National Institutes of Health, Bethesda, MD).

Nodal flow analysis. Red fluorescent 0.5μm Fluospheres (Invitrogen) were diluted 1:100 in PBS. 6-8 somite stage embryos were dechorionated manually and individually deposited into 50 μl pools of 1.2% low-melt agarose (Sigma) on 22mm square cover glass (VWR International). Embryos were positioned with the tailbud/KV down, tilted a few degrees to the side to aid in visualization of KV by light microscopy, and allowed to set. Microinjection of the diluted fluorescent beads was performed with the same glass needles used for morpholino injections. The needle followed a path through the yolk and entered through the ventro-lateral wall of KV. Injected embryos were allowed to rest 20 minutes before visualization. Bead movements were recorded using a CoolSNAP ES2 camera (Photometrics, Tuscon, AZ) on a Nikon TE300 inverted fluorescence microscope running Metamorph 7.6.2 software (Molecular Devices, Sunnyvale, CA). Z-stack assembly and other adjustments were performed in ImageJ v1.44 (National Institutes of Health, Bethesda, MD).

References

1. Amack, J. D. & Yost, H. J. The T box transcription factor no tail in ciliated cells controls zebrafish left-right asymmetry. *Curr Biol* **14,** 685–690 (2004).

2. Anderson, R. M. R. *et al.* Loss of Dnmt1 catalytic activity reveals multiple roles for DNA methylation during pancreas development and regeneration. *Dev Biol* **334,** 11–11 (2009).

3. Antic, D. *et al.* Planar cell polarity enables posterior localization of nodal cilia and left-right axis determination during mouse and Xenopus embryogenesis. *PLoS*

ONE **5,** e8999 (2010).

4. Borovina, A., Superina, S., Voskas, D. & Ciruna, B. Vangl2 directs the posterior tilting and asymmetric localization of motile primary cilia. *Nat Cell Biol* **12,** 407–412 (2010).

5. Chung, W.-S. & Stainier, D. Y. R. Intra-endodermal interactions are required for pancreatic beta cell induction. *Dev Cell* **14,** 582–593 (2008).

6. Cooper, M. S. & D'Amico, L. A. A cluster of noninvoluting endocytic cells at the margin of the zebrafish blastoderm marks the site of embryonic shield formation. *Dev Biol* **180,** 184–198 (1996).

7. Delmas, P. Polycystins: from mechanosensation to gene regulation. *Cell* **118,** 145–148 (2004).

8. Driever, W. *et al.* A genetic screen for mutations affecting embryogenesis in zebrafish. *Development* **123,** 37–46 (1996).

9. Essner, J. J., Amack, J. D., Nyholm, M. K., Harris, E. B. & Yost, H. J. Kupffer's vesicle is a ciliated organ of asymmetry in the zebrafish embryo that initiates left-right development of the brain, heart and gut. *Development* **132,** 1247–1260 (2005).

10. Essner, J. J. *et al.* Conserved function for embryonic nodal cilia. *Nature* **418,** 37–38 (2002).

11. Farooq, M. *et al.* Histone deacetylase 3 (hdac3) is specifically required for liver development in zebrafish. *Dev Biol* **317,** 336–353 (2008).

12. Field, H. A., Dong, P. D. S., Beis, D. & Stainier, D. Y. R. Formation of the digestive system in zebrafish. II. Pancreas morphogenesis. *Dev Biol* **261,** 197–208 (2003).

13. Fredriksson, R., Lagerström, M. C., Lundin, L.-G. & Schiöth, H. B. The G-protein-coupled receptors in the human genome form five main families. Phylogenetic analysis, paralogon groups, and fingerprints. *Mol. Pharmacol.* **63,** 1256–1272 (2003).

14. Haffter, P. *et al.* The identification of genes with unique and essential functions in the development of the zebrafish, Danio rerio. *Development* **123,** 1–36 (1996).

15. Hardt, von der, S. *et al.* The Bmp gradient of the zebrafish gastrula guides migrating lateral cells by regulating cell-cell adhesion. *Curr Biol* **17,** 475–487 (2007).

16. Hashimoto, M. & Hamada, H. Translation of anterior-posterior polarity into left-right polarity in the mouse embryo. *Curr Opin Genet Dev* **20,** 433–437 (2010).

17. Hashimoto, M. *et al.* Planar polarization of node cells determines the rotational axis of node cilia. *Nat Cell Biol* **12,** 170–176 (2010).

18. Hirokawa, N., Tanaka, Y. & Okada, Y. Cilia, KIF3 molecular motor and nodal flow. *Curr Opin Cell Biol* (2012). doi:10.1016/j.ceb.2012.01.002

19. Horne-Badovinac, S., Rebagliati, M. & Stainier, D. Y. R. A cellular framework for gut-looping morphogenesis in zebrafish. *Science* **302,** 662–665 (2003).

20. Howe, K. *et al.* The zebrafish reference genome sequence and its relationship to the human genome. *Nature* **496,** 498–503 (2013).

21. Huang, C.-J., Tu, C.-T., Hsiao, C.-D., Hsieh, F.-J. & Tsai, H.-J. Germ-line transmission of a myocardium-specific GFP transgene reveals critical regulatory elements in the cardiac myosin light chain 2 promoter of zebrafish. *Dev Dyn* **228,** 30–40 (2003).

22. Huang, S., Ma, J., Liu, X., Zhang, Y. & Luo, L. Geminin is required for left-right patterning through regulating Kupffer's vesicle formation and ciliogenesis in zebrafish. *Biochem Biophys Res Commun* **410,** 164–169 (2011).

23. Kimmel, C. B. C., Ballard, W. W. W., Kimmel, S. R. S., Ullmann, B. B. & Schilling, T. F. T. Stages of embryonic development of the zebrafish. *Dev Dyn* **203,** 253–310 (1995).

24. Kreiling, J. A., Prabhat, Williams, G. & Creton, R. Analysis of Kupffer's vesicle in zebrafish embryos using a cave automated virtual environment. *Dev Dyn* **236,** 1963–1969 (2007).

25. Kyte, J. & Doolittle, R. F. A simple method for displaying the hydropathic character of a protein. *J Mol Biol* **157,** 105–132 (1982).

26. Langenhan, T. *et al.* Latrophilin signaling links anterior-posterior tissue polarity and oriented cell divisions in the C. elegans embryo. *Dev Cell* **17,** 494–504 (2009).

27. Lee, J. D. & Anderson, K. V. Morphogenesis of the node and notochord: the

cellular basis for the establishment and maintenance of left-right asymmetry in the mouse. *Dev Dyn* **237,** 3464–3476 (2008).

28. Lele, Z., Bakkers, J. & Hammerschmidt, M. Morpholino phenocopies of the swirl, snailhouse, somitabun, minifin, silberblick, and pipetail mutations. *Genesis* **30,** 190–194 (2001).

29. Maisonneuve, C. *et al.* Bicaudal C, a novel regulator of Dvl signaling abutting RNA-processing bodies, controls cilia orientation and leftward flow. *Development* **136,** 3019–3030 (2009).

30. McGrath, J., Somlo, S., Makova, S., Tian, X. & Brueckner, M. Two populations of node monocilia initiate left-right asymmetry in the mouse. *Cell* **114,** 61–73 (2003).

31. Melby, A. E., Warga, R. M. & KIMMEL, C. B. Specification of cell fates at the dorsal margin of the zebrafish gastrula. *Development* **122,** 2225–2237 (1996).

32. Mintzer, K. A. *et al.* Lost-a-fin encodes a type I BMP receptor, Alk8, acting maternally and zygotically in dorsoventral pattern formation. *Development* **128,** 859–869 (2001).

33. Mullins, M. C. *et al.* Genes establishing dorsoventral pattern formation in the zebrafish embryo: the ventral specifying genes. *Development* **123,** 81–93 (1996).

34. Nasevicius, A. & Ekker, S. C. Effective targeted gene ‘knockdown’ in zebrafish. *Nat Genet* **26,** 216–220 (2000).

35. Nauli, S. M. & Zhou, J. Polycystins and mechanosensation in renal and nodal cilia.

Bioessays **26,** 844–856 (2004).

36. Nechiporuk, T., Urness, L. D. & Keating, M. T. ETL, a novel seven-transmembrane receptor that is developmentally regulated in the heart. ETL is a member of the secretin family and belongs to the epidermal growth factor-seven-transmembrane subfamily. *J Biol Chem* **276,** 4150–4157 (2001).

37. Niehrs, C. On growth and form: a Cartesian coordinate system of Wnt and BMP signaling specifies bilaterian body axes. *Development* **137,** 845–857 (2010).

38. Okabe, N., Xu, B. & Burdine, R. D. Fluid dynamics in zebrafish Kupffer's vesicle. *Dev Dyn* **237,** 3602–3612 (2008).

39. Park, T. J., Mitchell, B. J., Abitua, P. B., Kintner, C. & Wallingford, J. B. Dishevelled controls apical docking and planar polarization of basal bodies in ciliated epithelial cells. *Nat Genet* **40,** 871–879 (2008).

40. Peterson, R. T., Link, B. A., Dowling, J. E. & Schreiber, S. L. Small molecule developmental screens reveal the logic and timing of vertebrate development. *Proc Natl Acad Sci USA* **97,** 12965–12969 (2000).

41. Regard, J. B., Sato, I. T. & Coughlin, S. R. Anatomical profiling of G protein-coupled receptor expression. *Cell* **135,** 561–571 (2008).

42. Roszko, I., Sawada, A. & Solnica-Krezel, L. Regulation of convergence and extension movements during vertebrate gastrulation by the Wnt/PCP pathway. *Semin Cell Dev Biol* **20,** 986–997 (2009).

43. Sarmah, B., Latimer, A. J., Appel, B. & Wente, S. R. Inositol polyphosphates regulate zebrafish left-right asymmetry. *Dev Cell* **9,** 133–145 (2005).

44. Schwartz, T. W., Frimurer, T. M., Holst, B., Rosenkilde, M. M. & Elling, C. E. Molecular mechanism of 7TM receptor activation--a global toggle switch model. *Annu. Rev. Pharmacol. Toxicol.* **46,** 481–519 (2006).

45. Stacey, M. *et al.* The epidermal growth factor-like domains of the human EMR2 receptor mediate cell attachment through chondroitin sulfate glycosaminoglycans. *Blood* **102,** 2916–2924 (2003).

46. Stainier, D. Y. *et al.* Mutations affecting the formation and function of the cardiovascular system in the zebrafish embryo. *Development* **123,** 285–292 (1996).

47. Tabin, C. J. & Vogan, K. J. A two-cilia model for vertebrate left-right axis specification. *Genes Dev* **17,** 1–6 (2003).

48. Wallgard, E. *et al.* Identification of a core set of 58 gene transcripts with broad and specific expression in the microvasculature. *Arterioscler Thromb Vasc Biol* **28,** 1469–1476 (2008).

49. Wang, G. *et al.* The Rho kinase Rock2b establishes anteroposterior asymmetry of the ciliated Kupffer's vesicle in zebrafish. *Development* **138,** 45–54 (2011).

50. West, J. D., Leask, R. & Green, J. F. Quantification of the transition from oocyte-coded to embryo-coded glucose phosphate isomerase in mouse embryos. *J Embryol Exp Morphol* **97,** 225–237 (1986).

Chapter 3

Effects of *eltd1* knockdown on zebrafish hematopoietic and cardiovascular development

Introduction

G-protein-coupled receptors (GPCRs) play a key role in the regulation of the cardiovascular system. G protein-coupled receptors have been successfully targeted by numerous therapeutics including drugs that have transformed the management of cardiovascular disease. They regulate a variety of activities in cardiovascular system, from heart rate and contractility to myogenic tone of blood vessels (Kauffenstein *et al*., 2012). The fact that GPCRs can respond to variety of secreted hormones, peptides, proteins, lipids, and other compounds allows for long-range signaling.

In contrast to classical GPCRs, *Adhesion* GPCRs appear to participate in short range interactions with molecules on neighboring cells or in the extracellular matrix. Though they are widely expressed throughout the cardiovascular system (see Table 2, Chapter 1), their precise functions within it remain elusive. It is hypothesized that AdGPCRs play an important role in organizing cells into tissues; that is, orchestrating the polarity, cell-cell contacts, and spatial arrangement that add complexity to living tissues and maximize their intended functions. This activity is most likely to be observed during embryonic development, when organ systems are being rapidly assembled and tissues are becoming intertwined with one another.

During embryonic development, endothelial cells assemble the arborized tubular network of vessels that transports fluids, nutrients, blood cells, chemical messengers, and gasses to almost all tissues throughout the vertebrate body. Homotypic endothelial cell-cell adhesion is particularly important for the correct formation, networking and remodeling of vessels, and endothelial cells are remain in contact with one another by a complex network of transmembrane adhesion proteins anchored to the actin cytoskeleton.

How these interactions are initiated is not particularly well-understood and represents one question where the mysterious *Adhesion* GPCRs may be relevant.

Intimately related to the cardiovascular system are hematopoietic cells, most of which use blood vessels as a primary means of traversing through the vertebrate body. While much is understood about the signaling that regulates proliferation, differentiation, function, and survival of the various types of hematopoietic cells, less is known about the short-range interactions that regulate hematopoietic progenitors residing in stem cell niches.

The zebrafish represents an excellent model for the study of developmental angiogenesis and hematopoiesis due to the transparency of embryos and their ability to persist for several days even with severe defects of the blood and cardiovascular systems. We employed antisense oligonucleotide morpholinos targeting the zebrafish *eltd1* transcript in order to study the cardiovascular and hematopoietic roles of Eltd1. Our studies indicate that Eltd1 may regulate the development of hematopoietic stem cells (HSC) during zebrafish embryogenesis. In addition, we show that Eltd1 regulates the formation of several specific vascular structures in the zebrafish embryo, which may contribute to a hematopoietic defect. Additionally, we present data from cell-culture-based experiments aimed at characterizing the cellular and molecular mechanisms underlying Eltd1 function. These experiments represent a foundation and toolkit for further elucidation of Eltd1 function and signaling in the cardiovascular system.

Results

Eltd1 is expressed in mouse hematopoietic stem cells

We initially became interested in Eltd1/ETL while profiling GPCR expression in hematopoietic stem and progenitor cells (HSPC), with the goal to identify novel regulators of hematopoiesis. We isolated adult mouse $lin^{-}sca\text{-}1^{+}c\text{-}kit^{+}$ (LSK) cells from bone marrow using fluorescence-activated cell sorting (FACS). The LSK population contains hematopoietic progenitors that are able to reconstitute the bone marrow of a lethally-irradiated mouse in both the short- and long-term. Employing a qPCR-based array strategy with primer-probe sets that were designed and validated in our laboratory (Regard *et al*., 2008), we analyzed the GPCR repertoire of these cells. This analysis revealed several receptors with unknown contributions to hematopoiesis were abundantly expressed in LSK cells and enriched significantly compared to whole bone marrow, arguing for a potentially specific role in HSPC function (Figure 1).

Eltd1 was the second-most abundant GPCR we profiled in LSK cells, and expressed at levels several-folds higher than GPCRs with known roles in HSPC function, such as CXCR4, GPR105, and prostaglandin E receptor 3 (PTGER3). Further, *eltd1* transcript was 70-fold enriched in LSK cells compared to whole bone marrow. We additionally observed similar Eltd1 expression levels in HSPC isolated using an alternate strategy that also yields an enriched long-term repopulating subset of cells (SLAM, $CD150^{+}CD48^{-}CD41^{-}$). These data indicate that Eltd1 is abundantly expressed in bone marrow HSPC.

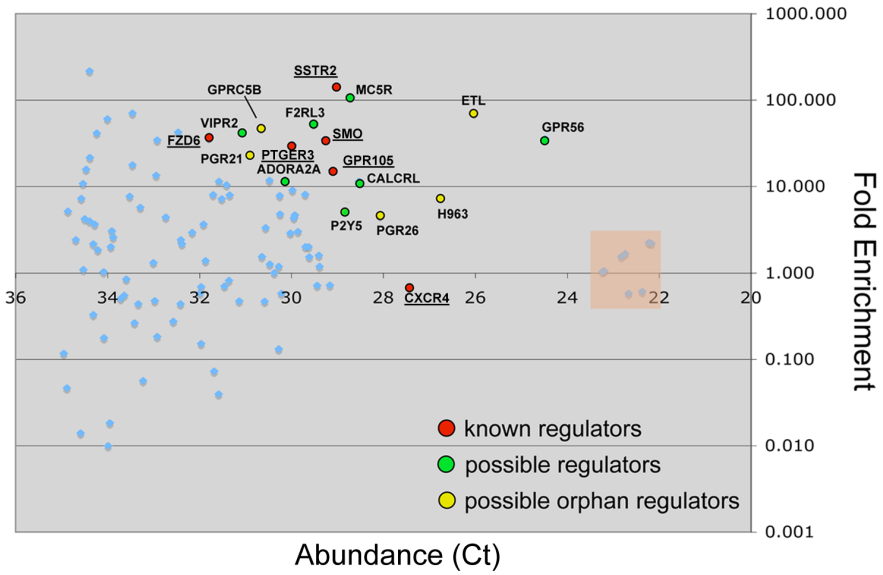

Figure 1. *Eltd1* expression in mouse HSPC isolated from adult bone marrow. LSK ($lin^-sca\text{-}1^+c\text{-}kit^+$) cells were isolated from adult mouse bone marrow and subjected to GPCR profiling. Results are plotted as abundance (cycle to threshold, Ct value, x-axis) vs. fold-enrichment as compared to total bone marrow (y-axis). Genes falling on the upper right of this graph are both abundantly expressed and enriched in LSK cells, and therefore of particular interest. Selected known regulators of HSPC are indicated with red circles and underlined. The green circles designate de-orphanized receptors with no established function in hematopoiesis. Orphan GPCRs of interest, including Eltd1, are noted with yellow circles. The shaded box indicates three duplicate housekeeping genes used as loading controls.

Knockdown of Eltd1 in zebrafish abrogates HSC development

To screen for the potential role of Eltd1 in HSPC function, we utilized morpholino-mediated knockdown in zebrafish embryos to assess how loss-of-function may impact hematopoietic progenitors. The transgenic zebrafish line *Tg(CD41:GFP)* expresses green fluorescence protein (GFP) under the control of the CD41 promoter and labels thrombocytes and early hematopoietic stem cells in the developing embryo (Lin *et al.*, 2005). Embryos injected with a splice-blocking morpholino targeting *eltd1* ($Eltd1_{ex10}MO$) exhibited significantly reduced GFP fluorescence in the trunk region, a site of definitive hematopoiesis in the zebrafish. Thrombocytes (GFP^{hi}), which are not thought to arise during the primitive wave of hematopoiesis, were nearly completely absent in morphants. GFP^{lo} cells, considered to be HSPC, were present (Figure 2A).

We sought to quantify thrombocytes and HSPC from control and Eltd1$_{ex10}$ morphants by homogenizing pooled 48 hpf embryos into a single-cell suspension and performing flow cytometry. GFP^{+} cells from control embryos were easily segregated into GFP^{hi} and GFP^{lo} populations. We enumerated approximately 230 HSC and 15 thrombocytes per control embryo. In contrast, Eltd1$_{ex10}$ morphants exhibited approximately a 2-fold reduction in both cell populations. This suggests that Eltd1 regulates HSPC function during the definitive wave of hematopoiesis in zebrafish.

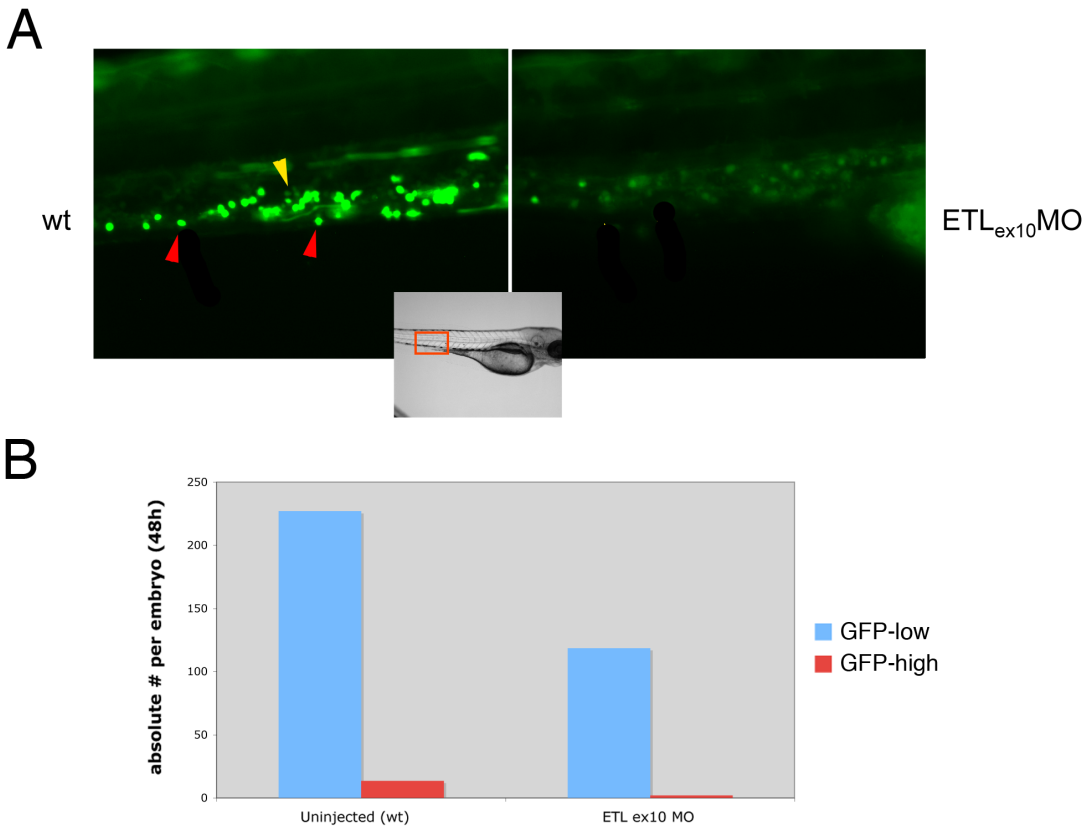

Figure 2. Knockdown of zebrafish Eltd1 impairs caudal hematopoiesis. (A) Epiflourescence images of control 48 hpf *Tg(CD41:GFP)* embryos and Eltd1$_{ex10}$ morphants. *Tg(CD41:GFP)* express GFP in HSC (dim) and thrombocytes (bright). Red arrows indicate examples of thrombocytes (GFP^{hi}), and the yellow arrow indicates an example of a HSC (GFP^{lo}). The inset indicates the region of the embryo that is depicted in fluorescence images. **(B)** Quantification of caudal hematopoiesis in control and Eltd1$_{ex10}$ morphants. Embryos were subjected to tissue disruption and FACS analysis to enumerate GFP+ hi and lo cells. Results are from 50 pooled control and morphant embryos and graphed as absolute numbers of GFP+ cells per embryo.

Eltd1 morphants exhibit cardiovascular failure

While studying the impaired hematopoiesis in Eltd1 morphants, we noticed that these embryos developed signs of cardiovascular failure as early as 30 hpf. The earliest symptom was a weak heartbeat that appeared to exhibit abnormal contractions compared to control morphants. Eltd1 morphants additionally developed rapidly progressive pericardial edema evident as early as 36 hpf that resulted in tamponade of the heart and a "string heart" phenotype by 4-5 dpf. These cardiac phenotypes were accompanied by a massive dilation of the caudal vein (CV) (Figure 3), resulting in a vessel that exhibited retarded flow and blood cell stasis.

A dilation of the swimbladder also became strikingly evident by 3-4 dpf. The swimbladder is a gas-filled organ postulated to be the teleost homolog of the mammalian lung on the basis of morphological and molecular similarities (Perry *et al*., 2001; Winata *et al*., 2009). We termed this phenotype "double-bubble" to reflect the two bubbles arising from pericardial edema and swimbladder dilation. 100% of morphants receiving the higher dose of Eltd1$_{ATG}$MO (1.2 ng) exhibited swimbladder dilation.

Specificity of the observed cardiovascular phenotypes was confirmed by the fact that both morpholinos produced all of the cardiovascular defects described in Figure 3. However, the Eltd1$_{ex10}$MO required a ten- to twenty-fold higher dose to produce the same effects as the Eltd1$_{ATG}$MO (data not shown).

These phenotypes suggest Eltd1 may regulate multiple aspects of cardiovascular development. The broad cardiovascular expression that has been reported for Eltd1 (Nechiporuk *et al*., 2001; Wallgard *et al*., 2008) supports this. In addition, data from our laboratory has quantified extremely high abundance of Eltd1 transcript in mouse lung

(Regard *et al*., 2008), and thus the swimbladder phenotype is not surprising. In sum, the cardiovascular phenotypes we observe in Eltd1 morphants are generally consistent with published expression data from mouse and suggest that Eltd1 expression and function in the cardiovascular system may be conserved from fish to mammals.

A

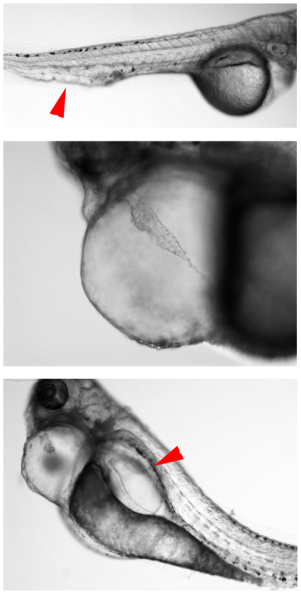

B

30 hpf	Weak heartbeat	Dilated CV	Blood pooling in CV lumen
Control MO	3/17 18%	1/17 6%	1/17 6%
$ETL_{ATG}MO$ 0.4 ng	14/33 42%	19/33 58%	15/33 45%
$ETL_{ATG}MO$ 1.2 ng	14/22 64%	14/22 64%	11/22 50%

76 hpf	Dilated CV	Blood pooling in CV lumen	Pericardial edema	Dead
Control MO	0/17, 0/16 0%	1/17, 0/16 0%	1/17, 0/16 0%	1/17
$ETL_{ATG}MO$ 0.4 ng	12/33, 12/31 39%	11/33, 11/31 35%	17/33, 17/31 55%	2/33
$ETL_{ATG}MO$ 1.2 ng	5/22, 5/15 33%	5/22, 5/15 33%	13/22, 13/15 87%	7/22

5 dpf	"Double bubble" phenotype	Normal	Dead
Control MO	0/17, 0/16 0%	16/17, 16/16 100%	1/17
$ETL_{ATG}MO$ 0.4 ng	19/33, 19/30 63%	11/33, 11/30 37%	3/33
$ETL_{ATG}MO$ 1.2 ng	15/22, 15/15 100%	0/22, 0/15 0%	7/22

Figure 3. Cardiovascular failure in $Eltd1_{ex10}$ and $Eltd1_{ATG}$ morphants. (A) Cardiovascular phenotypes observed in $Eltd1_{ex10}$ morphants at 76 hpf and 5 dpf. Failed caudal vein (CV) plexus in 76 hpf embryo, top panel. Pericardial edema in 5 dpf embryo, middle panel. "Double bubble" phenotype in 5 dpf embryo, bottom panel, with swimbladder noted by the arrowhead. **(B)** Quantification of cardiovascular

phenotypes in 30 hpf (top), 76 hpf (middle), and 5 dpf (bottom) control and Eltd1$_{ATG}$ morphants. The same embryos are followed through all three timepoints. Percentages shown are calculated using embryos alive at the time of scoring.

Eltd1 is expressed in mouse endothelium

While profiling murine tissues and cells for GPCR expression, we found Eltd1 to be expressed abundantly in neonatal microvascular endothelium purified from skin (Figure 4A). Levels of Eltd1 transcript reached threshold within 1-2 cycles of GPCRs that have known roles in endothelial cell function, including PAR1 (F2R) (Griffin *et al*., 2001), S1P1 (EDG1) (Liu *et al*., 2000), and Frizzled 4 (FZD4) (Descamps *et al*., 2011).

Because the presence of RNA is not necessarily an indicator of protein expression and functional relevance, we asked whether Eltd1 protein can be visualized in murine vasculature. We found that anti-Eltd1 antibody reacted strongly with the vasculature of whole-mount mouse tracheal preparations, overlapping significantly with the expression pattern exhibited by PECAM. Intriguingly, while the expression levels of PECAM were largely consistent between arterioles, venules, and capillaries, Eltd1 protein seemed to vary in expression levels across different vessels. From this experiment we are unable to conclusively determine whether Eltd1 protein is found on endothelial cells, vascular smooth muscle cells (VSMCs), or both. However, immunostaining for smooth muscle α-actin would serve to clarify this.

A

Gene	Ct value
B-ACTIN	16.126562
B-ACTIN	16.247782
CYCLOPHILIN	16.76797
CYCLOPHILIN	16.771036
MS9	17.966215
MS9	18.053833
GAPDH	18.455254
GAPDH	18.896454
F2R	21.135649
EDG1	21.295341
P2Y5	21.720003
KIAA0758	22.072834
EDG3	22.29946
RAI3	22.616604
CD97	22.79398
ETL	22.807127
TM7SF1	23.126211
EDG5	23.26157
GPR10	23.389374
AGR9	23.570963
FZD4	23.5889
TM7SF3	23.743725
HTR2A	24.168465
CXCR4	24.185343
PGR10	24.202919
TPRA40	24.20949
GPR23	24.217594
HTR1B	24.284704
FZD2	24.306892
FZD6	24.328295
ADORA2B	24.389568
GPR56	24.400545
LEC1	24.440865
PGR26	24.501728
LEC2	24.595057
PTGIR	24.620663
EDG2	24.630291
FZD1	24.687908
PTGER1	24.728373
PGR21	24.761179
RDC1	24.990774

B

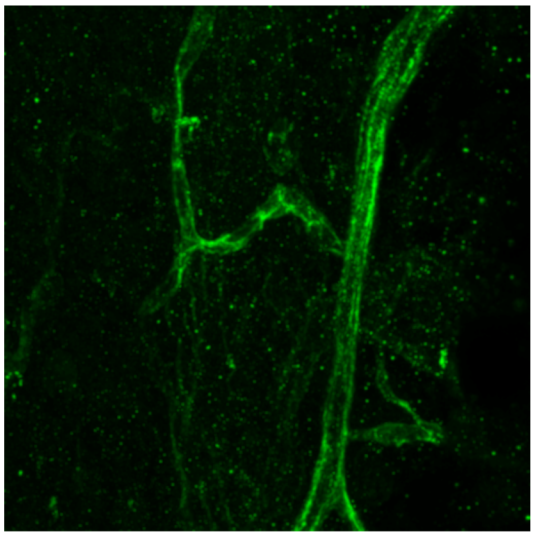

anti-ETL

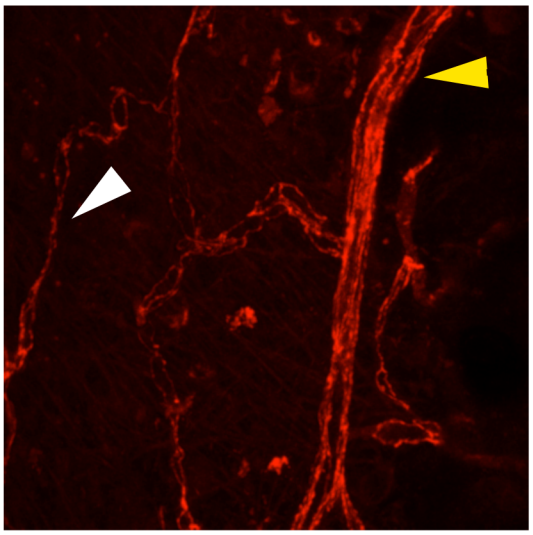

anti-PECAM

Figure 4. Eltd1 expression in mouse microvasculature. (A) GPCRs abundantly expressed in mouse endothelial cells purified from neonatal skin. B-actin, cyclophilin, MS9, and GAPDH are housekeeping genes in the array. GPCRs with known roles in endothelial cells are highlighted in green. **(B)** Fluorescence immunostaining of Eltd1 protein expression in mouse trachea. 100x magnification. Eltd1 expression pattern (top panel) largely overlaps that of PECAM (bottom panel). Yellow arrowhead indicates an arteriole. White arrowhead indicates a capillary.

Eltd1 morphants exhibit defects in the angiogenesis of several vascular structures

Given the published data on murine *eltd1* expression and our own observations of Eltd1 protein expression, we investigated the vascular anatomy of eltd1 morphants.

The intersegmental vessels (ISVs) are a frequent site of vascular study because of their metameric organization and relatively simple anatomy. At approximately 22 hpf, endothelial cells sprout from the dorsal aorta and grow dorsally along the intersomitic fissures to the dorsal roof of the neural tube, forming the segmental arteries (SA). They are joined approximately 10 hours later by sprouts from the posterior cardinal vein (PCV), which anastomose with some segmental arteries to produce segmental veins (SV) (Isogai *et al*., 2003; Yaniv *et al*., 2006). Together, the SAs and SVs are described as the ISVs. The primary mechanism for ISV formation is sprouting angiogenesis. Using *Tg(Flk-1:eGFP)* transgenic zebrafish (Jin *et al*., 2005), we found ISV formation in *eltd1* morphants to be normal, with vessels sprouting from the dorsal aorta and migrating dorsally. At doses of morpholino approaching those that produce mild convergence-extension/trunk defects, we noticed a disorganization of ISVs as opposed to the sharply angled metameric pattern that results from migration of the sprout between the chevron-shaped somites. This was likely due to trunk patterning defects though we cannot yet exclude a cell-autonomous role for Eltd1 in ISV patterning. Overall, these observations suggest that Eltd1 does not regulate sprouting angiogenesis of the ISVs but may regulate ISV patterning via non-cell-autonomous mechanisms.

We were also able to rule out a role for Eltd1 in vasculogenesis, the process by which *de novo* vessels form via the specification and coalescence of angioblasts. As is thought to be true for the axial vessels of all vertebrates, both the dorsal aorta (DA) and

the posterior cardinal vein (PCV) form by this process. We observed that the DA and PCV in Eltd1$_{ATG}$ and Eltd1$_{ex10}$ morphants arose normally.

We additionally looked to characterize vascular regions independent of the trunk and tail, where defects are less likely to be secondary to the convergence-extension phenotype of *eltd1* morphants. In the head, we found vasculature to be underdeveloped or abnormally patterned as compared to control morphants, which was evident at 32 hpf. Although the middle cerebral vein (MCeV) appeared to form normally in *eltd1* morphants, vascular development anterior to this vessel was severely impaired, with vessels such as the mesencephalic vein (MsV) and prosencephalic artery (PrA) absent from *eltd1* morphants at 48 hpf (Figure 5A). Additionally, the central arteries (CtA) were severely underdeveloped at 48 hpf, and we frequently observed intracranial hemorrhages at this site when Eltd1 morpholinos were injected into *Tg(Flk-1:eGFP)*;*Tg(gata-1:dsRed)* double-transgenic embryos. These data suggest Eltd1 may regulate the angiogenesis of specific cranial vessels.

The common cardinal veins (CCV) are located in the anterior trunk of the embryo, where they wrap around the yolk, converging craniofacially at the sinus venosus to connect to endocardial endothelial cells of the heart (Isogai *et al*., 2001). These vessels return venous blood to the heart. In *eltd1* morphants, we observed the CCVs to be underdeveloped and/or delayed (Figure 5A).

Finally, the subintestinal vein (SIV) of *eltd1* morphants failed to descend from the PCV as it did in control embryos (Figure 5B). At 48 hpf, it was absent from *eltd1* morphants. The SIV is additionally notable in that it does develop and descend in *silent heart* mutants, which lack a heartbeat and do not have blood flow (Montero-Balaguer *et al*.,

2009).

Our results indicate that most gross vascular patterning in the zebrafish embryo is not dependent on Eltd1. However, Eltd1 may regulate the angiogenesis of specific vessels in the head and anterior trunk regions of the embryo.

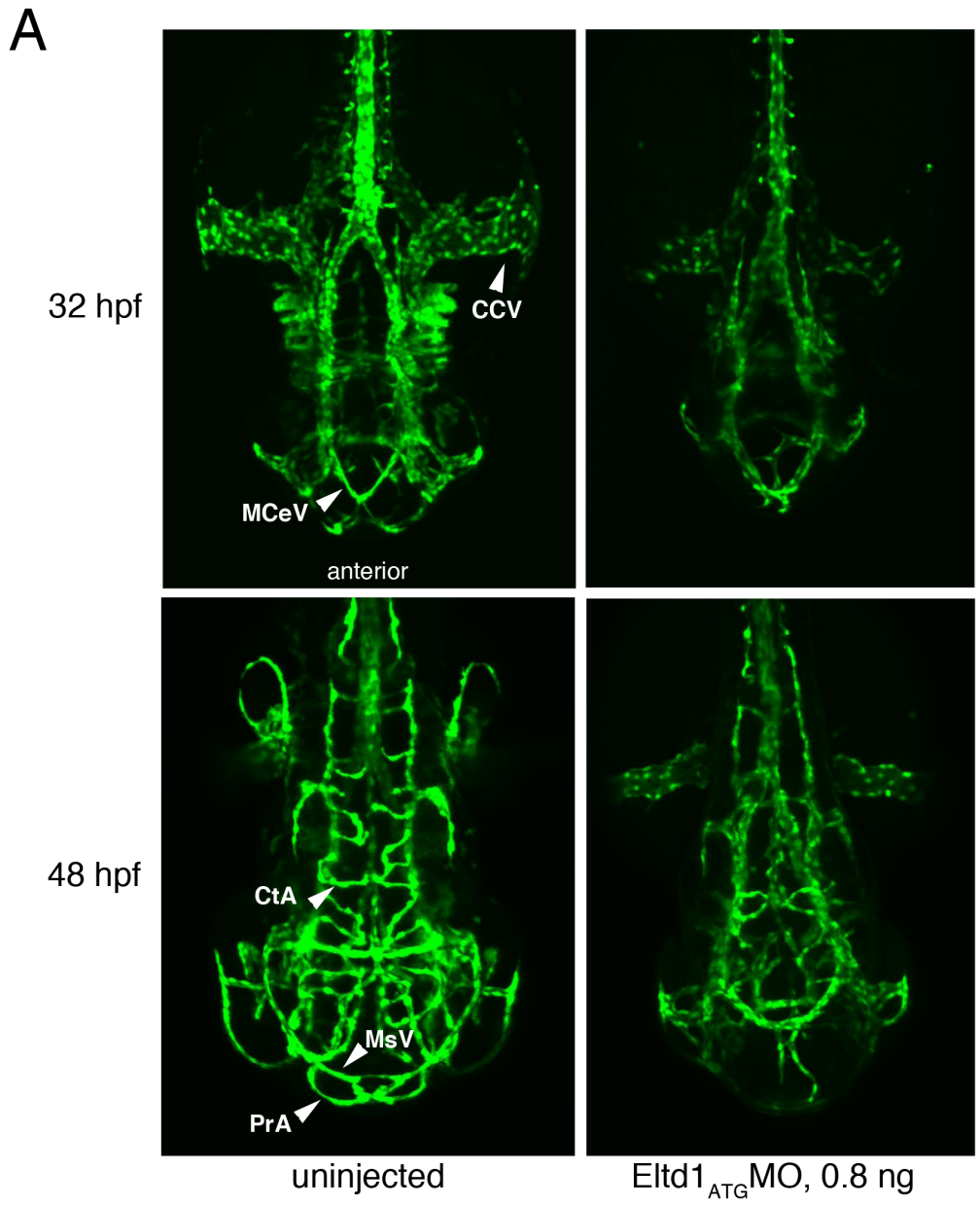

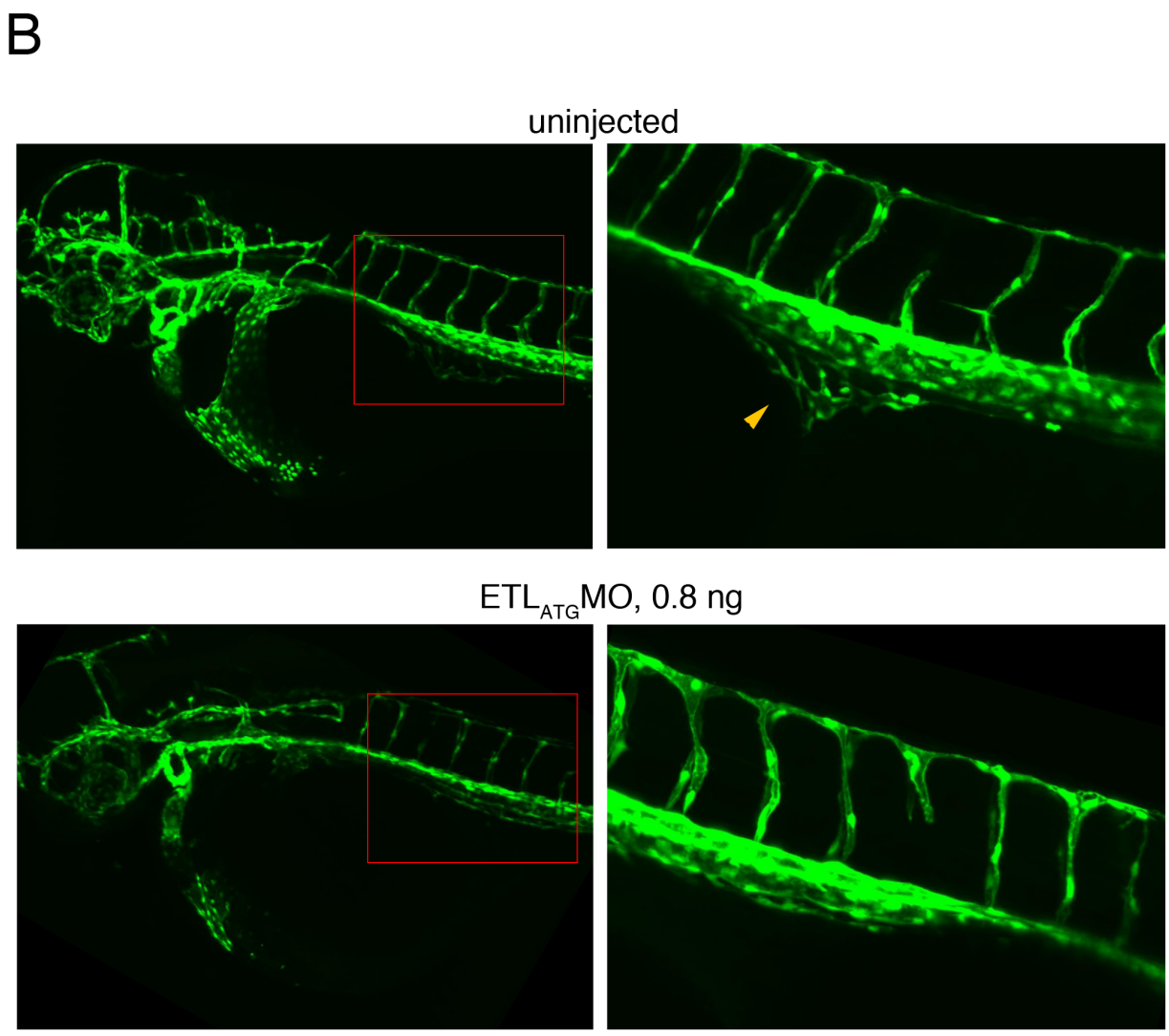

Figure 5. Impaired vascular development in Eltd1$_{ATG}$ morphants. (A) Confocal Z-stack immunofluorescence images of coronal slices through 32 hpf (top row) and 48 hpf (bottom row) *Tg(Flk-1:eGFP)* embryos that were uninjected or injected with 0.8 ng of Eltd1$_{ATG}$MO. CCV, common cardinal vein; MCeV, middle cerebral vein; CtA, central arteries; MsV, mesencephalic vein; PrA, prosencephalic artery. **(B)** Confocal Z-stack immunofluorescence images of sagittal slices through 48 hpf *Tg(Flk-1:eGFP)* embryos that were uninjected (top row) or injected with 0.8 ng of Eltd1$_{ATG}$MO (bottom row). The subintestinal vein (SIV) is indicated by the arrowhead. The right column shows a 20x magnification of the region outlined by the red boxes in a different embryo.

The caudal vein in eltd1 morphants does not form a vascular plexus

We noted that 64% of *eltd1* morphants exhibited a dilated caudal vein (CV) at 30 hpf. To study this phenomenon in greater detail, we conducted time-lapse confocal fluorescence imaging of *Tg(Flk-1:eGFP) eltd1* morphants. In control embryos at 24 hpf, the caudal vein was a large single vessel. Endothelial cells comprising this vein

displayed protrusive activity over the next several hours, forming dynamic filopodia that extended and retracted to form connections around the vessel. These cellular behaviors resulted in the formation of a vascular plexus in the posterior tail, occupying the space between the caudal vein, and dorsal aorta. In $Eltd1_{ATG}$ morphants, the endothelium could be seen extending filopodia but these seemed to retract prior to making sustained contact with other cells. This led to the failure of caudal plexus formation, resulting in the persistence of the primitive, dilated caudal vein.

The caudal plexus, along with associated mesenchymal cells, serves as the migratory target for hematopoietic stem cells originating in the ventral wall of the dorsal aorta. These cells take up residence amongst the endothelial cells of the caudal plexus, initiating definitive hematopoiesis at this site (Jin *et al*., 2007). The abrogated formation of the caudal plexus in *eltd1* morphants is thus likely responsible for the lower numbers of HSPC we observed.

Mouse Eltd1 localizes to the plasma membrane and cell-cell contacts when expressed in HEK293T cells

Given the potential for studying Eltd1 function in cell culture assays of angiogenesis, we generated C-terminal fluorescent protein fusions for real-time visualization of Eltd1 protein. eGFP and Ruby were fused to the C-terminus of Eltd1, separated by a 3x SGA linker to allow for flexibility of the fusion protein. As expected, mEltd1-eGFP localized to plasma membrane and cytoplasmic vesicles when transfected into HEK293T cells. eGFP fluorescence was particularly strong at cell-cell junctions (Figure 6). This was observed whether two contacting cells were both $eGFP^+$ or not, implying that homotypic interactions *in trans* are not the cause of mEltd1-eGFP

concentration at the cell-cell interface. The overexpression of mEltd1-eGFP had no obvious effects on the proliferation, survival, morphology, or motility of HEK293T cells during routine culture that we could observe.

We next moved to expressing these constructs in more relevant cell types. Given the reported expression of *Eltd1* in mouse smooth muscle, we transfected the MOVAS (mouse aortic smooth muscle) cell line with mEltd1-eGFP. Although MOVAS cells expressed the fusion protein at far lower levels than HEK293T cells, we were still able to observe localization of mEltd1-GFP at sites of filopodial contact between cells (Figure 6). Our subcellular localization results from HEK293T and MOVAS cells suggest Eltd1 is recruited to cell-cell junctions, either by a ligand present on the contacting cell or by cis binding partners that localize to sites of cell-cell contact.

We were unable to successfully express mEltd1-eGFP or mEltd1-Ruby constructs in several types of endothelial cells. MS-1 cells (miles seven, a mouse pancreatic microvascular endothelial cell line), EA.hy926 cells (a human endothelial cell line derived from umbilical vein), and HUVEC (human umbilical vein endothelial cells) all failed to show fluorescence after transfection. Given that endothelial cells are notoriously difficult to transfect with common transfection reagents, we cloned the mEltd1-FP into a lentivector for stable and efficient transduction. The mEltd1-eGFP lentivirus efficiently transduced HEK293T cells, and control lentivirus harboring eGFP alone efficiently transduced all three endothelial cell types. However, we were again unable to achieve expression of mEltd1-eGFP in any of the three endothelial cell types, though we did note cells that transiently exhibited some GFP-positivity quickly detached from the dish and appeared to undergo apoptosis. Several possibilities may explain these

observations. The most straightforward explanation is that Eltd1-eGFP protein is specifically toxic to endothelial cells in the large doses typically delivered during transfection. However, lowering the amount of DNA in transient transfections did not have any effect. Additionally, transduction with lentivirus typically leads to the random integration of only a few copies of the transgene into the transduced cell's genome. Another possibility is that the cultured endothelial cells we were using do not possess the required biosynthetic machinery to process or correctly fold the nascent mEltd1-eGFP protein. A more interesting hypothesis is that endothelial cells are particularly sensitive to the "on" state of Eltd1, which may arise as a result of overexpression as for many GPCRs. This may not be well-tolerated by endothelial cells in a non-physiologic two-dimensional context.

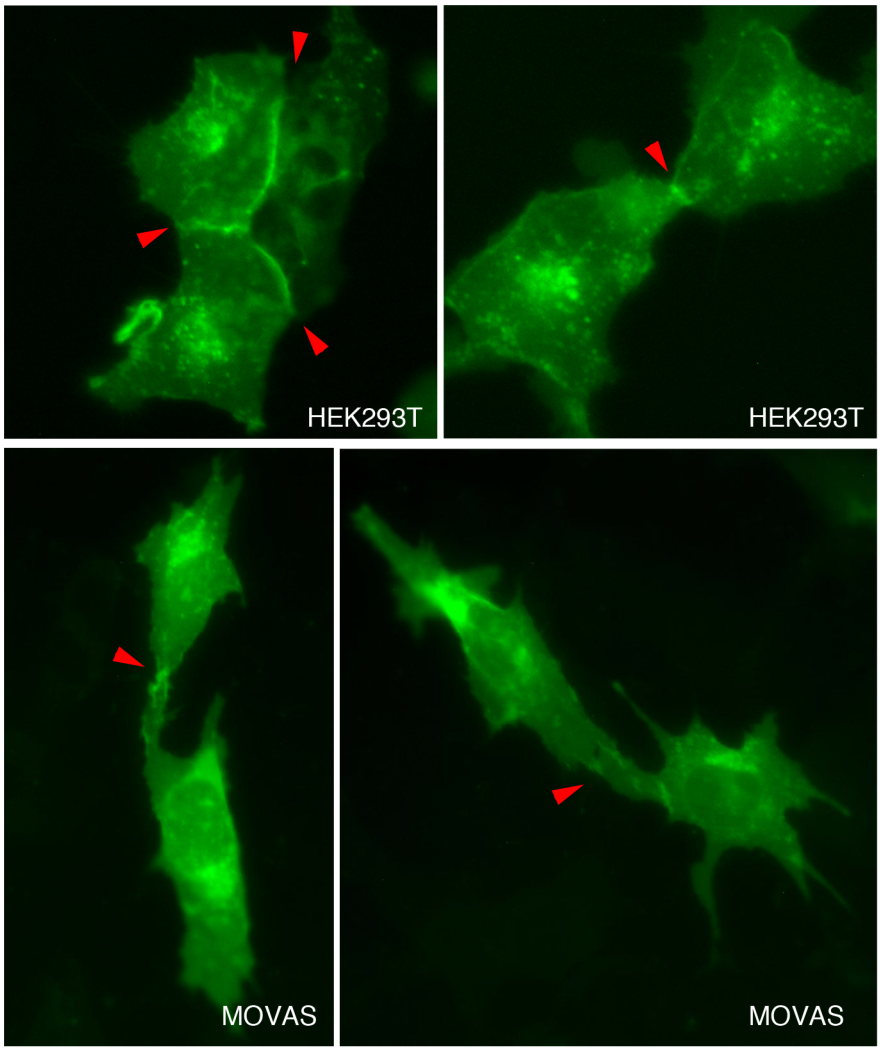

Figure 6. Subcellular localization of Eltd1 in HEK293T and MOVAS cells. mEltd1-GFP was transfected into HEK293T cells (top) and MOVAS (mouse aortic smooth muscle cells, bottom) cells on fibronectin-coated glass coverslips. The cells were replated and imaged ~80h after transfection. Arrowheads indicate GFP fluorescence at sites of cell-cell contact.

GPS cleavage is dispensable for Eltd1 localization to plasma membrane in HEK293T cells

A long-standing controversy in the *Adhesion* GPCR field has centered around whether cleavage at the GPS is required for trafficking of the receptor to the plasma membrane. To address this question for Eltd1, we generated two mutant mEltd1-eGFP

constructs with amino acid substitutions of the P1 and P1' residues at the GPS cleavage site (L454A and T455G). These mutations would be predicted to inhibit autoproteolysis of the receptor. Both mEltd1-eGFP(L454A) and mEltd1-eGFP(T455G) localized to the plasma membrane and cell-cell contacts in HEK293T cells, indistinguishable from the receptor with an unmutated GPS (Figure 7). Western blotting of whole cell lysates confirmed that the two mutant proteins were not cleaved. Thus, GPS cleavage is dispensable for trafficking Eltd1 to the plasma membrane in HEK293T cells. This result is direct visual confirmation of what was previously indirectly observed by Nechiporuk *et al*. with a similar mutant of rat Eltd1 (2001).

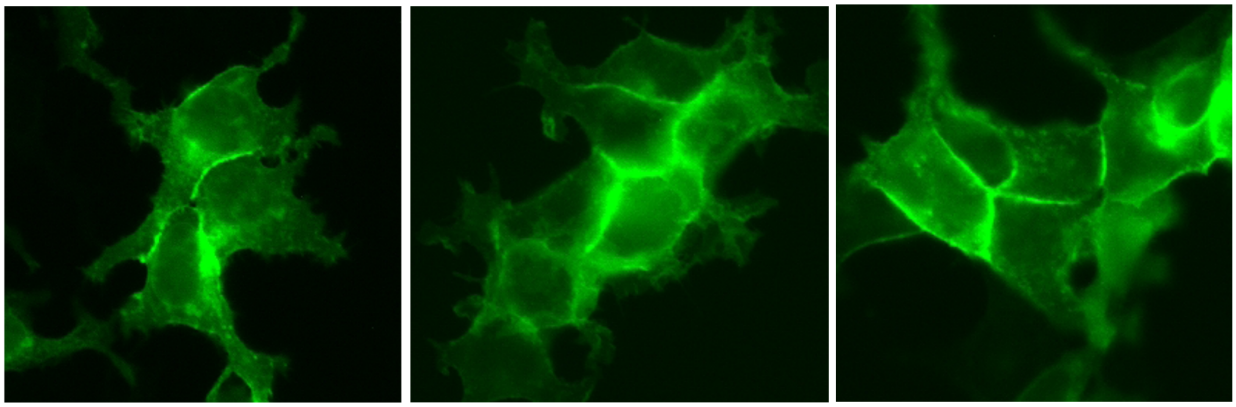

Figure 7. Subcellular localization of Eltd1 GPS cleavage site mutants. mEltd1-eGFP constructs were transfected into HEK293T cells on fibronectin-coated glass coverslips. The cells were replated and imaged ~72 h after transfection.

Eltd1 co-localizes with Vangl2 in HEK293T cells

The left-right asymmetry and convergence-extension defects we reported in Chapter 2 highlight the planar cell polarity (PCP) pathway as a potential interacting signaling pathway for Eltd1. Studies of mouse epidermal planar polarization have shown Celsr1, an AdGPCR, interacts physically with the core PCP protein Vangl2, and the two

proteins are dependent on one for trafficking to the membrane (Devenport *et al*., 2008). We thus hypothesized that if Eltd1 is indeed a participant in the PCP pathway, Vangl2 may be a binding partner. We tagged the N-terminus of mVangl2 with monomeric Ruby (mRuby-mVangl2) and co-transfected it with mEltd1-eGFP into HEK293T cells. Both fusion proteins were localized to the plasma membrane and to the tips of filopodia, and appeared to co-localize at cell-cell junctions (Figure 8), hinting at a possible physical interaction. Alternatively, they may simply be recruited to similar membrane subdomains or junctional complexes. Pilot attempts to co-immunoprecipitate eGFP-Vangl2 with FLAG-tagged Eltd1 have been unsuccessful thus far.

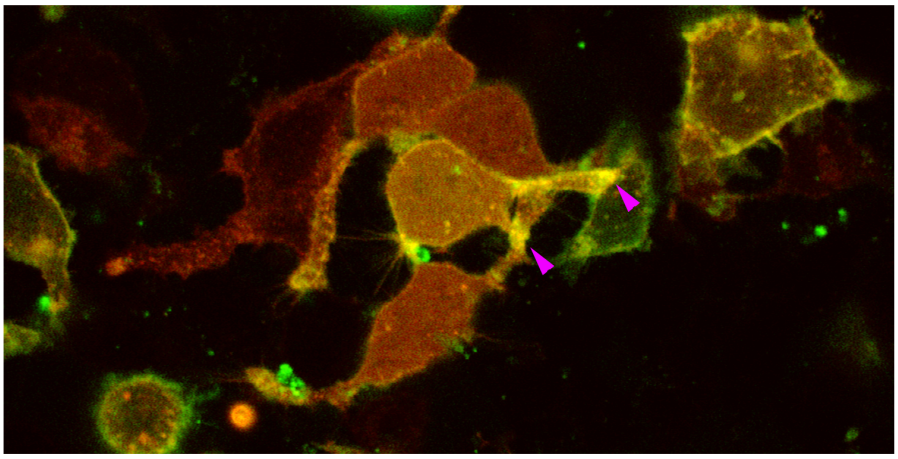

Figure 8. Co-localization of Eltd1 and Vangl2 in HEK293T cells. mEltd1-eGFP and mRuby-mVangl2 constructs were transfected into HEK293T cells on fibronectin-coated glass coverslips. The cells were replated and imaged ~48 h after transfection.

Discussion

In this work we have described cardiovascular *eltd1* morphant phenotypes, which outline a potential role for this orphan receptor in the regulation of hematopoiesis, cardiac development, angiogenesis of specific vascular regions, and development of the

swimbladder. Some of these phenotypes may be secondary to the early developmental defects reported in Chapter 2. However, they are likely independent of the convergence-extension and LR asymmetry defects we reported in Chapter 2 (with the exception of trunk defects contributing to disorganization of ISVs), given that the low doses (0.4 – 1.2 ng) of $Eltd1_{ATG}$ morpholino that resulted in cardiovascular phenotypes did not produce the early developmental defects.

More likely is that some of these phenotypes are secondary to one another. For example, angiogenesis, at least in some vessels, has been hypothesized to be flow-dependent on the basis of endothelial gene expression regulation by fluid shear stress and the response of endothelial cells to pulsatile flow (Malek & Izumo, 1995; Cullen *et al*., 2002). A reduction in cardiac output due to a primary cardiac defect in *eltd1* morphants might result in secondary vascular defects, such as underdeveloped cranial vasculature or the failed remodeling of the caudal plexus. In such an instance, the hematopoietic defect we observe could be considered tertiary to a primary heart defect. Alternatively, given that Eltd1 is expressed in heart, blood vessels and HSPC, it may have cell-autonomous roles in all of these tissues. Transplantation of *eltd1* morphant endothelium into wild-type embryos (and vice versa) will begin to address the cell autonomy of the cardiovascular phenotypes observed.

In this work, we did not attempt to study a potential primary heart defect in *eltd1* morphants, although we did note that hearts of morphants beat slowly and abnormally. A recent study has addressed the role of Eltd1 in cardiac function and reported that loss of Eltd1 in mice leads to exacerbated cardiac hypertrophy in response to aortic-banding-induced pressure overload (Xiao *et al*., 2012). Notably, the authors did not report any

defective angiogenesis, edema, or other signs related to cardiovascular dysfunction, in contrast to our results from zebrafish. However, this was the first published study using *eltd1* knockout mice, and as such there may be other, easily overlooked phenotypes present. The lungs would be particularly interesting to inspect and functionally challenge in the knockout animals. Given that Eltd1 is expressed abundantly there and that *eltd1* morphants exhibited a swimbladder phenotype, it is possible that Eltd1 knockout mice harbor some non-lethal defect in tissue organization in the lungs.

The idea that Eltd1 may be involved in regulating tissue polarity, possibly by interacting with PCP components, is an exciting prospect because it suggests PCP may be active in endothelium. Indeed, PCP components are known to be expressed widely, and though the structure of blood vessels makes it conceptually difficult to grasp how such a pathway might operate, several lines of investigation are indicating that PCP proteins do indeed have a role in angiogenesis (Cirone *et al*., 2008; Descamps *et al*., 2011; Sundberg *et al*., 2011). From this perspective, the defect we observe in the common cardinal vein (CCV) of *eltd1* morphants is particularly intriguing, in that it is also reported to occur in *pipetail* mutants (*wnt5a*) (Cirone *et al*., 2008). *Pipetail* mutants also exhibit loss of the anterior-most vessels of the head. Further supporting the role for PCP in endothelium, endothelial cells produce wnt5a, which promotes their growth and survival (Wright *et al*., 1996).

Materials and Methods

Generation of cDNA. Total RNA was isolated from purified endothelial cells with Trizol. The RNA was further purified using the RNEasy Mini Kit (Qiagen). cDNA was synthesized using the iScript cDNA synthesis kit (Bio-Rad).

qPCR profiling. Primer-probe sets used for GPCR profiling have been described (Regard *et al*., 2008). qPCR assays were performed in a 384-well format with an ABI7900HT, Platinum qPCR mix (Invitrogen) and 10 ml reactions. Cycle threshold (Ct) values were collected at 0.2 for all samples; Ct values for individual GPCRs were compared to Ct values for four internal controls (B-actin, cyclophilin, GAPDH, and ribosomal protein S9).

Zebrafish strains and husbandry. Wild-type AB, wild-type TL, *Tg(cmlc2:GFP)* (Huang *et al*., 2003), *Tg(Flk:GFP)* (cite), and *Tg(Gata-1:dsRed)* (cite) zebrafish (*Danio rerio*) strains were raised in the SCVRB facility at 28.5˚C. Embryos for experiments were obtained from natural matings and cultured at 28˚C – 32˚C in sterile-filtered fish water. The developmental stages of embryos were determined according to morphological criteria (Kimmel *et al*., 1995). Embryos were manually dechorionated for experiments using #5 fine forceps (Fine Science Tools, Foster City, CA).

Microscopy. For time-lapse imaging, live zebrafish embryos were manually dechorionated, anesthetized with 0.1% w/v tricaine (Sigma), and mounted in 50 µl drops of 1.2% low-melt agarose (Sigma) on glass slides or in glass-bottomed 35mm petri dishes

(Mattek, Ashland, MA). Time-lapse images (every 5 min. for 8 h) were captured using a Coolsnap ES2 CCD camera (Photometrics, Tuscon, AZ) attached to a Nikon Eclipse TE300 inverted microscope running Metamorph v7.6.2 (Molecular Devices, Sunnyvale, CA). Confocal imaging was carried out on a Bio-Rad MRC 1024ES confocal system attached to a Nikon TE300 microscope. Images were captured using Lasersharp2000 v5.2 (Bio-Rad, Hercules, CA) and further processed using ImageJ v1.44 (National Institutes of Health, Bethesda, MD).

References

1. Cirone, P. *et al.* A role for planar cell polarity signaling in angiogenesis. *Angiogenesis* **11,** 347–360 (2008).
2. Cullen, J. P. *et al.* Pulsatile flow-induced angiogenesis: role of G(i) subunits. *Arterioscler Thromb Vasc Biol* **22,** 1610–1616 (2002).
3. Descamps, B. *et al.* Frizzled 4 Regulates Arterial Network Organization Through Noncanonical Wnt/Planar Cell Polarity Signaling. *Circ Res* (2011). doi:10.1161/CIRCRESAHA.111.250936
4. Devenport, D. & Fuchs, E. Planar polarization in embryonic epidermis orchestrates global asymmetric morphogenesis of hair follicles. *Nat Cell Biol* **10,** 1257–1268 (2008).
5. Griffin, C. T., Srinivasan, Y., Zheng, Y. W., Huang, W. & Coughlin, S. R. A role for thrombin receptor signaling in endothelial cells during embryonic development. *Science* **293,** 1666–1670 (2001).

6. Isogai, S. S., Horiguchi, M. M. & Weinstein, B. M. B. The Vascular Anatomy of the Developing Zebrafish: An Atlas of Embryonic and Early Larval Development. *Dev Biol* **230,** 24–24 (2001).

7. Isogai, S., Lawson, N. D., Torrealday, S., Horiguchi, M. & Weinstein, B. M. Angiogenic network formation in the developing vertebrate trunk. *Development* **130,** 5281–5290 (2003).

8. Jin, H. H., Xu, J. J. & Wen, Z. Z. Migratory path of definitive hematopoietic stem/progenitor cells during zebrafish development. *Blood* **109,** 5208–5214 (2007).

9. Jin, S.-W. S., Beis, D. D., Mitchell, T. T., Chen, J.-N. J. & Stainier, D. Y. R. D. Cellular and molecular analyses of vascular tube and lumen formation in zebrafish. *Development* **132,** 5199–5209 (2005).

10. Kauffenstein, G. G., Laher, I. I., Matrougui, K. K., Guérineau, N. C. N. & Henrion, D. D. Emerging role of G protein-coupled receptors in microvascular myogenic tone. *Cardiovasc Res* **95,** 223–232 (2012).

11. Lin, H.-F. *et al.* Analysis of thrombocyte development in CD41-GFP transgenic zebrafish. *Blood* **106,** 3803–3810 (2005).

12. Liu, Y. *et al.* Edg-1, the G protein-coupled receptor for sphingosine-1-phosphate, is essential for vascular maturation. *J Clin Invest* **106,** 951–961 (2000).

13. Malek, A. M. A. & Izumo, S. S. Control of endothelial cell gene expression by flow. *J Biomech* **28,** 1515–1528 (1995).

14. Montero-Balaguer, M. *et al.* Stable vascular connections and remodeling require full expression of VE-cadherin in zebrafish embryos. *PLoS ONE* **4,** e5772 (2009).

15. Nechiporuk, T., Urness, L. D. & Keating, M. T. ETL, a novel seven-

transmembrane receptor that is developmentally regulated in the heart. ETL is a member of the secretin family and belongs to the epidermal growth factor-seven-transmembrane subfamily. *J Biol Chem* **276,** 4150–4157 (2001).

16. Perry, S. F., Wilson, R. J., Straus, C., Harris, M. B. & Remmers, J. E. Which came first, the lung or the breath? *Comp. Biochem. Physiol., Part A Mol. Integr. Physiol.* **129,** 37–47 (2001).

17. Regard, J. B., Sato, I. T. & Coughlin, S. R. Anatomical profiling of G protein-coupled receptor expression. *Cell* **135,** 561–571 (2008).

18. Sundberg, T. B. *et al.* Disruption of Wnt planar cell polarity signaling by aberrant accumulation of the MetAP-2 substrate Rab37. *Chem. Biol.* **18,** 1300–1311 (2011).

19. Wallgard, E. *et al.* Identification of a core set of 58 gene transcripts with broad and specific expression in the microvasculature. *Arterioscler Thromb Vasc Biol* **28,** 1469–1476 (2008).

20. Winata, C. L. *et al.* Development of zebrafish swimbladder: The requirement of Hedgehog signaling in specification and organization of the three tissue layers. *Dev Biol* **331,** 222–236 (2009).

21. Yaniv, K. K. *et al.* Live imaging of lymphatic development in the zebrafish. *Nat Med* **12,** 711–716 (2006).

Publishing Agreement

It is the policy of the University to encourage the distribution of all theses, dissertations, and manuscripts. Copies of all UCSF theses, dissertations, and manuscripts will be routed to the library via the Graduate Division. The library will make all theses, dissertations, and manuscripts accessible to the public and will preserve these to the best of their abilities, in perpetuity.

Please sign the following statement:

I hereby grant permission to the Graduate Division of the University of California, San Francisco to release copies of my thesis, dissertation, or manuscript to the Campus Library to provide access and preservation, in whole or in part, in perpetuity.

Author Signature

6/14/13
Date